A MAGNETICALLY TRIGGERED, TARGETED THERAPEUTIC DRUG DELIVERY SYSTEM FROM POLYMER MICELLES

by

AMANDA LOUISE GLOVER

DAVID E. NIKLES, COMMITTEE CHAIR

CAROLYN CASSADY
SHANLIN PAN
SHANE STREET
YUPING BAO

A DISSERTATION

Submitted in partial fulfillment of the requirements
for the degree of Doctor of Philosophy
in the Department of Chemistry
in the Graduate School of
The University of Alabama

TUSCALOOSA, ALABAMA

2014

ABSTRACT

Current chemotherapeutic treatment options rely on delivering high doses of toxic chemicals to a patient in the hopes that some of the drug will kill the cancer. This method of treatment leads to side effects ranging from hair loss to healthy cell mutation. To combat the potential for these side effects a method of delivery for therapeutics has been developed from polymer micelles housing the drug that specifically targets and binds to cancer cells. Not only can the cancer cells be targeted directly, thus reducing the detrimental side effects, but temporal control of therapeutic delivery can be achieved by a magnetically triggered mechanism. In the semi-crystalline core of the micelles, magnetic nanoparticles are housed with the therapeutic drug. Once an alternating current (ac) magnetic field is applied to the micelles, the magnetic particles heat, allowing the cores to melt, which allows the drug to diffuse from the cores of the micelles.

DEDICATION

For Ryan P. Stafford.

LIST OF ABBREVIATIONS AND SYMBOLS

$°C$	Degree Celcius
δ	chemical shift
λ_{EM}	emission wavelength
λ_{EX}	excitation wavelength
λ_{max}	maximum wavelength
µm	micrometer
ac	alternating current
CL	poly(ε-caprolactone)
CMC	Critical Micelle Concentration
cRGDfk	cyclic[arginine-glycine-aspartate-D-phenylalanine-lysine ($AcSCH_2CO$)]
D_h	hydrodynamic diameter
DLS	dynamic light scattering
EG	poly(ethylene glycol)
EPR	Enhanced Permeation and Retention Effect
GPC	gel permeation chromatography
h	hour
HIFU	high intensity focused ultrasound
IR	infrared
LA	poly(L-Lactide)

LCST	lower critical solution temperature
MeO	methoxy
mL	milliliter
mM	millimolar
M_n	number average molecular weight
NIR	near infrared radiation
nm	nanometer
NMR	nuclear magnetic resonance
NPs	magnetic nanoparticles
N_2	nitrogen gas
nm	nanometer
OH	hydroxyl
PCL	Polycaprolactone
PEG	Polyethylene glycol
PLA	Poly-L-lactide
QD	quantum dot
TEM	transmission electron microscopy
THF	tetrahydrafuran
UV	ultraviolet radiation
<	Less than
=	Equal to

ACKNOWLEDGMENTS

I could not have achieved even a fraction of the work presented here without my mentor David E. Nikles. He was quick to teach me to believe in my own intuition and intellect through the course of this project. I am indebted to Stephen Woski for encouragement when I was ready to throw the towel in and take a Master's Degree. Many lively discussions from our collaborator Christopher S. Brazel and his students, James Bennett and Rhythm Shah, kept the brainstorming and creativity alive when we seemed to hit walls. I would also like to thank Yuping Bao for allowing me to use her dynamic light scattering instrument and David E. Graves at the for allowing us to use his differential scanning microcalorimeter and his fluorimeter.

I had the great pleasure of mentoring many undergraduate students. They taught me as much as I taught them. In particular, I would like to thank M. Adam Beg, Lindsey Cobb, Jesse Gettinger, Margaret Johnson, Ben McCormik, Morgan Whitaker for staying on the project during the entirety of their undergraduate experience. Also, the graduate student members of my lab group, especially S. Keith McNeil and Kimberly Anderson reminded me that I was not alone in this process and not being alone is sometimes all the will one needs to move forward.

Finally I have to thank the most important people in my life, my family. My parents, Roy Glover, Vicki Prest and Jim Prest, believed in me even when I did not believe in myself. P. Nigel Glover and O. Lucas Stafford have kept me company through many long nights. I am particularly indebted to my husband, Ryan P. Stafford. He has been a rock in my life, giving me a reason for being each and every day.

CONTENTS

LIST OF TABLES

LIST OF FIGURES

CHAPTER 1

INTRODUCTION

1.1 Statement of Problem

In the treatment of cancer by chemotherapy, the patient is oftentimes harmed by the therapeutic drug as much as by the disease. This is because traditional chemotherapy is not delivered directly to the cancer site, but rather nonspecifically affects healthy systems as well as compromised systems. Additionally, many anti-cancer drugs are poorly soluble in aqueous systems. There is a need for the development delivery vehicles to allow the drugs to become bioavailable. In an effort to gain spatial and temporal control of the delivery of chemotherapeutics such a system needs to be developed that allows clinicians to target the delivery of therapeutics directly to the site of the cancer and trigger the delivery of the cancer drug only after it has reached the cancer site.

1.1.1 Cancer Death Rates

According to the American Cancer Society in 2014 an estimated half a million people will die as a result of cancer and 1.7 million new cases of cancer will be diagnosed in the United States alone.[1] This makes cancer the second leading cause of death in the United States next to heart disease. In 2010 65% of deaths worldwide were due to noncommunicable diseases and of those 15% were cancer related deaths, this equates to 8 million cancer deaths worldwide in

2010.[2] The American Cancer Society predicts this will mean 13.1 million deaths world-wide due to cancer in 2030. Currently cancer therapy options include surgery to remove diseased tissue, radiation therapy, and chemotherapy. This dissertation will focus on an improved delivery method for chemotherapy.

1.1.2 State of the Art in Cancer Chemotherapy

The first chemotherapeutic was discovered based on the autopsy results of soldiers from the First World War. Mustard gas was shown to destroy the lymphatic systems of exposed soldiers, and it was proposed that this effect would be helpful in the fight against lymphatic tumors. Although the end result was tumor regression of a non-Hodgkin's lymphoma the tumor eventually came back.[3] Since then chemotherapy has evolved to include many drug classes and targeted therapies.

1.2 Drug Delivery Systems

Modern chemotherapeutics often times rely on nanoscale carriers to deliver drugs to the site of the cancer. These are usually nanoparticles made from either metals like gold[4] or iron oxides,[5] or amphiphilic molecules such as lipids and copolymers that self-assemble into nanostructures.[6] An amphiphilic molecule is a molecule that has a hydrophobic, or water hating, tail and a hydrophilic, or water loving, head. In selective solvents, such as water, the amphiphile will self-assemble into a variety of different nanostructures. In such nanostructures the tails line up surrounded by solvated heads. Copolymers are amphiphilic molecules with hydrophobic tails and hydrophobic heads. One of the simplest examples of nanostructures that amphiphilic molecules make are spherical micelles. In spherical micelles, upon reaching a certain concentration in water (deemed the Critical Micelle Concentration or CMC) the amphiphilic molecules can self-assemble into a sphere. The core of the sphere excludes water and contains hydrophobic portions

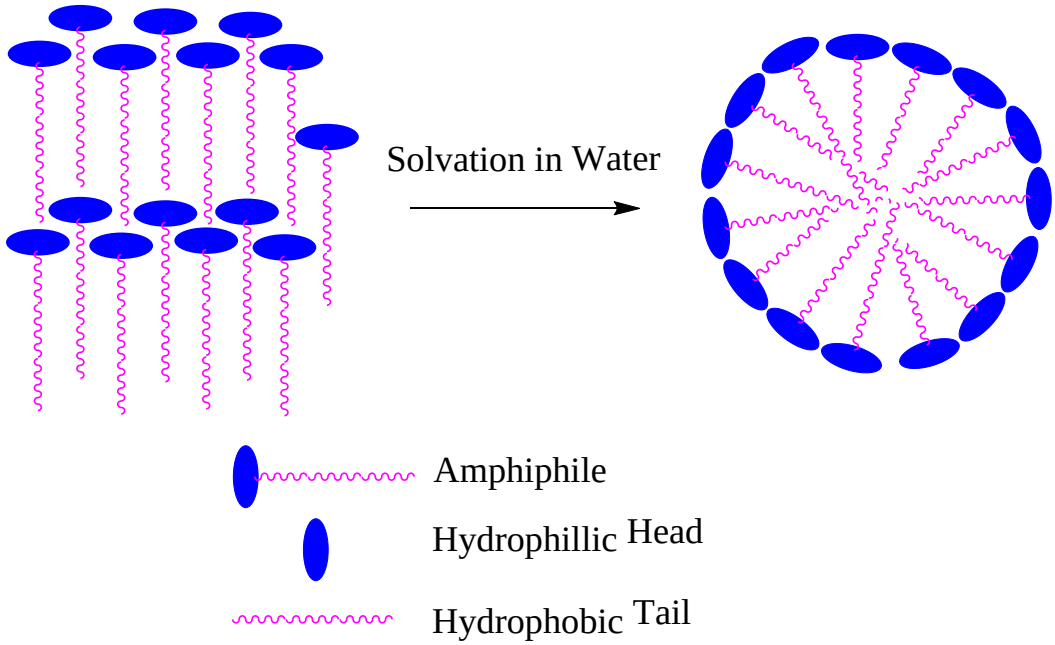

Figure 1.1. Schematic of micellization from amphiphilic molecule where hydrophobic tails exclude water, creating a hydrophobic core. The hydrophilic heads solvate the micelle core.

of the molecules and the hydrophilic portions form a corona that is solvated by water molecules. These structures have diameters ranging from 20—100 nm.[7] A schematic of micellization is shown in Figure 1.1. Other nanostructures that have been used for drug delivery and can be formed by amphiphilic molecules such as worm-like micelles,[8] polymersomes,[9] and nanocapsules.[10] The focus of this dissertation will be spherical micelle drug carriers made from amphiphilic block diblock and triblock copolymers.

The aforementioned nanostructures made from amphiphilic molecules can act as carriers for therapeutic small molecules[11], genes,[12] or proteins.[10, 13] In the case of small molecules held by spherical micelles, hydrophobic drugs can reside in the hydrophobic cores of the micelles.[14] The ability to house drugs that have limited solubility in aqueous environments overcomes one problem of modern chemotherapeutics. Effectively solubilizing the drugs in polymer allows the

drug to become more bioavailable as long as there is a trigger mechanism to release the drug from its hydrophobic housing. Triggering mechanisms will be discussed in section 1.2.1.

Once drug is solubilized and the mechanism of delivery is determined the drug delivery system must also be able to reach the cancer cells. Amphiphilic nanosystems containing polyethylene glycol (PEG) as the hydrophilic group are widely used for drug delivery because of the fact that PEG decreases opsonization of nanoparticles solubilized by PEG.[15] Additionally, micelles are in a size range that allows them to escape renal clearance and liver filtration.[16] These traits allow nanoparticles under 200 nm to stay in the body longer and result in accumulation of nanoparticles in tumor tissues because of the increased and leaky vasculature.[17] This is called the Enhanced Permeation and Retention effect or EPR effect. This effect allows nanosystems with drugs in them get the drugs to the tumor tissues even without ligands to direct the nanoparticles to the disease sites. The issue with these stealthy nanoparticles is they still have many side effects and are not only passively targeted to the cancer cells. To increase the probability that drug delivery systems reach the disease site targeting mechanisms have been developed. These result in active rather than passive targeting of diseased cells. Active targeting will be discussed further in Section 1.2.2.

1.2.1 Triggered Drug Delivery Systems

Delivering the drug payload to a disease site in a nano-package alone is not sufficient for therapy. A mechanism must be in place that will release the drug into a cell once the nanodelivery system reaches tumor tissues and cells. This is where sophisticated triggering mechanisms for delivery must be in place. These mechanisms are divided into two categories: internally triggered release and externally triggered release. Internal triggering mechanisms rely on differences and properties internal to cells to release drug. For internal triggered release

mechanisms there is no further control of when the drug releases once the delivery system is injected into patients. External release mechanisms rely on stimuli outside of the body to control release. Once a drug delivery system has reached its target, it is necessary use fields, light, or radiation to give the clinician the ultimate control of delivery. Oftentimes these externally triggered mechanisms are used in conjunction with imaging mechanisms.[9c] This allows one to detect the location of the disease site before releasing drug.

One strategy in internally triggered release is to rely on pH gradients in the body. This can be slight changes in pH like the difference between physiological conditions (pH = 7.4) and that inside tumor tissues (pH = 6.5-7.2), or certain organelles like the lysosomes (pH = 4.0-5.5) or endosomes (pH = 5.0-6.5) that are at a lower pH than the surrounding media.[18] When changes in the environmental pH occurs hydrophobic ester chains can hydrolytically degrade, thus falling apart and releasing drug (as is the case with polycaprolactone).[11] Another pH responsive mechanism relies on the formation of a covalent bond between the hydrophobic portion of the amphiphile and the drug. This bond, oftentimes hydrazone bond, can be broken at reduced pH resulting in the release of the drug. [19] Other internal mechanisms include redox active bonds in the nanostructure. For example, disulfide bonds can be used to cross-link the hydrophobic portion of the nanosystems.[20] The disulfide linkages, this time in the core of a polyionic complex polymersome, or PICsome, are stable until internalized in the cells. The reductive conditions inside cells allow the disulfide bond to break and release the therapeutic molecule.

This work will focus on an external release mechanism. As described above, externally triggered release mechanisms rely on an external stimulus to break apart the nanostructure. This can be done using light, ultrasound, infrared radiation, or a magnetic field. In the case of ultrasound mediated release mechanisms, the copolymer micelles are designed with weak bonds.

These bonds are susceptible to the mechanical stress provided by high intensity focused ultrasound (HIFU). Liang et. al. have recently developed copolymer micelles with a metal-ligand bond between the hydrophobic and hydrophilic blocks of their copolymer.[21] They demonstrated that the dyes pyrene and Nile Red could be eliminated from the micelles core upon treatment with HIFU. Temperature can also be used as a triggering mechanism. Thermo sensitive micelles can be prepared from block copolymers. In these polymers one block is soluble in water at a low temperature but insoluble at a higher temperature. This exploits the lower critical solution temperature (LCST) of the temperature sensitive block. LCST can be increased or decreased based on hydrophobic or hydrophilic residues on the copolymer.[22] Poly(N-isopropylacrylamide) (PNIPAAm) is one polymer that has been used for these purposes.[23] Nakayama et. al. were able to conjugate PNIPAAm to poly-D,L-lactide and PCL to form biodegradable temperature responsive micelles that increased doxorubicin release *in vitro* at 41 °C.[23c] Thermo-sensitive micelle applications can use focused ultrasound to create hyperthermia conditions.[24]

Light can also act as an external trigger for micelles or polymersomes which either incorporate a chromophore into the hydrophobic core or conjugated into the polymer structure.[18a, 24] In general the chromophores incorporated undergo a conformational shift upon exposure to either ultraviolet (UV) or near infrared (NIR) radiation. NIR can penetrate into the body deeper than UV and NIR responsive chromophores are a better option when choosing the delivery system. Light can also be exploited to render a photoresponsive polymer hydrophilic where it was once hydrophobic. Jiang et. al. used poly(ethylene glycol-pyreneylmethyl methacrylate) (PEG-PPyMA); upon exposure to UV light the pyrenylmethyl ester bond is cleaved leaving polymethacrylate and 1-pyrenemethanol monomers.[25] This ester cleavage

yielded a PEG-PMA copolymer that was completely hydrophobic, resulting in the dissolution of the micelles. Visible light can also be used to stimulate release from nanosystems using gold nanoparticles. Niikura et. al. have created gold nanoparticle vesicles which could be loaded with drugs or dyes at 62.5 °C.[26] They hypothesize that at elevated temperatures nanogaps between the gold nanoparticles open and drug can be loaded into the vesicles. When irradiated with a 532 nm laser these gold nanoparticle vesicles open again, due to heating of the gold nanoparticles under laser irradiation and drug was released.

The mechanism relied for the triggering of release from micelles in this dissertation will be alternating current (ac) magnetic field induced hyperthermia. Hyperthermia is the heating of cells or living systems above their physiological temperatures. Generally, a temperature range of 41 °C to 46 °C elicits hyperthermia temperatures which can trigger cell death or make cells more susceptible to chemotherapeutics.[27] In the case of this dissertation magnetic iron oxide nanoparticles (NPs) were used to heat in a radio frequency ac magnetic field. This was used to disrupt the crystallinity designed the core of the micelles and allow drug to diffuse out of the micelles.

1.2.2 Targeted Drug Delivery Systems

In the past two decades much work has been done to increase the efficacy of therapeutic nanocarriers. Initially, many of these devices relied on the aforementioned EPR effect in combination with "stealth" polymers such as polyethylene glycol as their mechanism of delivery. Liposomal doxorubicin hydrochloride (DOXIL) and albumin bound nanoparticle paclitaxel (Abraxane) are currently on the market in Japan and the United States for AIDs related Kaposi's sarcoma, ovarian cancer and breast cancer treatments to name a few.[28] Targeting mechanisms have been developed for use from ligands made from small molecules[9c], peptides[29], aptamers,[30]

or proteins.[31] These ligands will direct stealthy nanoparticles directly to the cancer sites decreasing the retention time of the EPR effect and increasing the tumor cell uptake.[6] Decreasing the retention time due of the nanoparticles should reduce the probability of side effects from the delivery system and drug.[28] Modern nanotherapeutics rely these specific targeting ligands that take the nanodevice directly to the disease site via some interaction with receptors on cell membranes or internal to the cells of interest. For this system a $\alpha_v\beta_3$ integrin targeting cyclic pentapeptide, cyclic-[Arg-Gly-Asp-$_D$-Phe-Lys(AcCH_2S-CO)] (cRGDfk), was attached to the corona of the micelles. These integrins are responsible for cell adhesion, differentiation among other processes and are overexpressed on the surface of tumor cells.[32]

1.3 Magnetothermally Triggered Polymeric Drug Delivery System

This dissertation will outline the formation of a targeted, externally triggered chemotherapeutic drug delivery system made from block copolymer spherical micelles. The micelles were comprised of diblock copolymers of poly(ethylene glycol-*b*-caprolactone) (MeO-

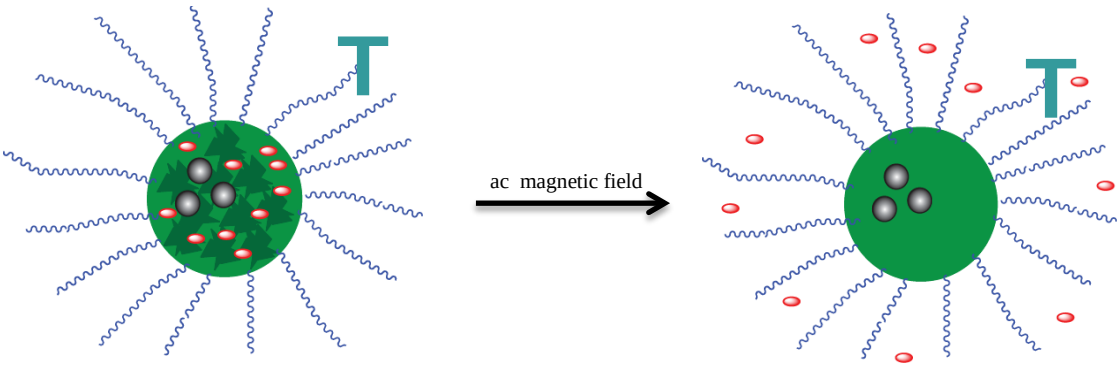

Figure 1.2. Schematic depicting magnetically triggered drug delivery system. The micelles core are comprised of amophous and crystalline PCL (green and dark green). The core holds doxorubicin (red ovals) and magnetic nanoparticles (gray spheres). The corona of the micelles is made of hydrophilic PEG (blue lines) and is attached to a targeting ligand, cRGD, (teal T). Upon exposure to an ac magnetic field the NPs in the core will heat, melting the crystalline PCL and allowing drug to diffuse to the cancer site.

EG_m-CL_n-OH) of varying molecular weights or the triblock terpolymer poly(ethylene glycol-*b*-caprolactone-*b*-lactide) (MeO-EG_m-CL_n-LA_p-OH). These polymers are biocompatible and biodegradable.[11, 33] Also, CL and LA can be crystalline at room temperature (25 °C) or physiological temperatures (37 °C). Semicrystalline PCL had a melting point in the range for hyperthermia treatment (~43 °C).[34] It was hypothesized that crystallinity will trap the drug in place and once the core is melted the drug housed within the core will be able to diffuse from the core of the micelle into the targeted cancer cells.

Magnetic NPs with hydrophobic surfaces were incorporated into the semicrystalline core of the micelles along with hydrophobic drug. By exposing the micelles to an ac magnetic field the NPs heat due to magnetic induction.[35] This is related to magnetic hyperthermia, except that the energy produced by the NPs may not result in heating in the extracellular matrix, but should be enough energy to heat the core of the micelles. The targeting peptide cRGD*fk* was attached to the corona of the micelle through a Michael Addition to a maleimide terminated PEG-PCL containing batch of micelles. This ligand binds to endocrines oftentimes overexpressed on cancer cells.[36] This allowed the micelles to stick to the surface of cells. Figure 1.2 shows a schematic of the drug delivery system described.

References

1. *Cancer Facts & Figures 2014*; American Cancer Soceity: Atlanta, 2014.

2. Rising Global Cancer Epidemic. http://www.cancer.org/acs/groups/content/@marketing/documents/document/acspc-036979.pdf (accessed March 9, 2013).

3. Chabner, B. A.; Roberts, T. G., Jr., Timeline: Chemotherapy and the war on cancer. *Nature reviews. Cancer* **2005,** *5* (1), 65-72.

4. Mieszawska, A. J.; Mulder, W. J. M.; Fayad, Z. A.; Cormode, D. P., Multifunctional Gold Nanoparticles for Diagnosis and Therapy of Disease. *Mol Pharmaceut* **2013,** *10* (3), 831-847.

5. Laurent, S.; Forge, D.; Port, M.; Roch, A.; Robic, C.; Vander Elst, L.; Muller, R. N., Magnetic Iron Oxide Nanoparticles: Synthesis, Stabilization, Vectorization, Physicochemical Characterizations, and Biological Applications. *Chemical Reviews* **2008,** *108* (6), 2064-2110.

6. Zhong, Y.; Meng, F.; Deng, C.; Zhong, Z., Ligand-directed active tumor-targeting polymeric nanoparticles for cancer chemotherapy. *Biomacromolecules* **2014,** *15* (6), 1955-69.

7. Riess, G., Micellization of block copolymers. *Prog Polym Sci* **2003,** *28* (7), 1107-1170.

8. (a) Geng, Y.; Discher, D. E., Hydrolytic degradation of poly(ethylene oxide)-block-polycaprolactone worm micelles. *J Am Chem Soc* **2005,** *127* (37), 12780-12781; (b) Kim, Y.; Dalhaimer, P.; Christian, D. A.; Discher, D. E., Polymeric worm micelles as nano-carriers for drug delivery. *Nanotechnology* **2005,** *16* (7), S484-S491; (c) Rajagopal, K.; Mahmud, A.; Christian, D. A.; Pajerowski, J. D.; Brown, A. E. X.; Loverde, S. M.; Discher, D. E., Curvature-Coupled Hydration of Semicrystalline Polymer Amphiphiles Yields flexible Worm Micelles but Favors Rigid Vesicles: Polycaprolactone-Based Block Copolymers. *Macromolecules* **2010,** *43* (23), 9736-9746.

9. (a) Pang, Z.; Gao, H.; Yu, Y.; Guo, L.; Chen, J.; Pan, S.; Ren, J.; Wen, Z.; Jiang, X., Enhanced Intracellular Delivery and Chemotherapy for Glioma Rats by Transferrin-Conjugated Biodegradable Polymersomes Loaded with Doxorubicin. *Bioconjugate Chemistry* **2011,** *22* (6), 1171-1180; (b) Adams, D. J.; Kitchen, C.; Adams, S.; Furzeland, S.; Atkins, D.; Schuetz, P.; Fernyhough, C. M.; Tzokova, N.; Ryan, A. J.; Butler, M. F., On the mechanism of formation of vesicles from poly(ethylene oxide)-block-poly(caprolactone) copolymers. *Soft Matter* **2009,** *5* (16), 3086-3096; (c) Yang, X. Q.; Grailer, J. J.; Rowland, I. J.; Javadi, A.; Hurley, S. A.; Matson, V. Z.; Steeber, D. A.; Gong, S. Q., Multifunctional Stable and pH-Responsive Polymer Vesicles Formed by Heterofunctional Triblock Copolymer for Targeted Anticancer Drug Delivery and Ultrasensitive MR Imaging. *Acs Nano* **2010,** *4* (11), 6805-6817.

10. Tang, R.; Kim, C. S.; Solfiell, D. J.; Rana, S.; Mout, R.; Velázquez-Delgado, E. M.; Chompoosor, A.; Jeong, Y.; Yan, B.; Zhu, Z.-J.; Kim, C.; Hardy, J. A.; Rotello, V. M., Direct

Delivery of Functional Proteins and Enzymes to the Cytosol Using Nanoparticle-Stabilized Nanocapsules. *ACS Nano* **2013,** *7* (8), 6667-6673.

11. Shuai, X.; Ai, H.; Nasongkla, N.; Kim, S.; Gao, J., Micellar carriers based on block copolymers of poly(epsilon-caprolactone) and poly(ethylene glycol) for doxorubicin delivery. *Journal of Controlled Release : Official Journal of the Controlled Release Society* **2004,** *98* (3), 415-26.

12. Patil, M. L.; Zhang, M.; Minko, T., Multifunctional Triblock Nanocarrier (PAMAM-PEG-PLL) for the Efficient Intracellular siRNA Delivery and Gene Silencing. *Acs Nano* **2011,** *5* (3), 1877-1887.

13. Bale, S. S.; Kwon, S. J.; Shah, D. A.; Banerjee, A.; Dordick, J. S.; Kane, R. S., Nanoparticle-Mediated Cytoplasmic Delivery of Proteins To Target Cellular Machinery. *Acs Nano* **2010,** *4* (3), 1493-1500.

14. Liu, J.; Lee, H.; Allen, C., Formulation of drugs in block copolymer micelles: drug loading and release. *Current Pharmaceutical Design* **2006,** *12* (36), 4685-701.

15. Gref, R.; Minamitake, Y.; Peracchia, M.; Trubetskoy, V.; Torchilin, V.; Langer, R., Biodegradable long-circulating polymeric nanospheres. *Science* **1994,** *263* (5153), 1600-1603.

16. Jones, M.-C.; Leroux, J.-C., Polymeric micelles – a new generation of colloidal drug carriers. *European Journal of Pharmaceutics and Biopharmaceutics* **1999,** *48* (2), 101-111.

17. Letchford, K.; Zastre, J.; Liggins, R.; Burt, H., Synthesis and micellar characterization of short block length methoxy poly(ethylene glycol)-block-poly(caprolactone) diblock copolymers. *Colloid Surface B* **2004,** *35* (2), 81-91.

18. (a) Du, J.; O'Reilly, R. K., Advances and challenges in smart and functional polymer vesicles. *Soft Matter* **2009,** *5* (19), 3544-3561; (b) Meng, F.; Zhong, Z.; Feijen, J., Stimuli-Responsive Polymersomes for Programmed Drug Delivery. *Biomacromolecules* **2009,** *10* (2), 197-209; (c) Carlsen, A.; Lecommandoux, S., Self-assembly of polypeptide-based block copolymer amphiphiles. *Current Opinion in Colloid & Interface Science* **2009,** *14* (5), 329-339; (d) Christian, D. A.; Cai, S.; Bowen, D. M.; Kim, Y.; Pajerowski, J. D.; Discher, D. E., Polymersome carriers: From self-assembly to siRNA and protein therapeutics. *European Journal of Pharmaceutics and Biopharmaceutics* **2009,** *71* (3), 463-474; (e) Nishiyama, N.; Kataoka, K., Current state, achievements, and future prospects of polymeric micelles as nanocarriers for drug and gene delivery. *Pharmacology & Therapeutics* **2006,** *112* (3), 630-648; (f) Park, I.-K.; Singha, K.; Arote, R. B.; Choi, Y.-J.; Kim, W. J.; Cho, C.-S., pH-Responsive Polymers as Gene Carriers. *Macromol Rapid Comm* **2010,** *31* (13), 1122-1133.

19. (a) Tyrrell, Z. L.; Shen, Y.; Radosz, M., Fabrication of micellar nanoparticles for drug delivery through the self-assembly of block copolymers. *Prog Polym Sci* **2010,** *35* (9), 1128-1143; (b) Xiong, X.-B.; Ma, Z.; Lai, R.; Lavasanifar, A., The therapeutic response to

multifunctional polymeric nano-conjugates in the targeted cellular and subcellular delivery of doxorubicin. *Biomaterials* **2010,** *31* (4), 757-768.

20. Matsumoto, S.; Christie, R. J.; Nishiyama, N.; Miyata, K.; Ishii, A.; Oba, M.; Koyama, H.; Yamasaki, Y.; Kataoka, K., Environment-Responsive Block Copolymer Micelles with a Disulfide Cross-Linked Core for Enhanced siRNA Delivery. *Biomacromolecules* **2008,** *10* (1), 119-127.

21. Liang, B.; Tong, R.; Wang, Z.; Guo, S.; Xia, H., High Intensity Focused Ultrasound Responsive Metallo-supramolecular Block Copolymer Micelles. *Langmuir* **2014,** *30* (31), 9524-9532.

22. Rijcken, C. J. F.; Soga, O.; Hennink, W. E.; Nostrum, C. F. v., Triggered destabilisation of polymeric micelles and vesicles by changing polymers polarity: An attractive tool for drug delivery. *Journal of Controlled Release* **2007,** *120* (3), 131-148.

23. (a) Kohori, F.; Sakai, K.; Aoyagi, T.; Yokoyama, M.; Yamato, M.; Sakurai, Y.; Okano, T., Control of adriamycin cytotoxic activity using thermally responsive polymeric micelles composed of poly(N-isopropylacrylamide-co-N,N-dimethylacrylamide)-b-poly(d,l-lactide). *Colloids and Surfaces B: Biointerfaces* **1999,** *16* (1–4), 195-205; (b) Liu, B.; Yang, M.; Li, R.; Ding, Y.; Qian, X.; Yu, L.; Jiang, X., The antitumor effect of novel docetaxel-loaded thermosensitive micelles. *European Journal of Pharmaceutics and Biopharmaceutics* **2008,** *69* (2), 527-534; (c) Nakayama, M.; Okano, T.; Miyazaki, T.; Kohori, F.; Sakai, K.; Yokoyama, M., Molecular design of biodegradable polymeric micelles for temperature responsive drug release. *Journal of Controlled Release* **2006,** *115* (1), 46-56.

24. Oerlemans, C.; Bult, W.; Bos, M.; Storm, G.; Nijsen, J. F.; Hennink, W., Polymeric Micelles in Anticancer Therapy: Targeting, Imaging and Triggered Release. *Pharmaceutical Research* **2010,** *27* (12), 2569-2589.

25. Jiang, J.; Tong, X.; Zhao, Y., A New Design for Light-Breakable Polymer Micelles. *J Am Chem Soc* **2005,** *127* (23), 8290-8291.

26. Niikura, K.; Iyo, N.; Matsuo, Y.; Mitomo, H.; Ijiro, K., Sub-100 nm Gold Nanoparticle Vesicles as a Drug Delivery Carrier enabling Rapid Drug Release upon Light Irradiation. *ACS Applied Materials & Interfaces* **2013,** *5* (9), 3900-3907.

27. Kuznetsov, A. A.; Leontiev, V. G.; Brukvin, V. A.; Vorozhtsov, G. N.; Kogan, B. Y.; Shlyakhtin, O. A.; Yunin, A. M.; Tsybin, O. I.; Kuznetsov, O. A., Local radiofrequency-induced hyperthermia using CuNi nanoparticles with therapeutically suitable Curie temperature. *J Magn Magn Mater* **2007,** *311* (1), 197-203.

28. Iwamoto, T., Clinical application of drug delivery systems in cancer chemotherapy: review of the efficacy and side effects of approved drugs. *Biological & Pharmaceutical Bulletin* **2013,** *36* (5), 715-8.

29. (a) Nasongkla, N.; Shuai, X.; Ai, H.; Weinberg, B. D.; Pink, J.; Boothman, D. A.; Gao, J., cRGD-Functionalized Polymer Micelles for Targeted Doxorubicin Delivery. *Angewandte Chemie International Edition* **2004,** *43* (46), 6323-6327; (b) Toti, U. S.; Guru, B. R.; Grill, A. E.; Panyam, J., Interfacial Activity Assisted Surface Functionalization: A Novel Approach To Incorporate Maleimide Functional Groups and cRGD Peptide on Polymeric Nanoparticles for Targeted Drug Delivery. *Mol Pharmaceut* **2010,** *7* (4), 1108-1117; (c) Kuai, R.; Yuan, W.; Qin, Y.; Chen, H.; Tang, J.; Yuan, M.; Zhang, Z.; He, Q., Efficient Delivery of Payload into Tumor Cells in a Controlled Manner by TAT and Thiolytic Cleavable PEG Co-Modified Liposomes. *Mol Pharmaceut* **2010,** *7* (5), 1816-1826.

30. Xu, W.; Siddiqui, I. A.; Nihal, M.; Pilla, S.; Rosenthal, K.; Mukhtar, H.; Gong, S., Aptamer-conjugated and doxorubicin-loaded unimolecular micelles for targeted therapy of prostate cancer. *Biomaterials* **2013,** *34* (21), 5244-5253.

31. Pang, Z.; Feng, L.; Hua, R.; Chen, J.; Gao, H.; Pan, S.; Jiang, X.; Zhang, P., Lactoferrin-Conjugated Biodegradable Polymersome Holding Doxorubicin and Tetrandrine for Chemotherapy of Glioma Rats. *Mol Pharmaceut* **2010,** *7* (6), 1995-2005.

32. Hersel, U.; Dahmen, C.; Kessler, H., RGD modified polymers: biomaterials for stimulated cell adhesion and beyond. *Biomaterials* **2003,** *24* (24), 4385-4415.

33. Nasongkla, N.; Bey, E.; Ren, J.; Ai, H.; Khemtong, C.; Guthi, J. S.; Chin, S.-F.; Sherry, A. D.; Boothman, D. A.; Gao, J., Multifunctional Polymeric Micelles as Cancer-Targeted, MRI-Ultrasensitive Drug Delivery Systems. *Nano Letters* **2006,** *6* (11), 2427-2430.

34. Glover, A. L.; Nikles, S. M.; Nikles, J. A.; Brazel, C. S.; Nikles, D. E., Polymer Micelles with Crystalline Cores for Thermally Triggered Release. *Langmuir* **2012,** *28* (29), 10653-10660.

35. Pradhan, P.; Giri, J.; Samanta, G.; Sarma, H. D.; Mishra, K. P.; Bellare, J.; Banerjee, R.; Bahadur, D., Comparative evaluation of heating ability and biocompatibility of different ferrite-based magnetic fluids for hyperthermia application. *Journal of Biomedical Materials Research Part B: Applied Biomaterials* **2007,** *81B* (1), 12-22.

36. Wang, Y.; Wang, X.; Zhang, Y.; Yang, S.; Wang, J.; Zhang, X.; Zhang, Q., RGD-modified polymeric micelles as potential carriers for targeted delivery to integrin-overexpressing tumor vasculature and tumor cells. *Journal of Drug Targeting* **2009,** *17* (6), 459-467.

CHAPTER 2

EXPERIMENTAL

2.1 Sources of Chemicals and Materials

All chemicals were purchased from Sigma-Aldrich Chemical Co. (Saint Louis, Missouri, United States) and were reagent grade or better and used as received unless otherwise noted. Polyethylene glycol monomethyl ether (MeO-PEG, $M_n \approx 2{,}000$ or 5,000) was dried by heating to 60 °C under vacuum overnight then stored in a desiccator over indicating Drierite®. The ε-caprolactone was distilled from calcium hydride and stored under nitrogen over 4 Å molecular sieves until used. Polyethylene glycol monomaleimide (MAL-PEG, $M_n = 3{,}400$) was purchased from Lasan Bio, Inc (Arab, Alabama, United States). Cyclo[Arg-Gly-Asp-D-Phe-Lys(Ac-SCH_2CO)] (cRGD*fk*) was purchased from Peptides International (Louisville, Kentucky, United States). Dialysis tubing was purchased from VWR International, Spectrapor 7, 50 kDa molecular weight cut off, regenerated cellulose membrane. Ultrapure water, 18 MΩ, was obtained from a Thermoscientific (Waltham, Massachusetts, United States) EasyPure II water purifier.

2.2 Synthesis of Polymers

2.2.1 Poly(ethylene glycol-*b*-caprolactone) (MeO-$(EG)_m$-$(CL)_n$-OH)

All diblock copolymers were prepared by the tin catalyzed ring opening polymerization of ε-caprolactone using a procedure adapted from Sosnik and Cohn.[1] The feed ratio, or amount

of material provided to the reaction, in moles for the ε-caprolactone to polyethylene glycol monomethyl ether was 5, 10, 20, or 40 for the diblocks made with MeO-EG, $M_n \approx 2{,}000$ or 20, 40, or 100 for MeO-EG $M_n \approx 5{,}000$. Briefly, a three neck round bottom flask fitted with a stir bar and a condenser was purged with N_2, then MeO-EG ($M_n \approx 2{,}000$ or 5,000) was added to the flask, then ε-caprolactone was added via a dried syringe to the reaction mixture. A catalytic amount of dibutyltin dilaurate was then added to the reaction mixture and the reactor was heated with an oil bath to the melt (155—160 °C) and stirred for 3 h to 3 days. The reaction mixture was then purified by recrystallization from hot acetone with ether. For the case of MeO-EG_{113}-CL_{107}-OH purified by repeatedly washing the solid obtained with methanol until the washes contained no material.

2.2.2 ^{1}H NMR Results for MeO-EG_m-CL_n-OH

MeO-$(EG)_{45}$-$(CL)_5$-OH ^{1}H NMR ($CDCl_3$) δ (ppm) 1.39 (m, 9 H), 1.64 (m, 20 H), 2.31 (m, 9 H), 3.38 (s, 3 H (set)), 3.64 (s, 180 H), 4.06 (t, 6 H), 4.22 (t, 2 H).

MeO-$(EG)_{43}$-$(CL)_{11}$-OH ^{1}H NMR ($CDCl_3$) δ (ppm) 1.38 (m, 23 H), 1.63 (m, 54 H), 2.32 (m, 23 H), 3.38 (s, 3 H (set)), 3.64 (s, 173 H), 4.06 (t, 19 H), 4.22 (t, 2 H).

MeO-$(EG)_{43}$-$(CL)_{20}$-OH ^{1}H NMR ($CDCl_3$) δ (ppm) 1.36 (m, 42 H), 1.61 (m, 80 H), 2.28 (t, 40 H), 3.36 (s, 3 H (set)), 3.62 (s, 172 H), 4.04 (t, 37 H), 4.20 (t, 3 H).

MeO-$(EG)_{53}$-$(CL)_{51}$-OH ^{1}H NMR ($CDCl_3$) δ (ppm) 1.39 (m, 102 H), 1.64 (m, 222 H), 2.30 (t, 100 H), 3.37 (s, 3 H (set)), 3.64 (s, 214 H), 4.05 (t, 98 H), 4.22 (t, 2 H).

MeO-$(EG)_{111}$-$(CL)_{17}$-OH ^{1}H NMR ($CDCl_3$) δ (ppm) 1.37 (m, 36 H), 1.61 (m, 75 H), 2.31 (t, 33 H), 3.38 (s, 3 H (set)), 3.64 (s, 448 H), 4.06 (t, 31 H), 4.22 (t, 2 H).

MeO-$(EG)_{113}$-$(CL)_{40}$-OH ^{1}H NMR ($CDCl_3$) δ (ppm) 1.39 (m, 84 H), 1.64 (m, 174 H), 2.30 (t, 78 H), 3.38 (s, 3 H (set)), 3.64 (s, 455 H), 4.06 (t, 75 H), 4.22 (t, 2 H).

MeO-$(EG)_{113}$-$(CL)_{107}$-OH ^{1}H NMR ($CDCl_3$) δ (ppm) 1.38 (m, 219 H), 1.64 (m, 460 H), 2.31 (t, 206 H), 3.38 (s, 3 H (set)), 3.64 (s, 456 H), 4.06 (tm 198 H).

2.2.3 Poly(ethylene glycol-*b*-caprolactone-*b*-lactide) (MeO-$(EG)_{109}$-$(CL)_{48}$-$(LA)_{43}$-OH)

The triblock was synthesized by first preparing MeO-EG_{113}-CL_{40}-OH as described above from the ring opening polymerization of ε-caprolactone onto methoxy terminated polyethylene glycol Mw 5,000 using tin (II) octanoate as the catalyst. Next, the prepared diblock was dried and put into a three neck round bottom under N_2 atmosphere with a condenser and stir bar attached. L-Lactide (1:25 molar ratio) was added to the flask. The reaction mixture was allowed to melt and eight drops of tin (II) octanoate was added to the flask. The reaction was allowed to run for 3 h. To isolate the final product the crude melt was allowed to solidify then dissolved in chloroform and gravity filtered to remove any impurities. The remaining solid was then triturated with methanol. The solid was isolated by centrifugation and dried in a desiccator overnight. The final yield was 3.42 g (32.7 %). ^{1}H NMR ($CDCl_3$) δ (ppm) 1.38 (m, 108 H), 1.58 (d, 122 H), 1.63 (m, 196 H), 2.30 (t, 96 H), 3.38 (s, 3 H (set)), 3.64 (s, 439 H), 4.05 (t, 88 H), 5.17 (m, 45 H). MeO-EG_{109}-CL_{48}-LA_{43}-OH.

2.2.4 Maleimide poly(ethylene glycol-*b*-caprolactone) (MAL-PEG-PCL-OH)

The maleimide terminated poly(ethylene glycol-*b*-caprolactone) was synthesized with a procedure adapted from Gao and coworkers.[2] A 10 mL round bottom flask was dried in a convection oven at 110 °C. Flask was equipped with magnetic stirring a nitrogen atmosphere. The flask was charged with polyethylene glycol monomaleimide (0.5004 g, 0.147 mmol), ε-

caprolactone (0.41 mL, 3.7 mmol) and tin (II) octanoate (5 drops). The flask was heated with an oil bath at 71 °C and allowed to stir at that temperature for 80 hours. After this the viscous liquid was allowed to cool to room temperature under N_2. Upon cooling the product solidified. The product was dissolved in a minimum of tetrahydrofuran and enough hexane was added to the point of imminent precipitation. The solution was placed in the freezer overnight at -30 °C whereupon the polymer crystallized. The polymer was isolated by vacuum filtration and rinsed with cold hexane. Yield, 0.8682 g. ^{1}H NMR ($CDCl_3$) δ (ppm) 1.38 (m, 61.1 H), 1.64 (m, 113.8 H), 2.30 (m, 53.5 H), 3.64 (s, 328.0 H), 4.06 (t, 47.7 H), 4.22 (t, 5.7 H), 6.70 (s, 1.8 H). MAL-CH_2CH_2-$(OCH_2CH_2)_{82}$-$(OCOCH_2CH_2CH_2CH_2CH_2)_{28}$-OH.

2.3 Polymer Micelles

In creating micelles several different formulations were used and they will be referred to as generations of micellization.

2.3.1 Generation I Micelle Preparation

Generation I micelles were made by simple dissolution in water. For example, 8.1 mg (0.002 mmol) MeO-PEG_{42}-PCL_{19}-OH was weighed in a tarred 100 mL volumetric flask. Ultrapure H_2O (18 MΩ, 70 mL) was added to the polymer and the flask was capped and put in a warm water bath (60 °C) until the turbid solution became clear. Once clear the flask was allowed to come to room temperature and then ultrapure H_2O was added to the line (100 mL total). The resulting solution was 0.081 g/L, 0.02 mM or 22 times the critical micelle concentration (CMC). Solutions made by Generation I method were used for differential scanning microcalorimetry (DSC), critical micelle concentration (CMC) determination with pyrene, and dynamic light scattering (DLS) measurements.

2.3.2 Generation II Micelle Preparation

It was determined early on that the eventual loading of drug and magnetic nanoparticles would not be achieved with Generation I micelles because there was no solvent that the hydrophobic materials would be soluble in. The first attempt to develop a method for loading materials into the cores of the micelles was done by Generation II micelles. To make blank micelles in this method tetrahydrafuran (THF) filtered through a 0.20 µm syringe filter to use as the solvent selective for both blocks. First MeO-PEG_{43}-PCL_{20}-OH was weighed into a small vial, then filtered THF (10 mL) was added to dissolve the polymer completely. The polymer/THF solution was then added drop wise to ultrapure H_2O until a 50/50 mixture of THF to water was reached with stirring with a stir flea. The solution was kept at reduced pressure for 1 week, until the solution volume decreased by half and THF could no longer be detected. Finally the was diluted to 70 mL with ultrapure H_2O, capped, and stirred in a 60 °C water bath until turbidity cleared. Once cooled the solution was diluted to the final volume in a 100 mL volumetric flask. The final solution concentration was 2.488 g/L, 0.6145 mM and 670 times the CMC. This solution was used for DSC.

2.3.3 Generation III Micelle Preparation

Generation II proved difficult to reproduce and took over one week to make. In an effort to improve reproducibility Generation III was developed. To improve reproducibility an addition funnel was set to add about 1 drop/sec of a set amount of water to a THF/polymer solution in a volumetric flask. Briefly, MeO-PEG_{43}-PCL_{20}-OH (24.6 mg, 0.00607 mmol) was weighed into a 100 mL volumetric flask equipped with a stir flea. The polymer was dissolved in filtered THF (0.20 µm, 2 mL) and ultrapure H_2O was added drop wise with an addition funnel

set to deliver 1 drop every 10 sec while stirring. The solution was kept at reduced pressure for 1 week for the THF to evaporate. After the THF had evaporated, ultrapure H_2O (20 mL) was added to the flask, the flask was capped and then heated to 50 °C to reduce turbidity, cooled then diluted to the final volume of 100 mL. The final concentration was 0.242 g/L, 0.0598 mM or 65 times the CMC. This method was used for DSC and temperature dependent DLS.

2.3.4 Generation IV Micelle Preparation

Attempts were to make magnetic micelles by Generation III; however, it was found that the magnetic nanoparticles stuck to the stir flea rather than dispersing into the cores of the micelles. Because of this Generation IV was developed without using stirring of any kind but rather probe sonication to mix the solutions. To make blank micelles, MeO-PEG_{43}-PCL_{20}-OH (10.2 mg, 0.0025 mmol) was weighed in a small vial and dissolved in filtered THF (0.20 µm, 2 mL). The THF/polymer solution was added drop wise with a pasture pipet to the ultrapure H_2O (10 mL) in a small jar with probe sonication using a Branson 184UV probe sonicator. The micelles were allowed to self-assemble overnight while THF evaporated in an open hood. Once the THF evaporated, the micelles were transferred to a 25 mL volumetric flask and diluted to a final concentration of 0.408 g/L, 0.101 mM or 110 times the CMC.

2.3.5 Generation V Micelle Preparation

To increase loading percentages, Generation V was developed by loading into water above the melting point of the polymers (60 °C). Generation V micelles were made identically to Generation IV micelles; however, the ultrapure H_2O in the jar during probe sonication was heated to 90 °C before adding THF solutions. It was determined that the drugs (doxorubicin and

dibucaine) could decompose at such high temperatures so Generation IV was the final generation of micelles used for drug release studies.

For loading drug or dye and magnetic nanoparticles generally the procedure for Generation IV and V were used.

2.3.6 Doxorubicin Loaded Generation IV Micelles

To load the anti-cancer drug doxorubicin into the core of the micelles, Generation IV was employed. First doxorubicin hydrochloride (5.0 mg, 0.0086 mmol) and the desired copolymer (10-20 mg) were weighed into two separate tarred vials. The polymer was then dissolved in filtered THF (1.0 mL) and the doxorubicin hydrochloride was dissolved in 1.0 mL DMSO with 10 µL triethylamine to afford the deprotonated doxorubicin. The polymer solution was then added to the doxorubicin solution and the resulting mixture was added drop wise to a small jar of ultrapure water (18 MΩ, 10 mL) with probe sonication. The final micelle solution was then kept in the hood overnight in the dark to allow the THF to evaporate. The next day the solution was dialyzed (50 kDa MWCO dialysis membrane) against ultrapure (1 L) water with dialysate changes at 3 h, 6 h, 12 h and taken off dialysis at 24 h. At each time point a sample of the dialysate was saved for mass balance analysis. If aggregates were present at this point the solution was filtered through 0.45 µm syringe filter and diluted to 25 mL with ultrapure water in a volumetric flask. Drug loading was determined by the absorption spectrum at 485 nm.

2.3.7 Dibucaine Loaded Generation IV Micelles

The procedure for dibucaine loaded micelles was similar to doxorubicin loaded micelles except deprotonated dibucaine was prepared in bulk by extraction of the hydrochloride salt from water and triethylamine with chloroform. After dialysis every sample of dibucaine loaded

micelles provided precipitated drug except for the MeO-EG_{113}-CL_{107}-OH, so the micelles were filtered through 0.45 µm syringe filters. Drug loading was determined by the absorption spectrum at 327 nm.

2.4 Synthesis of Magnetic Nanoparticles

2.4.1 Magnetite Nanoparticles (11 nm and 10 nm)

Magnetite nanoparticles (11 nm and 10 nm) were prepared with some modification via the synthesis from Sun et. al.[3] Briefly, iron (III) acetylacetonate (2 mmol) was added to a three-neck round bottom flask containing 1,2-hexadecanediol (10 mmol), oleic acid (6 mmol), and oleylamine (6 mmol) in benzyl ether (20 mL) under N_2 atmosphere. The reaction mixture was then refluxed in the benzyl ether. Allowing for violent reflux for ~3 h produced 8 nm nanoparticles that were presumably magnetite. A gentle 3 h reflux controlling the reflux temperature at ~300 °C yielded the 11 nm nanoparticles. Particles were precipitated from the reaction mixture with ethanol and separated via centrifugation. The supernatant was removed and the particles were dispersed in hexanes with oleic acid/oleyl amine and again precipitated with ethanol. This process was repeated for each batch of nanoparticles until the supernatant was colorless and clear. Both batches were analyzed via transmission electron microscopy (TEM), infared spectroscopy (IR), X-ray photoelectron spectroscopy (XPS), and X-ray powder diffraction (XRD).

2.4.2 Seeded Magnetite Nanoparticles (18 nm)

Magnetite nanoparticles (18 nm) were made by first using the modified Sun synthesis described in 2.4.1 to produce 11 nm nanaoparticles. These particles were then used to nucleate the reaction producing 18 nm nanoparticles. This process was also done according to the Sun

procedures (REF). First, the nanoparticles were loaded into a reaction flask containing more iron(III) acetylacetoneate (2 mmol), 1,2-hexadecanediol (10 mmol), oleic acid (6 mmol) and oleylamine (6 mmol) in benzyl ether. The reaction mixture was held at a temperature of 210 °C for 5 min, then the temperature was lowered to 200 °C for the next 2 h. Finally, the reaction was refluxed for 1 h, allowed to cool to room temperature then worked up as described previously.

2.4.3 Magnetite Nanoparticles (24 nm)

Iron (III) oleate was prepared by the metathesis reaction of iron (III) chloride and sodium oleate. The iron oleate was thermally decomposed in refluxing octadecene to give magnetite nanoparticles that were spherical and 24 ± 2 nm in diameter. The particles were washed with ethanol, then hexanes and a small amount of acetone to remove the octadecene.[4]

2.5 Characterization of Materials

For confirmation of copolymer structure ^{1}H NMR was performed using Bruker (Billerica, Massachusetts, United States) 360 MHz, 500 MHz or 750 MHz NMR. For copolymer structure determination, deuterated chloroform was used. Deuterated water was used for determination of attachment of targeting ligand onto maleimide PEG-PCL. Copolymers were also analyzed using gel permeation chromatography (GPC) to determine molecular weight, using phenomenex Phenogel 5 u 10E4A and Phenogel 5u 110A columns with dimensions of 300 x 7.80 mm 5 u. The mobile phase was 100 % chloroform.

Critical micelle concentrations (CMCs) were determined using pyrene as a fluorescent probe and a Varian Cary Eclipse fluorescence spectrometer with a water-thermostatted cell holder for variable temperature measurements. Generally, micelles were loaded with pyrene by

either generation I or generation IV methods where a 6.04 μM aqueous (Type I water) solution of pyrene was used in place of pure Type I water for making a concentrated stock solution of the micelles. From these stock solutions, a range of concentrations of the copolymer were prepared by weight using the aqueous solution of pyrene. To determine CMC, the fluorescence emission spectra at 390 nm were taken at ambient temperature with excitation wavelengths of 338 nm (I_{338}) and 333 nm (I_{333}). The ratio (I_{338}/I_{333}) was then plotted as a function of the polymer concentration. For temperature dependent CMC measurements of the series of polymers prepared with polyethylene glycol monomethyl ether $M_n \approx 2{,}000$, each polymer's emission intensity at 390 nm at I_{338} and I_{333} was determined at from 10 °C to 70 °C at 1 °C intervals. For MeO-EG_{113}-CL_{106}-OH and MeO-EG_{107}-CL_{48}-LA_{43}-OH copolymers the same was done for each solution with temperature intervals being 10 °C to 75 °C every 1 °C or 10 °C to 80 °C every 2 °C respectively.

The size of the micelles was determined by dynamic light scattering (DLS) and transmission electron microscopy (TEM). DLS was performed on a Zetasizer Nano ZS ZEN3600 (Malvern Instruments, Worcestershire, UK). Generally the hydrodynamic diameters were determined from number average DLS. TEM was performed using Silicon Monoxide coated 300 mesh Cu grids (Electron Microscopy Sciences, Hatfiled, PA) where the grids were placed on filter paper then the micelle solution was dropped onto the grid in layers allowing each drop to dry between applications. After the final application of micelles a 2% phosphomolybdic acid solution (in ethanol, for blank micelles) was added to stain the micelles. These grids were then allowed to dry at least 24 h before imaging with a FEI 200 kV TEM (Tecnai, Hillsboro, OR). NIH ImageJ software was used to determine the size of the micelle cores seen on the TEM images. This gave a distribution of micelle sizes. Micelle crystallinity was determined using

differential scanning microcaloirimetry (DSC) which is a solution phase DSC technique. Micelles were prepared from each generation in ultrapure water (18 MΩ) and loaded into a VP-DSC microcalorimeter (MicroCal). The scans were run from 10 °C to 90 °C with a temperature ramp of 60 °C per hour. Magnetic nanoparticles (NPs) were analyzed by TEM (FEI F-20, Tecnai, Hillsboro, Oregon, US) to determine size and morphology.

2.6 Drug Release Studies

Drug release was first simulated using a hot water bath rather than magnetic field to screen for the best polymer/drug combination to use for magnetically triggered release studies. Several different methods were used in the development of the understanding of the system including isothermal and pulsatile temperature profiles. Different dialysis membranes were also employed for mimicking release kinetics.

2.6.1 Isothermal Release Sampling from Dialysate

All release simulation methods used a shaker bath and dialysis to simulate drug release inside the body. This bath was set at either 27 °C, 37 °C, 47 °C, 57 °C, or 67 °C with the shaker set at 22 RPM. All dialysis reservoirs (50 mL centrifuge tubes) were filled with ultrapure H_2O (12 mL) and put in jars to hold them upright in the baths and allowed to equilibrate to temperature at least 3 h before the release experiment started. The same was done for a reservoir of ultrapure water used for replenishing the dialysate once a sample was taken. On the day of the experiment the dialysis devices, 50 kDa MWCO Float-a-Lyzers (Spectrum Laboratories, Inc., Rancho Dominguez, California, US), were prepared as per package instructions and loaded with Generation IV or V micelles loaded with either doxorubicin or dibucaine (1.2—1.5 mL). A small string was attached to each device to make sampling easier and the devices were dropped

into the previously equilibrated centrifuge tubes. The release experiments were kept in one bath the entirety of the experiment at a regulated temperature. At regular intervals 2.00—3.00 mL dialysate was removed and replaced with fresh ultrapure H_2O. These samples were analyzed at either 327 nm (dibucaine loaded) or 485 nm (doxorubicin loaded) and compared to a calibration curve to determine the amount of drug released at each time interval.

2.6.2 Isothermal release sampling from retentate

Large jars with ultrapure H_2O (300 mL) were put in the shaker baths at least 3 h before starting release experiments to equilibrate to temperature. 50 kDa MWCO regenerated cellulose dialysis membranes (Spectrum Laboratories, Inc., Rancho Dominguez, California, US) were prepared as per package instructions. Generation IV or V micelles loaded with either dibucaine or doxorubicin were loaded into the membranes and dropped into the jars in the shaker bath kept at a predefined temperature throughout the experiment. At regular intervals the retentate was removed from the dialysis membrane and the absorbance at either 327 nm or 485 nm was taken. The sample was then placed back into the dialysis membrane and allowed to continue dialyzing until the next sample was taken. Like the previous method the absorbance was compared to a calibration curve and the amount of drug remaining in the dialysis membrane at each time interval was calculated and compared with the amount of drug that was loaded into the dialysis membrane. The first time point for each replicate was at t = 0 h.

2.6.3 Pulsatile Release Sampling from Retentate

Pulsatile release was set up just as the isothermal release with sampling from the retentate (2.5.2) was set up except for pulsatile release two jars were equilibrated in two different baths, one at 37 °C and one at 57 °C. The dialysis membrane containing the micelles was moved

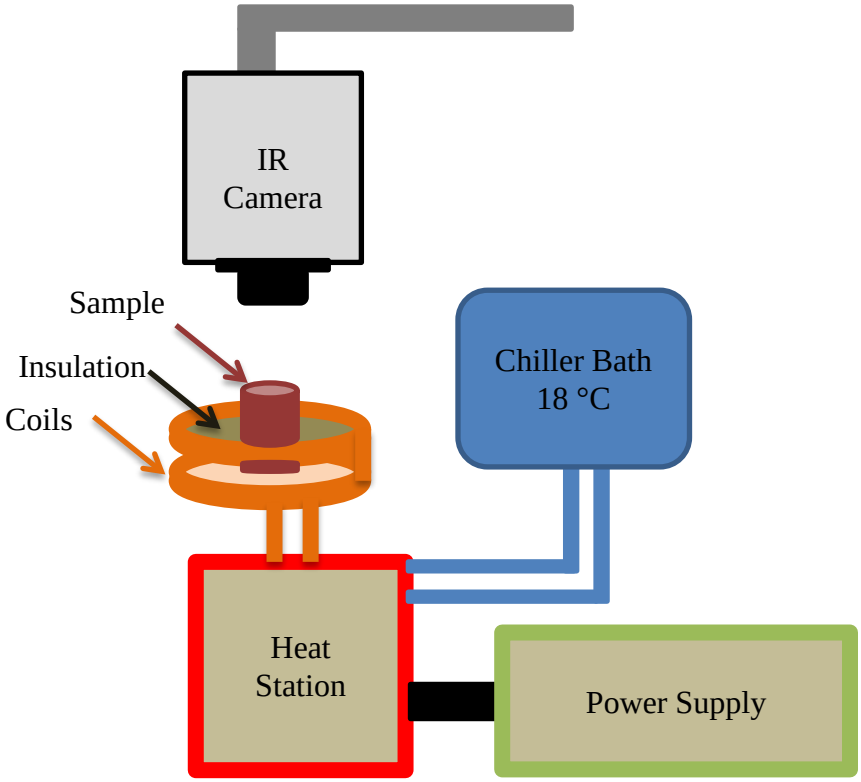

Figure 2.1. Magnetic induction heating coil set up.

between the jars at regular intervals and the retentate was sampled at regular time intervals using UV-Vis spectrophotometer just as described above.

2.7 Heating Studies

2.7.1 Hyperthermia Coils Set Up

All magnetic heating experiments were performed using custom designed hyperthermia coils (Induction Atmosphere, Rochester, NY) with a 5 kW power supply (Novastar 5 kW, Ameritherm, Scottsville, NY) connected to a heat station which is attached to the coils. The coils used to generated the field are hollow to allow circulating water to pass through to minimize temperature rise in the coils themselves. Water was circulated through the coils using a chiller bath (Model JT1000, Koolant Koolers, Kalamazoo, MI) set at 18 °C. The coils

themselves have a 4 cm inner diameter with 2-turns in 1.2 cm height separated from two more turns by 2 cm total giving a total of 4-turns for the coil set up, see figure 2.1. Samples were set up in the center of a section of turns and insulated with either foam or air to minimize non-specific heating from the surface of the coils to the samples.

2.7.2 Micelles for Magnetic Heating

Several set of micelles were prepared with NPs. The first sets of micelles with MNPs were prepared using 8 nm MNPs (see synthesis 2.4.1). Briefly, NPs (8 nm, 2.5 mg) and MeO-EG_{43}-CL_{20}-OH (10.0 mg) were weighed into two separate vials. These were dispersed or dissolved in THF (filtered 0.45 μm, 1.00 mL each). The polymer solution was then pipetted into the MNP dispersion and the solution was placed in a sonicating bath for 10 min to ensure full dispersion. Finally the polymer/NP solution was added to Type I water (10 mL) with probe sonication according to Generation IV techniques (see section 2.3.4). These micelles were analyzed using TEM and DLS and were used to try magnetic heating.

Additional micelles were prepared with the 8 nm NPs incorporating ~4 nm Zn coated CdSe quantum dots (QDs, Ocean Nanotech, San Diego, California, US). This was done in an effort to quantify nano-temperature changes in the cores' of the micelles by fluorescence. A fiber optic fluorescence probe (Ocean Optics, Dunedin, Florida, US) was used to measure the fluorescence of the micelles while a fiber optic temperature probe (Optotemp 2000) simultaneously measured the temperature of the micelles when exposed to the magnetic field, Figure 2.7.2. TEM and DLS were also performed on these micelles.

Other micelles were prepared for magnetic heating, again without the addition of small molecules for drug release; from the 11 nm and 18 nm MNPs (see synthesis sections 2.4.1-2). Four sets of micelles were made with the two types of MNPs and the MeO-EG_{43}-CL_{20}-OH and MeO-EG_{113}-CL_{106}-OH copolymers. The procedure was similar to that above however much more material was used to increase micelle and MNP concentrations and the total volume was decrease to 5 mL Type I water to increase chance for observable magnetic heating. Additionally, these micelles were filtered post evaporation to remove large, undispersed nanoparticle aggregates. Table 2.1 shows the amounts of materials used to create the micelles for heating. The goal was to achieve about 20 g/L MNP concentration because this has been shown to give significant heating above room temperature by our group.[5]

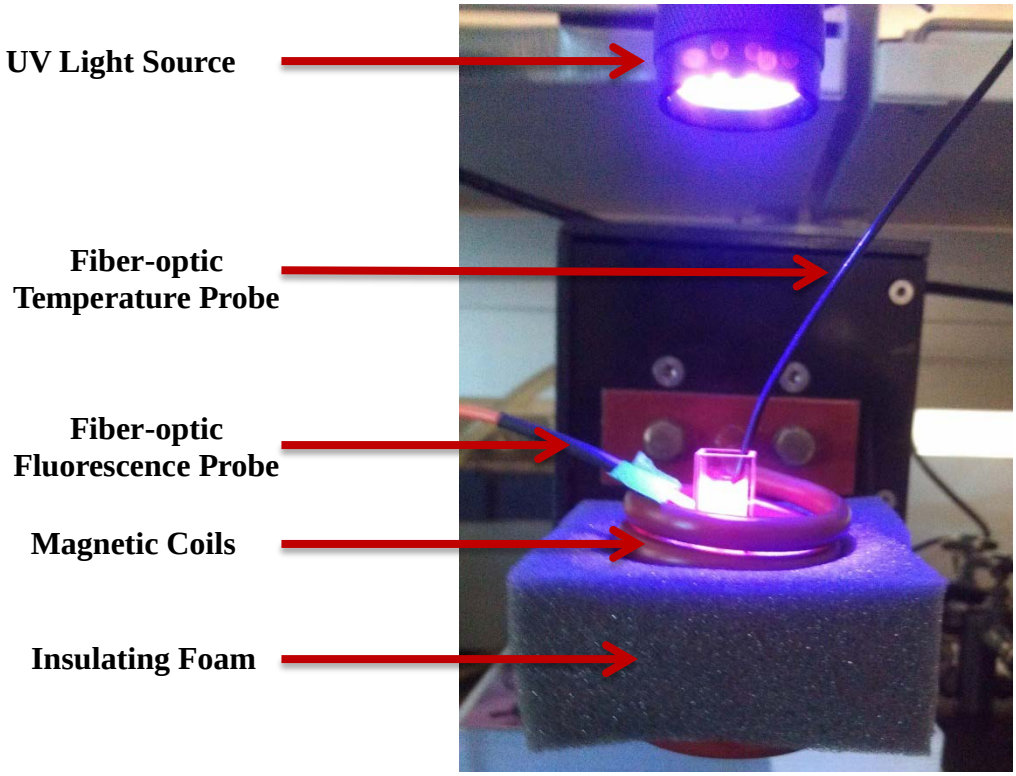

Figure 2.2. Hyperthermia coil set up for measuring local temperature of micelles' cores by QD fluorescence.

Table 2.1. Materials used for magnetic heating of micelles made from 11 nm and 18 nm nanoparticles.

Polymer	Polymer Amount (mg)	MNP Type	MNP Amount (mg)
MeO-EG_{43}-CL_{20}-OH	26.0	11 nm	156.9
	26.0	18 nm	101.4
MeO-EG_{113}-CL_{106}-OH	25.8	11 nm	163.0
	25.9	18 nm	101.7

2.7.3 Magnetically Triggered Drug Release

Finally micelles were prepared for magnetically triggered drug release using the magnetic coils. This was done by first weighing 24 nm MNPs (80.4 mg), MeO-EG_{113}-CL_{107}-OH (81.4 mg, 0.00473 mmol), and dibucaine (57.9 mg, 0.169 mmol) into three separate vials. The polymer and dibucaine were dissolved in filtered THF (0.45 µm, 3 mL and 2 mL respectively). The polymer and dibucaine solutions were then added to the MNPs' vial and this was allowed to sonicate in a sonicating bath for 20 min. The polymer/drug/MNP solution was then added drop wise to Type I water (15 mL) with probe sonication. The solution was then split into two aliquots and each aliquot was dialyzed in regenerated cellulose membranes (SpectraPor 7, 50 kDa MWCO, Spectrum Labs) against 2 L Type I water total. Dialysate was changed at 3 h 7 h and taken off dialysis at 20 h. Once off dialysis the micelles were filtered through 0.45 µm syringe filters (Nylon, VWR) and diluted to 25 mL in a volumetric flask.

For magnetically triggered release every sample was run in triplicate including the controls. For the first set of samples, exposed to the magnetic field for 30 min, six 1.2 mL

aliquots of the micelles were transferred into six micro centrifuge tubes (Eppendorf, Hamburg, Germany). Three of these samples were allowed to sit at ambient temperature and three were put into a three sample holder and exposed to the magnetic field (427 kHz, 750 V, 780 G) for 30 min. Each sample was labeled either control A-C (ambient) for 30 A-C (exposed) and were transferred one at a time into one of six rehydrated dialysis devices (Float-A-Lyzers, 50 kDa MWCO, Spectrum Labs). Once the sample was transferred to the Float-A-Lyzer it was placed in a 50 mL plastic centrifuge tube equilibrated in a 27 °C bath with Type I water (12 mL). The samples were then kept in a 27 °C shaker bath. Samples of the dialysate (4.00 mL) were taken at 30 min, 120 min, 500 min and 1440 min, replacing the 4.00 mL with fresh type I water each time for each sample. This experiment was repeated the next day for 1 h exposure to the field. To quantify the amount of dibucaine in each dialysate sample the absorbance values at 327 nm were compared to a calibration curve of dibucaine in water at 327 nm.

2.8 Micelles for Cell Studies

2.8.1 cRGDfk-Mal-PEG-PCL-OH/MeO-EG_{43}-CL_{20}-OH/PKH26 Micelles for HEK293 Cell Studies

To obtain micelles for cell studies a hydrophobic rhodamine derivative dye, PKH26 (Sigma-Aldrich Chemical Co., Saint Louis, Missouri, US), was used for detecting the micelles. The dye was loaded into the core of micelles using Generation IV procedures and either HEPES/EDTA (50 mM/10 mM) buffer. Two sets of micelles were created, one with Mal-(EG)-(CL)-OH at 40% (by molar) which was attached to the peptide cRGD*fk* and one with just the MeO-EG_{43}-CL_{20}-OH both contained the PKH26 dye. For the micelles with cRGD*fk* attached, first weighed out Mal-(EG)-(CL)-OH (3.0 mg, 5.3 X 10^{-4} mmol) and MeO-EG_{43}-CL_{20}-OH (7.7

mg, 1.9 X 10^{-3} mmol) into a small vial and dissolved in THF (filtered 0.2 μm, 1.9 mL). To this vial added a 1.0 mM ethanol solution of PKH26 dye (100 μL, 1.0 X 10^{-4} mmol). This solution was then added drop wise to HEPES/EDTA buffer (50 mM/10 mM, 10 mL) with probe sonication. The jar was then covered with aluminum foil and left in the hood overnight for solvent to evaporate. The next day the micelle solution was transferred to round bottom flask equipped with a stir flea and to it was added a solution of c[RGD*fk*(Ac-SCH_2CO)] (0.9 mg, 1.0 X 10^{-3} mmol) in HEPES/EDTA incubated with 5.5 mM hydroxylamine to deprotect the thiol. This solution was allowed to stir overnight for the Michael Addition to take place at the maleimide terminus of the PEG. The next day the solution was put on dialysis in a 50 kDa MWCO dialysis membrane against 1 L of the buffer. The dialysate was changed at 3 h, 6 h, 24 h and taken off dialysis at 30 h. Once off dialysis the micelles were transferred to a volumetric flask and diluted to their final concentration of 10 mL resulting in 22 % by mole targeted micelles solution (0.77 g/L, 0.19 mM solution of MeO-EG_{43}-CL_{20}-OH, and a 0.3 g/L, 0.053 mM solution of cRGD*fk* terminated polymer). Dynamic light scattering (DLS) showed an average hydrodynamic radius of 250 nm by distribution analysis with some larger aggregates present.

2.8.2 Non-targeted MeO-EG_{43}-CL_{20}-OH micelles for HEK293 studies

Micelles for the control for the HEK293 studies were prepared as Generation IV and in a method similar to above for targeted micelles. Briefly MeO-EG_{43}-CL_{20}-OH (10.7 mg, 2.6 X 10^{-3} mmol) was dissolved in THF (0.2 μm, 1.9 mL) and a 1.0 mM solution in ethanol of PKH26 was added to the THF solution. The dye/polymer solution was then added drop wise to HEPES/EDTA (50 mM/10 mM, 10 mL) with probe sonication and allowed to sit in the hood overnight in the dark. The micelle solution was then dialyzed against the 1 L of the buffer at 4 °C in 50 kDa MWCO dialysis membrane with dialysate changes occurring at 3 h, 7 h, 19 h, and

taken off at 28 h. The final micelle solution was then diluted to 10 mL with buffer in a volumetric flask and stored in the dark at 4 °C. DLS showed an average hydrodynamic radius of 250 nm with some larger aggregates present.

2.8.3 MeO-EG_{43}-CL_{20}-OH Micelles for Jurkat Studies

Micelles for Jurkat cell studies were prepared similarly to micelles for HEK293 cells (2.8.1 and 2.8.2) except that buffer solution was phosphate buffered saline (PBS) and the amount of cRGDfk incorporated into the MAL-PEG-PCL-OH micelles was 5 %. Jurkat cells are T lymphocyte cells.

2.8.4 cRGDfk-Mal-(EG)-(CL)-OH Micelles for ^{1}H NMR Studies

The purpose of this experiment was to assure that peptide was adding to the maleimide by Michael addition. Mal-(EG)-(CL)-OH (50.8 mg, 8.9 X 10^{-3} mmol) was weighed and dissolved in THF (1.0 mL). Then the buffer (HEPES/EDTA 50 mM/10 mM) was added until the solution was cloudy. Then c[RGDfk(AC-SCH_2CO)] (4.0 mg) and dissolved in the buffer (200 µL) and combined peptide with the polymer and allowed the reaction mixture to stir overnight. The next day the solution was dialysed (3500 Da MWCO) against the HEPES/EDTA buffer with a dialysate change at 6 h and 24 h and taken off dialysis at 48 h. Once off dialysis the solution was lyophilized to remove the water then taken for ^{1}H NMR in $CDCl_3$ and D_2O.

References

1. Sosnik, A.; Cohn, D., Poly(ethylene glycol)-poly(epsilon-caprolactone) block oligomers as injectable materials. *Polymer* **2003,** *44* (23), 7033-7042.

2. Nasongkla, N.; Shuai, X.; Ai, H.; Weinberg, B. D.; Pink, J.; Boothman, D. A.; Gao, J., cRGD-Functionalized Polymer Micelles for Targeted Doxorubicin Delivery. *Angewandte Chemie International Edition* **2004,** *43* (46), 6323-6327.

3. Sun, S. H.; Zeng, H.; Robinson, D. B.; Raoux, S.; Rice, P. M.; Wang, S. X.; Li, G. X., Monodisperse MFe2O4 (M = Fe, Co, Mn) nanoparticles. *J Am Chem Soc* **2004,** *126* (1), 273-279.

4. Park, J.; An, K.; Hwang, Y.; Park, J.-G.; Noh, H.-J.; Kim, J.-Y.; Park, J.-H.; Hwang, N.-M.; Hyeon, T., Ultra-large-scale syntheses of monodisperse nanocrystals. *Nat Mater* **2004,** *3* (12), 891-895.

5. Shah, R. R. D., T. P.; Glover, A. L.; Nikles, D. E.; Brazel, C. S. , Impact of magnetic field parameters and iron oxide nanoparticle properties on heat generation for use in magnetic hyperthermia. *J Magn Magn Mater* **under revision, 2014**.

CHAPTER 3

POLYMER MICELLES

The drug delivery system was assembled from block copolymer micelles containing either polycaprolactone (CL) or polycaprolactone and polylactide (CL-LA) hydrophobic blocks with polyethylene glycol (EG) hydrophilic blocks. Magnetic nanoparticles (NPs) and hydrophobic drug would be contained inside the hydrophobic cores of the micelles. Before the drug or the MNPs could be put into the cores of the micelles, several pieces of information were needed.

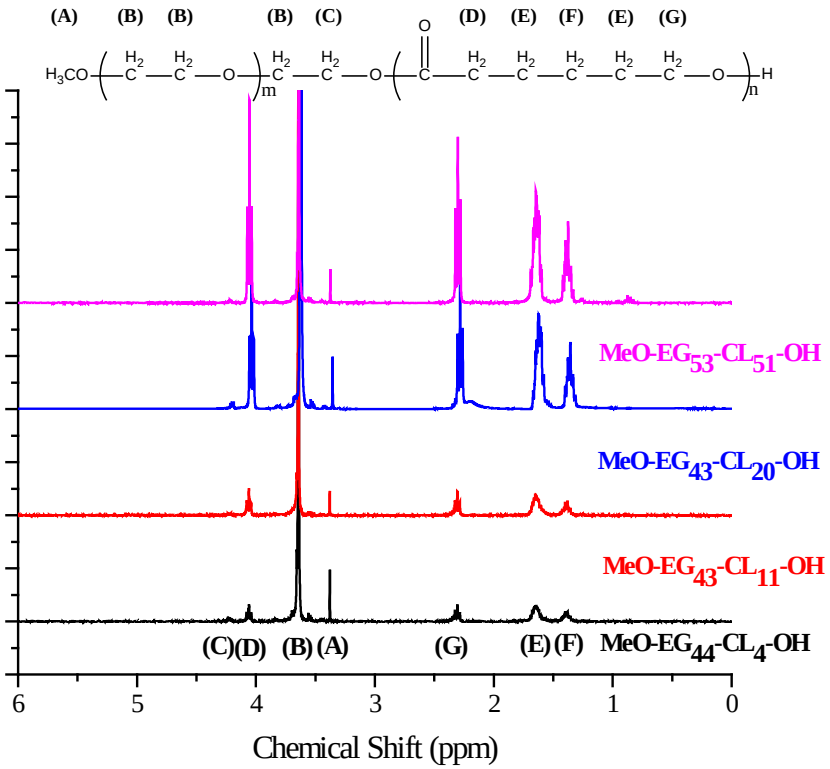

Figure 3.1. ^{1}H NMR spectrum for MeO-EG$_m$-CL$_n$-OH copolymers prepared from MeO-PEG MW ≈ 2,000.

First, the copolymers had to be characterized to determine the degree of polymerization and the molecular weights. Then micelles had to be created without anything inside of them and characterized for critical micelle concentration (CMC) and size. These micelles will be referred to as blank micelles for this text. Additionally, the best method for self-assembly was determined as well as the characterization of the thermal properties of the micelles because the final package was designed to be temperature responsive based on the CL's melting profiles.

3.1 Characterization of the Polymers

The degrees of polymerization of the EG, CL and LA block were determined by ^{1}H NMR. For the MeO-EG_m-CL_n-OH copolymers, the integration of the peak at δ = 3.38 ppm for the terminal methyl group of the EG block was set to 3.00 protons. The remaining protons were

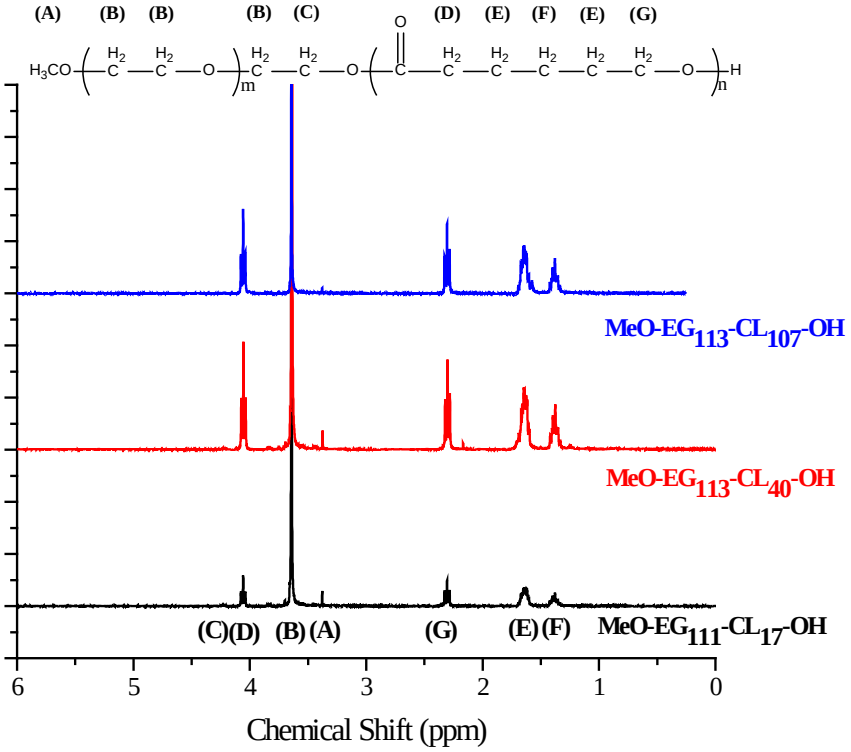

Figure 3.2. ^{1}H NMR spectrum for MeO-EG_m-CL_n-OH copolymers prepared from MeO-PEG MW ≈ 5,000.

then integrated and the degree of polymerization was determined for the EG by integrating the signal at 3.64 ppm ((A), Figure 3.2) and subtracting 2 for the linker protons and dividing by 4 because that signal corresponds to the two methylene groups on the PEG which contains 4 protons total. Each of the polycaprolactone signals at 1.38 ppm, 1.64 ppm, 2.31 ppm, and 4.06 ppm were integrated and divided by the number of protons each signal corresponds to (two, four, two, two). The integrals were then averaged to determine the average degree of polymerization for each polymer ((D)-(G) Figure 3.1). In Figure 3.1, the ^{1}H NMR for all of the copolymers made with MeO-PEG, M_n ~ 2,000 (EG2000) along with the basic structure of the MeO-EG_m-CL_n-OH copolymer are shown. The peaks are labeled and correspond to the protons on the shown structure. It is important to note that as the CL chain length increased the peak corresponding to the linking glycol shrinks in relation to the other peaks (C, Figure 3.1).

This is more evident in figure 3.2 which shows the ^{1}H NMR spectra of the polymers

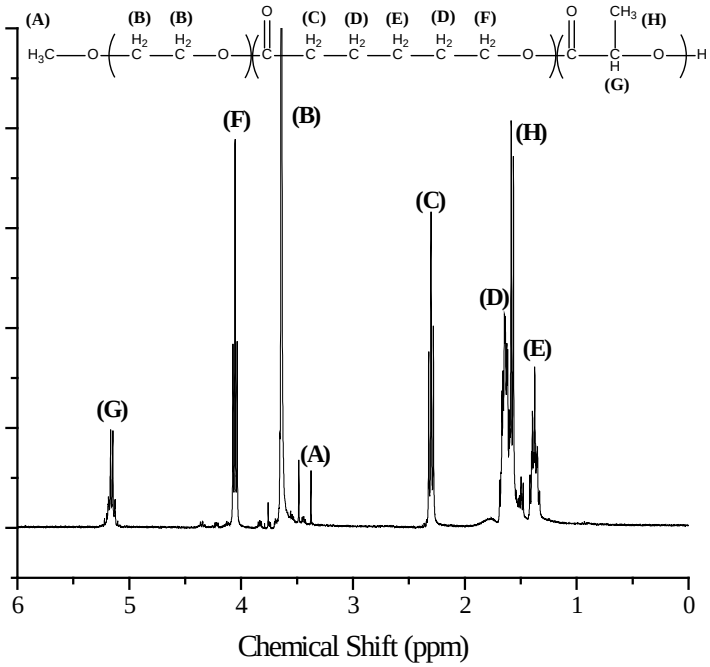

Figure 3.3. ^{1}H NMR spectrum of MeO-EG_{109}-CL_{48}-LA_{43}-OH

made with MeO-PEG M_n ~ 5,000 (EG5000). The peaks for the C labeled methylenes are barely visible in the spectrum for MeO-EG_{113}-CL_{40}-OH and are no longer visible at all for the MeO-EG_{113}-CL_{107}-OH polymer. In the ^{1}H NMR for the triblock copolymer containing polylactide (LA, MeO-EG_{109}-CL_{48}-LA_{43}-OH, Figure 3.3) the linker peak is barely visible. The spectrum is comparable to the ^{1}H NMR for the diblock MeO-EG_{113}-CL_{40}-OH (Figure 3.2, red) because the polylactide was grown from lactic acid onto that diblock copolymer. The extra signals present at 5.17 ppm (multiplet, G) for the methine and the methyl at 1.59 and 1.57 ppm (doublet, H) were from the polylactide. Table 3.1 summarizes the degrees of polymerization for each block and molecular weights from ^{1}H NMR and GPC. The table compares the target of degree of polymerization with the observed value determined by ^{1}H NMR.

Table 3.1. Results for degrees of polymerization and molecular weights from ^{1}H NMR and GPC for MeO-EG_m-CL_n-OH and MeO-EG_m-CL_n-LA_p-OH copolymers.

Polymer Goal	Actual m[a]	Actual n[a]	Actual p[a]	M_n (g/mol)[a]	M_n (g/mol)[b]	M_w (g/mol)[b]
MeO-EG_{45}-CL_5-OH	44	4	n/a	2,424	3,872	4,280
MeO-EG_{45}-CL_{10}-OH	43	11	n/a	3,178	4,758	5,191
MeO-EG_{45}-CL_{20}-OH	43	20	n/a	4,204	4,555	5,952
MeO-EG_{45}-CL_{40}-OH	53	51	n/a	8,178	n/a	n/a
MeO-EG_{113}-CL_{20}-OH	111	17	n/a	6,854	7,383	10,353
MeO-EG_{113}-CL_{40}-OH	113	40	n/a	9,564	7,993	12,073
MeO-EG_{113}-CL_{100}-OH	113	107	n/a	17,202	n/a	n/a
MeO-EG_{113}-CL_{40}-LA_{50}-OH	109	48	43	13,393	13,026	18,753

[a] repeat units and M_n as determined by 360 MHz ^{1}H NMR, [b] M_n and M_w as determined by GPC

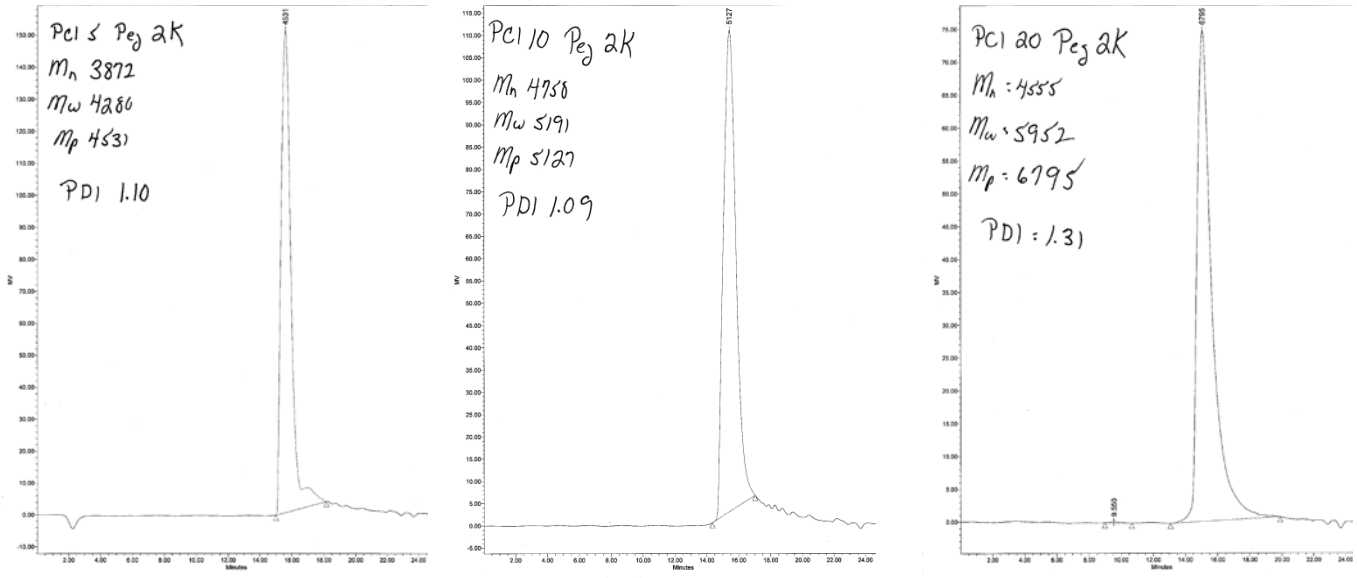

Figure 3.4. GPC traces for MeO-EG_{44}-CL_4-OH(left), MeO-EG_{43}-CL_{11}-OH(middle), and MeO-EG_{43}-CL_{20}-OH(right) copolymers done against a polystyrene standard.

Gel permeation chromatography (GPC) was performed on the copolymers to determine the number and weight average molecular weights. This was done using a 6.1 kDa polystyrene standard for reference. In Table 3.1, it is clear that there is not a lot of agreement between the NMR and GPC data. In GPC the polymer chains are separated by size. The size is determined by the hydrodynamic radius in solution. It is reasonable to assume that the polystyrene standard

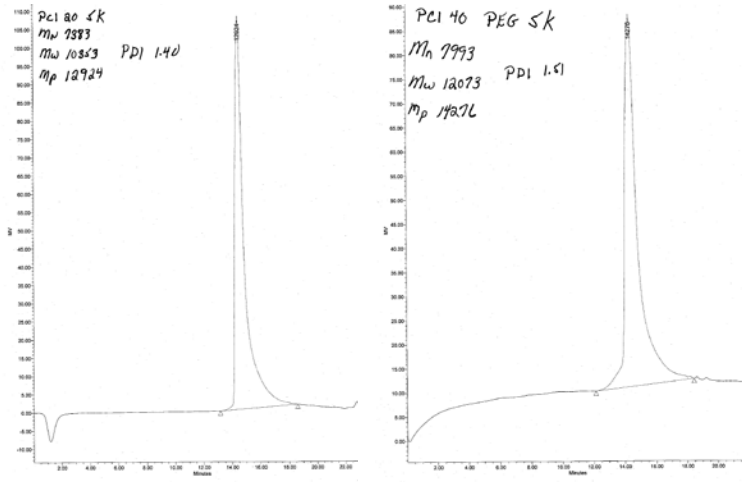

Figure 3.5. GPC traces of MeO-EG_{111}-CL_{17}-OH and MeO-EG_{113}-CL_{40}-OH against a polystyrene standard.

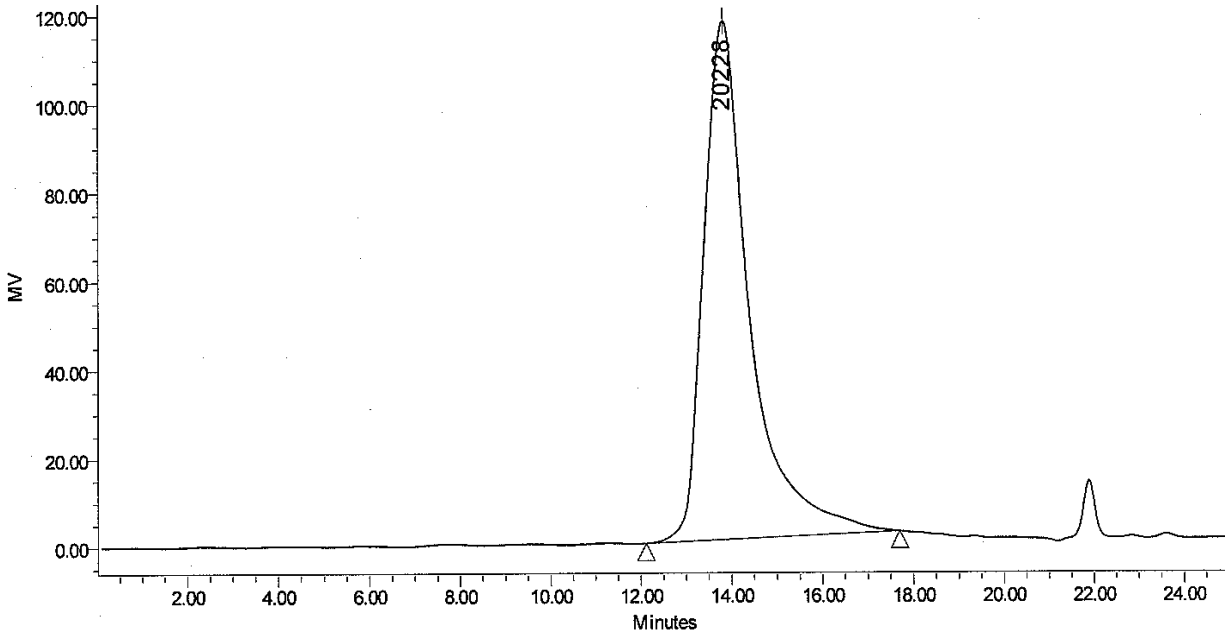

Figure 3.6. GPC trace for MeO-EG_{109}-CL_{48}-LA_{43}-OH done against a polystyrene standard.

was not a good standard for the diblocks. In THF the different polymers may have different degrees of solvation, which can affect the hydrodynamic radius. Accordingly the molecular weight determined by GPC for the diblock is not necessarily the true molecular weight, but a molecular weight relative to the polystyrene standard. To determine the molecular weight of the diblock properly we would need a PEG-PCL diblock standard with a well-defined molecular weight and a narrow polydispersity. Such standards were not available. In this work the molecular weight obtained by GPC were reported. However, the number average degree of polymerization (M_n) was used. The only one that closely resembles the initial M_n as determined by ^{1}H NMR was for the MeO-EG_m-CL_n-LA_p-OH polymer where M_n as determined by ^{1}H NMR was 13,393 g/mol compared to that of 13,026 g/mol from GPC.

3.2 Characterization of Micelles and Optimization of Micelle Procedures

3.2.1 Determination of Critical Micelle Concentration

The first order of business for each set of copolymer micelles was to determine the critical micelle concentration (CMC). The CMC is the concentration at which an amphiphilic material forms micelles. Solutions at varying concentration of copolymer and constant concentration of pyrene were prepared via Generation I or Generation IV, and the fluorescence intensity was measured at 390 nm for two excitation wavelengths (λ_{EX} = 333 nm or 338 nm). The CMC could be determined by plotting the ratio of emission intensity at 390 nm between the two excitation wavelengths (I_{338}/I_{333}) vs. the log of polymer concentration. The shape of the curve

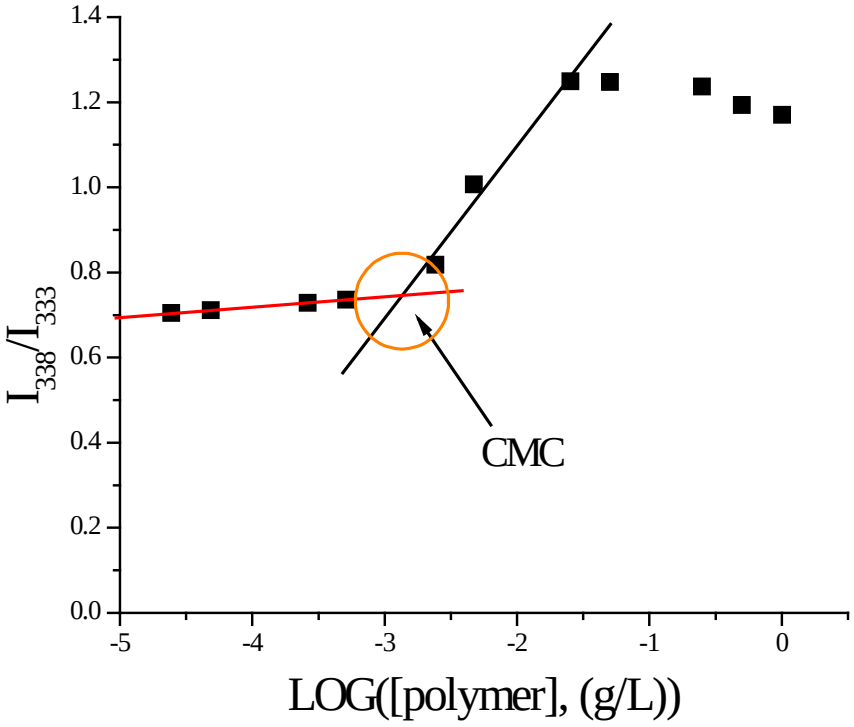

Figure 3.7. CMC curve for MeO-EG_{109}-CL_{48}-LA_{43}-OH as determined by plotting the pyrenene fluorescence intensity ratios at 390 nm of two excitation wavelengths (λ_{EX} = 333 nm/(λ_{EX} = 338 nm) vs. the log of polymer concentration. The CMC is at the intercept of the two lines.

Table 3.2. Critical Micelle Concentration (CMC) of six copolymers as determined by pyrene fluorescence. The CMC is reported at three temperatures, room temperature (27 °C), body temperature (37 °C), and above the melting point of the CL core (57 °C).

Polymer	f_{PHIL}	Gen.	CMC (mg/L, 25 °C)	CMC (mg/L, 37 °C)	CMC (mg/L, 57 °C)
MeO-EG_{44}-CL_4-OH	0.80	I	41	46	52
MeO-EG_{43}-CL_{11}-OH	0.60	I	3.9	8.1	10
MeO-EG_{43}-CL_{20}-OH	0.45	I	4.0	3.8	7.5
MeO-EG_{53}-CL_{51}-OH	0.29	I	2.9	1.9	4.9
MeO-EG_{113}-CL_{107}-OH	0.29	I	1.4	2.8	3.4
MeO-EG_{113}-CL_{50}-LA_{46}-OH	0.36	IV	2.1[a]	2.4[b]	4.7[c]

[a]As determined at 26 °C, [b]As determined at 38 °C, [c]As determined at 58 °C

(Figure 3.7) allowed for two fit lines to be obtained, one below the CMC where the intensity ratio is below 1 and one fit line as the CMC was approaching saturation with the ratio being between 1 and 1.3. Because pyrene is hydrophobic it will go into the core of the micelles. Once micelles are formed and the fluorescence intensity ratio was above 1.3 whereas when pyrene is in a hydrophilic environment, not in the core of the micelle, the ratio will be less than 1. The intersection of the two lines previously described is the CMC. The CMC curve for the MeO-EG_{109}-CL_{48}-LA_{43}-OH triblock copolymer is shown in Figure 3.7 with the CMC values for six of the described polymers tabulated in Table 3.2.1. The CMC at room temperature, at body temperature, and above the melting point of the micelles is described along with the ratio of hydrophilic character for each copolymer. The CMC decreased with decreasing hydrophilic

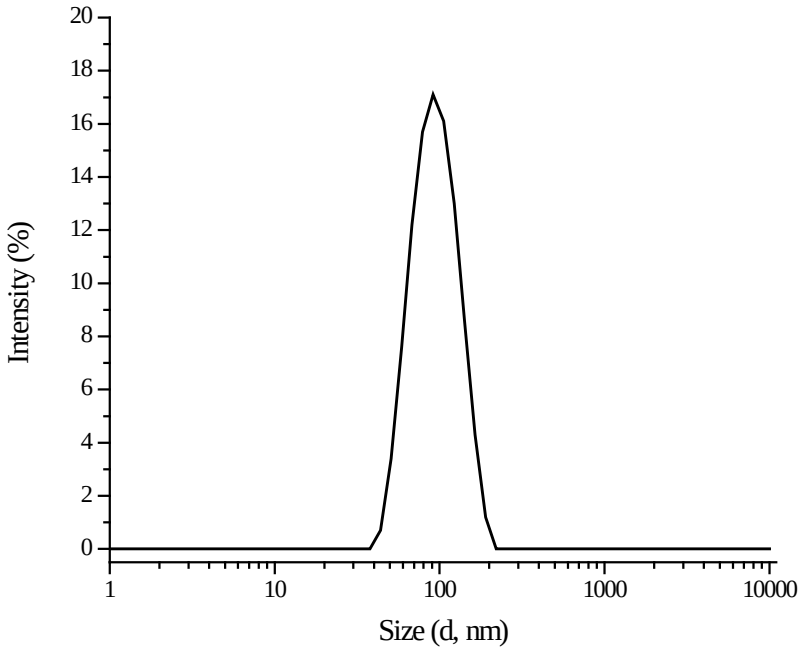

Figure 3.8. Intensity distribution DLS showing the size of the MeO-EG_{43}-CL_{20}-OH micelles made by Generation I method to be about 91 nm diameter.

character (f_{PHIL}) and increased with temperature. All of the copolymers that the CMC was determined for were prepared by Generation I except for the MeO-EG_{109}-CL_{48}-LA_{43}-OH because that copolymer could not be dissolved in water directly at a high concentration.

3.2.2 Optimization of Micellization Procedure

After completing CMC work it was necessary to begin understanding the phase behavior of both empty and loaded micelles. To do this a method had to be developed that would allow for micellization at concentrations two to ten times the CMC as well as allowing for the incorporation of hydrophobic components upon self-assembly. This was the main problem with generation I micelles; they would not allow for hydrophobic components to be introduced into the aqueous self-assembly media without precipitation or phase separation. Because many in the field were already using a selective solvent system, Generations II-V were developed.[1]

Generation II and Generation III micelles were born of the same principle: introduce a solvent, miscible with water that could be selective for hydrophobic blocks as well as hydrophobic components. This solvent also had to be volatile enough to leave the system on its own with simple evaporation. The solvent arrived upon was THF. One method to determine which micellization technique was working better was to run dynamic light scattering (DLS) on the micelle samples made by different generations and see how the sizes and distribution of sizes compared. The first sample run on DLS was of MeO-EG_{43}-CL_{20}-OH prepared by direct dissolution (Generation I). This showed micelles with a hydrodynamic diameter (D_h) of 91 nm according to the intensity distribution, seen in Figure 3.8.

When DLS was obtained for the same polymer micelles prepared by solvent evaporation method (Generation II), the D_h of the micelles was 250 nm by intensity distribution, but the same sample showed a D_h of 120 nm for number distribution results (Figure 3.9). Generation II was a slow evaporation technique where the container holding the micelles had a small opening, thus increasing the time it took to evaporate the THF.

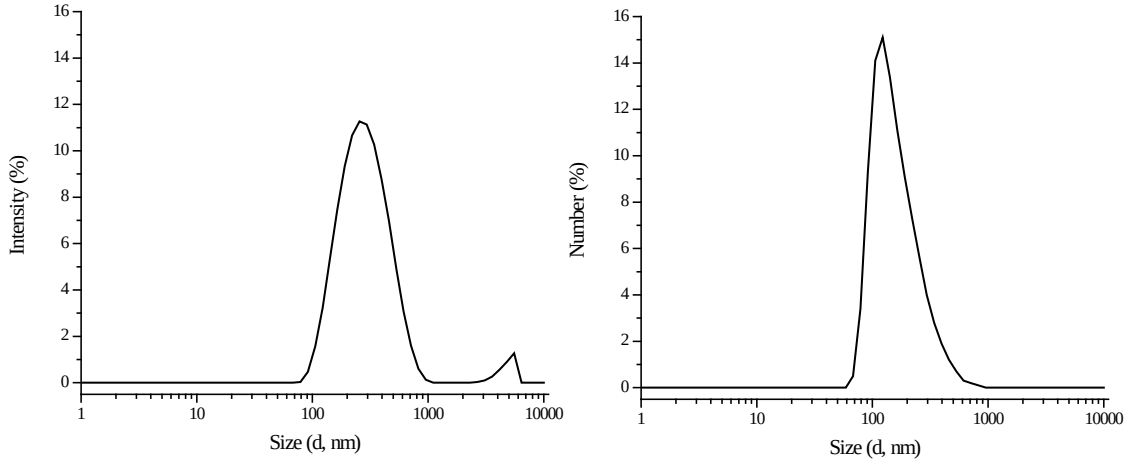

Figure 3.9. Intensity distribution (left) and number distribution (right) DLS for MeO-EG_{43}-CL_{20}-OH prepared by Generation II, solvent evaporation, showing 250 nm D_h or 120 nm D_h respectively.

In DLS the intensity distribution is a function of the cumulants fit of the correlation function obtained during the experiment. Because larger particles scatter more light the intensity distribution is often time skewed towards the larger particles in solution if the particles are not highly monodispersed. The number distribution from DLS is more of a true representation of the major species in solution; however it introduces more error into the measurement as it is derived from the intensity distribution results. When DLS was first performed intensity distribution was exclusively analyzed. Because intensity distribution is skewed more towards the larger particles

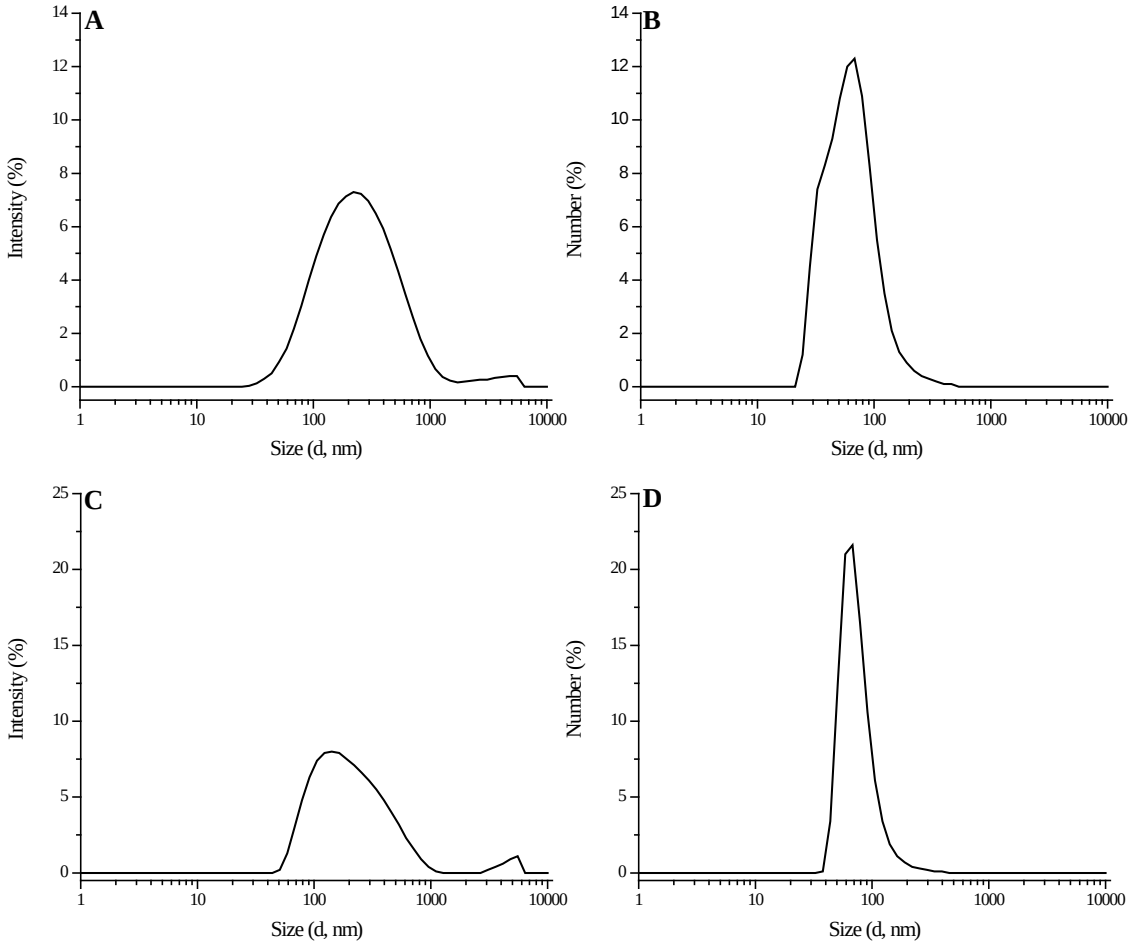

Figure 3.10. DLS for blank MeO-EG_{43}-CL_{20}-OH micelles (A and B) and magnetic MeO-EG_{43}-CL_{20}-OH micelles (C and D) where the intensity distribution showed a D_h of 250 nm for blank (A) and 160 nm for magnetic (C). The number distribution shows 68 nm for both blank (B) and magnetic (D) with the magnetic showing a lower polydispersity.

in solution, eventually both distributions were used to get a full picture of what the size distribution actually was. Regardless of the results from DLS it was imperative to move to a solvent/solvent system because of the need for a solvent selective to hydrophobic moieties.

Generation II and III were used to prepare micelles loaded with magnetic nanoparticles (NPs) as a proof of concept. This venture proved unsuccessful, mainly because it was unclear as to whether or not the nanoparticles were dispersing into the self-assembly matrix. This was because visible amounts of nanoparticles were sticking to the magnetic stir fleas used to mix the micelle solutions. Next, a combination of solvent evaporation and probe sonication was examined as a possible method for the best dispersion of the micelles with NPs. Again, blank micelles were prepared first using Generation IV methods based on literature procedures.[2] This yielded micelles that had a 250 nm D_h by intensity distribution and 68 nm D_h by number distribution, as shown in Figure 3.10. The intensity distribution showed little difference from the

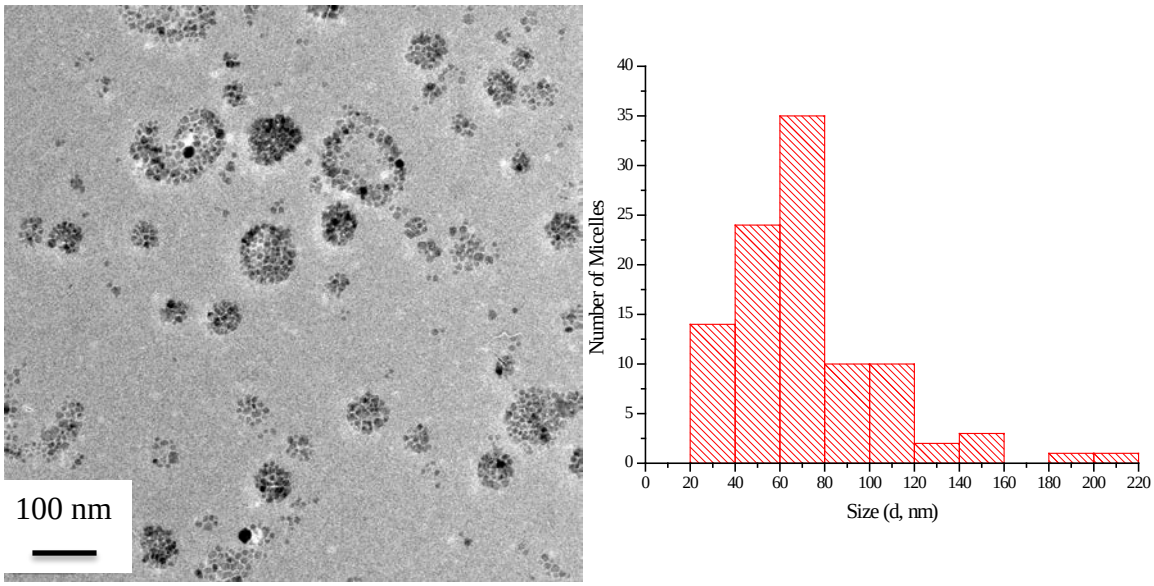

Figure 3.11. TEM image, with a 100 nm scale bar, of magnetic micelles where many MNPs were incorporated into each micelle's core (left) and histogram from ImageJ analysis showed the clusters at 70 ± 30 nm in diameter.

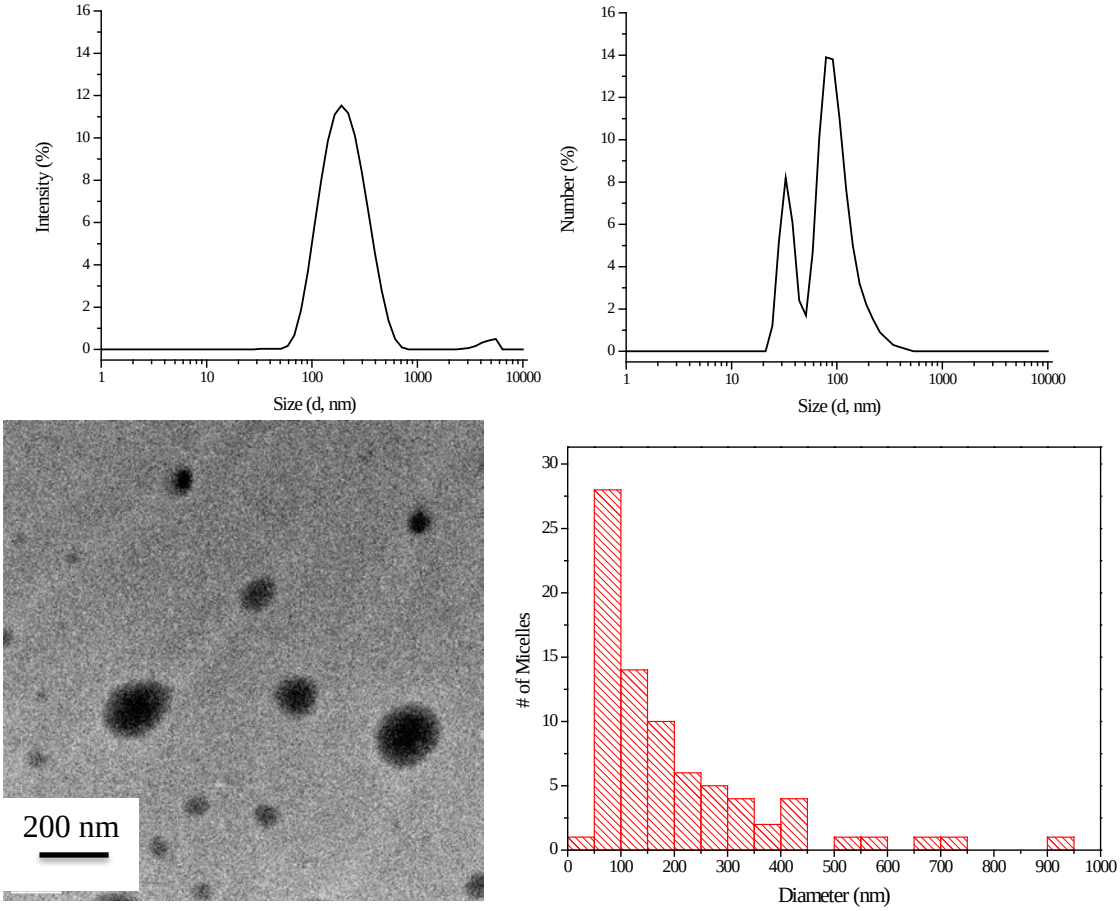

Figure 3.12. Intensity distribution (top left) and number distribution (top right) DLS along with TEM image (bottom left) and results from ImageJ analysis (bottom right) for blank MeO-EG_{44}-CL_4-OH micelles.

Generation II and III micelles; however, the number distribution indicated that there was a large population of sub-100 nm micelles in solution.

NPs (8 nm, 0.18 g/L) were loaded into MeO-EG_{43}-CL_{20}-OH micelles made by Generation IV to determine if this was indeed a viable alternate method for making micelles. DLS, Figure 3.10 C and D, showed that the intensity average was only skewed to 160 nm diameter and the number distribution showed micelles that were still 68 nm in diameter The polydispersity was lower for the micelles with MNPs incorporated than the blank micelles. This became true for most micelle sets, showing that MNPs incorporation actually helped the self-assembly of the micelles.

TEM images showed clusters of spherical nanoparticles, presumably in the core of the micelles, Figure 3.11 (left). NIH ImageJ was used to determine the diameter of the clusters of nanoparticles and the average diameter was similar to the hydrodynamic diameter determined by DLS. The average size of the clusters of particles was 70 ± 30 nm. This is shown by the histogram in Figure 3.11 (right). At this point Generation IV was determined to be the most efficient way to incorporate hydrophobic materials into the cores of the micelles.

3.2.3 Size Determination by DLS and TEM

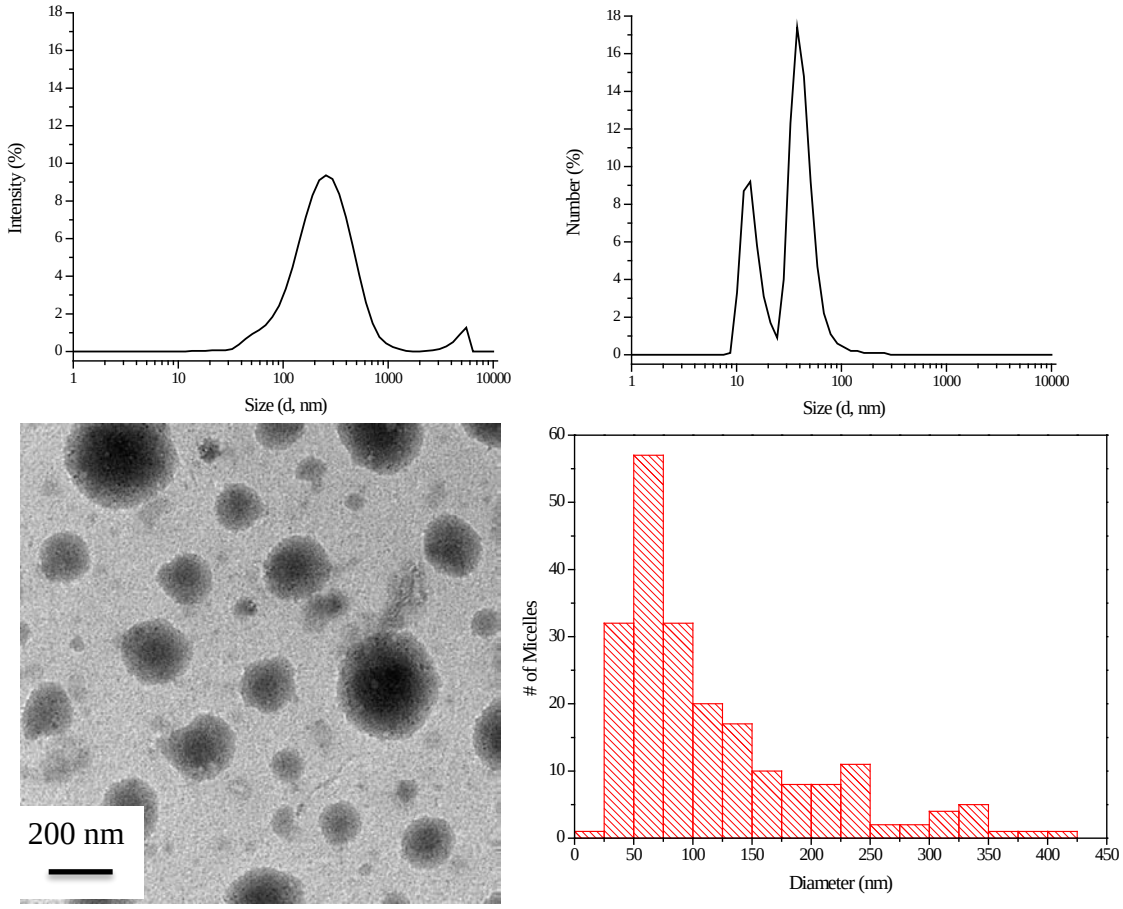

Figure 3.13. Intensity distribution (top left) and number distribution (top right) DLS along with TEM image (bottom left) and results from ImageJ analysis (bottom right) for MeO-EG_{43}-CL_{11}-OH.

Blank micelles were prepared for all of the copolymers by Generation IV methods. TEM samples for the micelles made with MeO-EG_{44}-CL_4-OH, MeO-EG_{43}-CL_{20}-OH, MeO-EG_{53}-CL_{51}-OH were prepared by dropping the micelles onto a 300 mesh Cu grid coated with carbon and stained with phosphomolybdic acid (0.2 %). For MeO-EG_{43}-CL_{11}-OH and MeO-EG_{108}-CL_{48}-LA_{43}-OH TEM samples were prepared on silicon monoxoide coated 300 mesh Cu grids and again stained with phosphomolybdic acid. The TEM images were processed using NIH ImageJ software to determine the area of the micelles which could be converted to diameters and histograms were made for each of the micelles.

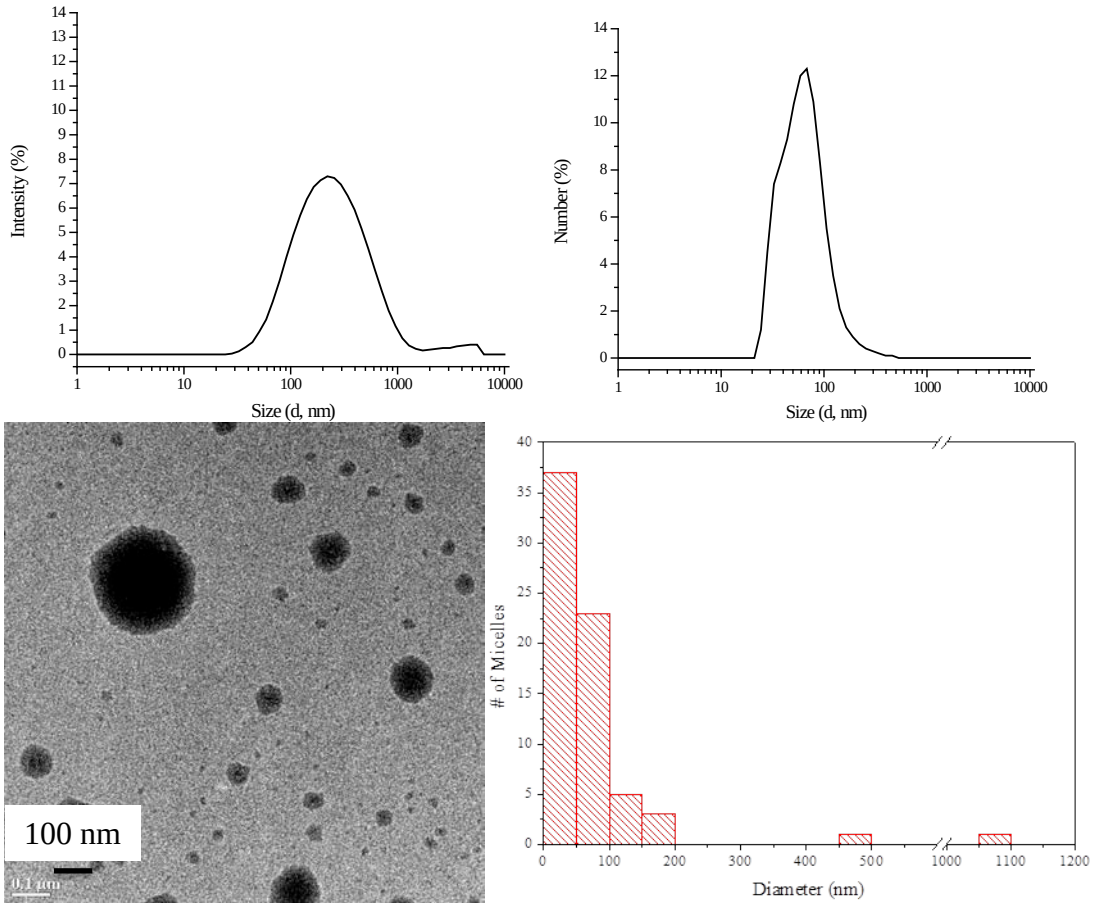

Figure 3.14. Blank MeO-EG_{43}-CL_{20}-OH micelles intensity and number distribution DLS (top left, top right) showing Dh of 70 nm and 220 nm respectively and TEM (bottom left) with a scale bar of 100 nm with histogram showing average diameter of 98 ± 270 nm (bottom right).

Figure 3.12 shows the intensity (top left) and number distribution (top right) results for the D_h of the MeO-EG_{44}-CL_4-OH micelles from DLS. The intensity distribution indicated that the hydrodynamic diameter of the micelles was 190 nm and the number distribution, which was bimodal, showed two D_h at 33 nm and 80 nm. TEM of blank micelles stained showed an average diameter of 190 ± 160 nm. The imaged micelles were generally spherical in size as seen in Figure 3.12 (bottom left). The large standard deviation can be attributed to a few outliers above 500 nm diameter as seen in the histogram (Figure 3.12 bottom right). Because micelles loaded with drug and nanoparticles were generally filtered through a 0.45 µm syringe filter these

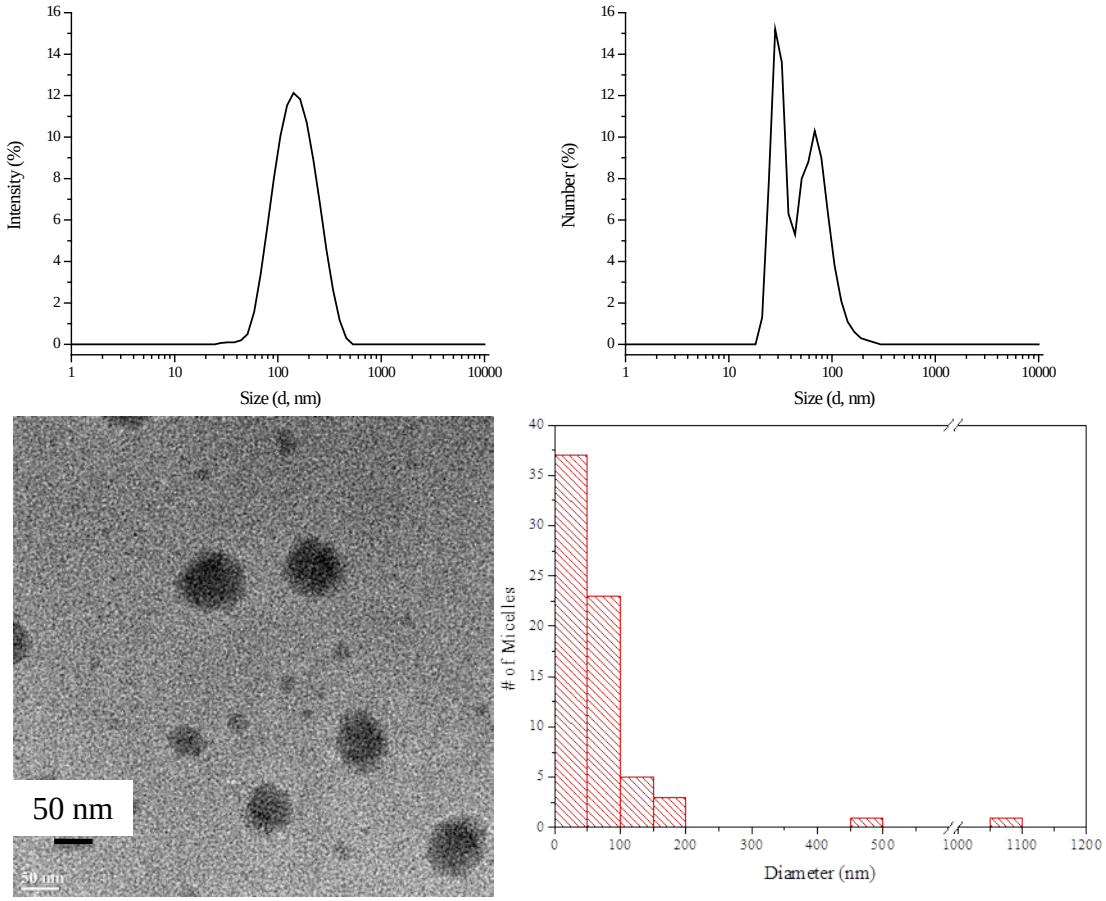

Figure 3.15. Blank MeO-EG_{53}-CL_{51}-OH micelles intensity and number distribution DLS (top left, top right) showing Dh of 30 nm and 70 nm and 140 nm respectively and TEM (bottom left) with a scale bar of 50 nm with histogram showing average diameter of 79 ± 140 nm (bottom right).

larger micelles would not be seen in the loaded micelle batches. Interestingly, 35% of the micelles were between 50 nm and 100 nm in diameter. This agrees with the number average results from DLS whereas the average diameter of the micelles, skewed to the higher numbers was more in line with the intensity average results.

A similar trend is true for the MeO-EG_{43}-CL_{11}-OH micelles, where the intensity distribution DLS (Figure 3.13, top left) showed much larger diameter micelles than the number distribution DLS results (figure 3.13 top right). The D_h for intensity distribution was 260 nm and the results from the number distribution were again bimodal and showed 14 nm and 38 nm diameter micelles. After analyzing 212 micelles using ImageJ, the TEM showed 56% of the micelles had a diameter between 25 nm and 100 nm but the average was still higher than that at 120 ± 80 nm. This time the results from TEM lay right between the results from the two different DLS methods.

The same analysis was performed for MeO-EG_{43}-CL_{20}-OH (Figure 3.14), MeO-EG_{53}-CL_{51}-OH (Figure 3.15), and MeO-EG_{107}-CL_{48}-LA_{43}-OH (Figure 3.16). Both MeO-EG_{43}-CL_{20}-OH and MeO-EG_{107}-CL_{48}-LA_{53}-OH showed a single peak in the number distribution DLS as well as the intensity distribution DLS. The two polymers made the same size micelles according to the number distribution at 70 nm (Figure 3.14 and Figure 3.16, top right). According to intensity distribution DLS the 220 nm diameter MeO-EG_{43}-CL_{20}-OH micelles were larger by almost 100 nm than both the MeO-EG_{53}-CL_{51}-OH and the MeO-EG_{107}-CL_{48}-LA_{53}-OH micelles which were 140 nm diameter (Figures 3.14, 3.15 and 3.16 top left).

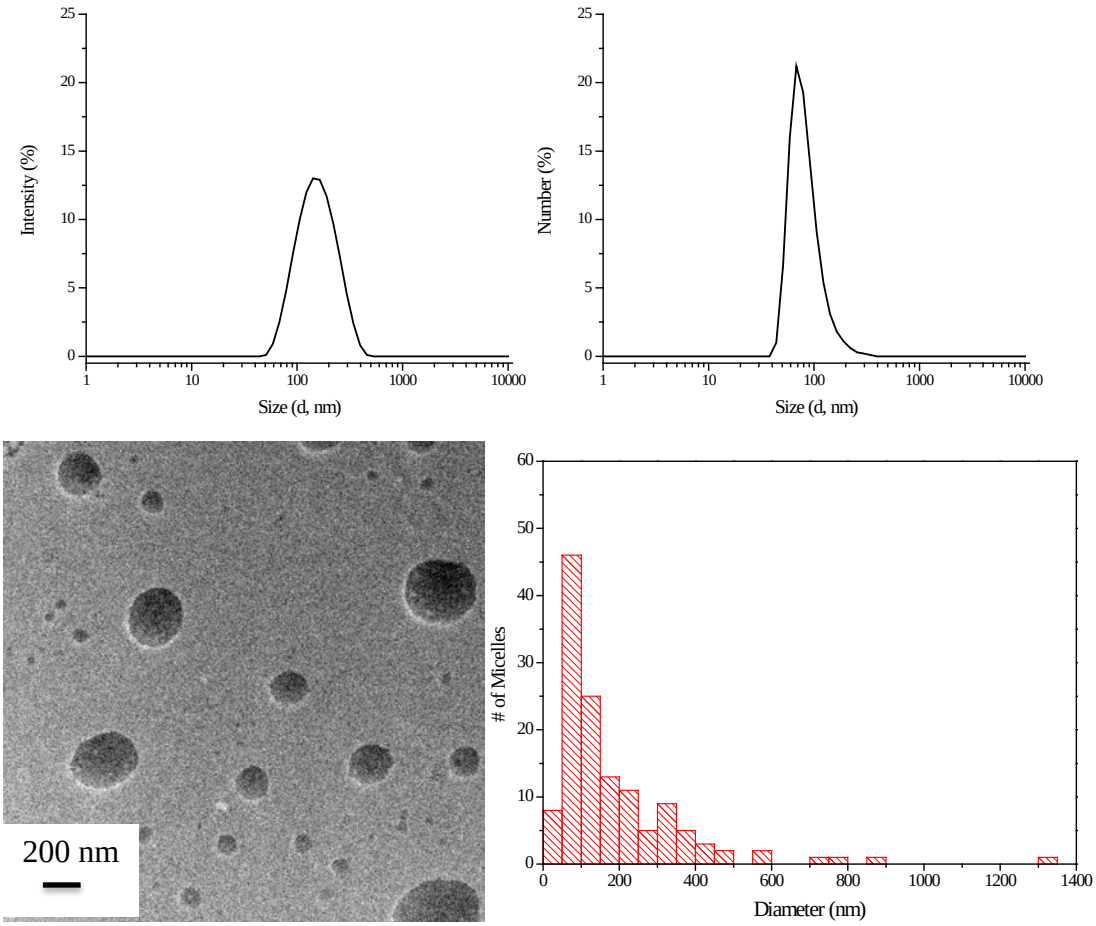

Figure 3.16. Blank MeO-EG_{107}-CL_{48}-LA_{43}-OH micelles intensity and number distribution DLS (top left, top right) showing D_h of 70 nm and 140 nm respectively and TEM (bottom left) with a scale bar of 200 nm with histogram showing average diameter of 190 ± 180 nm (bottom right)

TEM imaging gives statistics on a relatively small population where as DLS samples a vastly greater population. For the EG2000, CL20 and CL51 micelles, the TEM average diameter agrees well with the number distribution analysis from TEM (Figures 3.14 and 3.15, bottom right). However the histogram displays some micron sized artifacts which increase the standard deviation to larger than the average diameter of the micelles. This is true for every sample except the EG2000, CL10 micelles where no structures in the TEM are above half a micron in diameter (Figure 3.13). For MeO-EG_{107}-CL_{48}-LA_{43}-OH the TEM indicated that the micelles were on

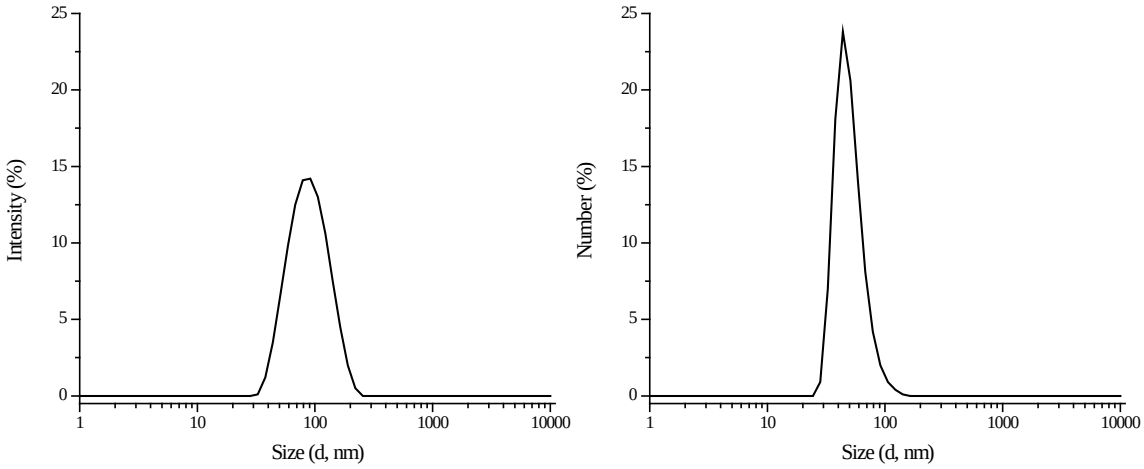

Figure 3.17. Intensity distribution (left) and number distribution(right) DLS of MeO-EG_{113}-CL_{107}-OH blank micelles showing a D_h of 91 nm and 44 nm respectively.

average larger than even the intensity distribution DLS indicated at 190 ± 180 nm (Figure 3.16 bottom right).

The TEM for MeO-EG_{113}-CL_{107}-OH proved difficult to obtain without drug inside of the micelles. DLS was performed on the blank micelles resulting in the most ideal micelles of all of the polymers because even without filtration all of the micelles were sub-100 nm. The DLS, Figure 3.17 shows 91 nm D_h micelles by intensity distribution (left), meaning that the larger species seen in the previous micelles were not present. The D_h by number distribution (Figure 3.17, right) was similar to the other blank polymeric micelles at 44 nm D_h.

3.2.4 Phase Behavior of Blank Micelles with Temperature

For all of the copolymers the CMC increased with temperature (Table 3.2 and Figure 3.18). When diblock polymers are placed in water at concentrations above the CMC there is an equilibrium between polymer chains aggregated into micelles and individual polymer chain freely dissolved in the aqueous phase. Entropy favors dissolution and it was expected that

increasing temperatures would shift the equilibrium toward dissolution. Indeed the CMC increased with increasing temperature.[3] For all of the micelles except MeO-EG_{44}-CL_4-OH micelles, the CMC when above the melting point of the core of the micelles is about double that of the CMC at room temperature. Knowing this it was important to perform future temperature

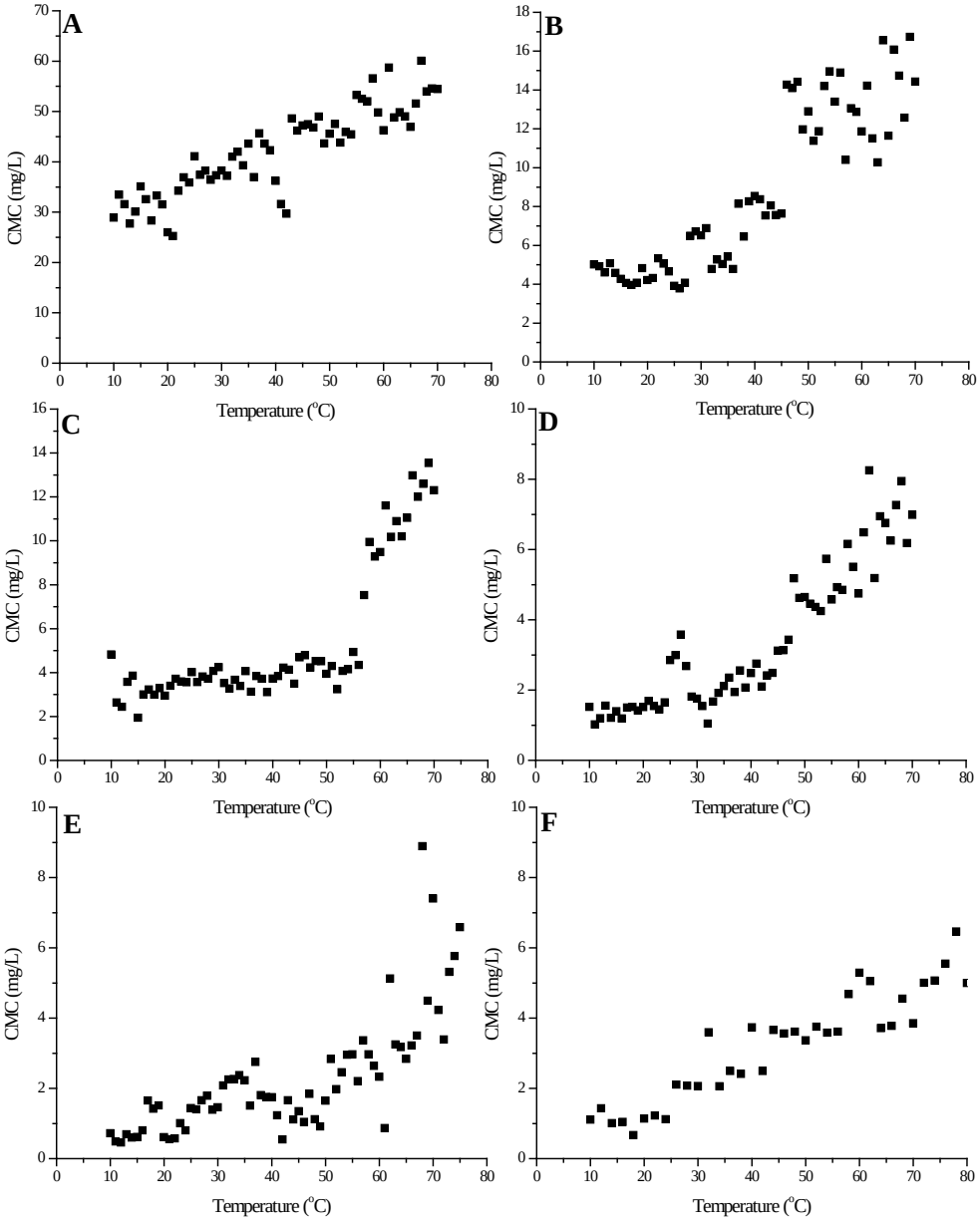

Figure 3.18. Temperature dependent CMC curves for MeO-EG_{44}-CL_4-OH (A), MeO-EG_{43}-CL_{11}-OH (B), MeO-EG_43-CL_{20}-OH (C), MeO-EG_{53}-CL_{51}-OH (D), MeO-EG_{113}-CL_{107}-OH (E), MeO-EG_{113}-CL_{48}-LA_{43}-OH (F).

dependent experiments, namely DSC and DLS, at a concentration at least twice the room temperature CMC. Typically experiments were performed at polymer concentrations of 1 g/L or 100 to 1,000 times the CMC.

The phase behavior of the blank polymer micelles was looked at by differential scanning microcalorimetry (DSC) and temperature dependence DLS. DSC was used to determine the melting point and the percent crystallinity for the polycaprolactone in the core of the micelles. Temperature dependent DLS gave insight as to what was happening to the size of the micelles

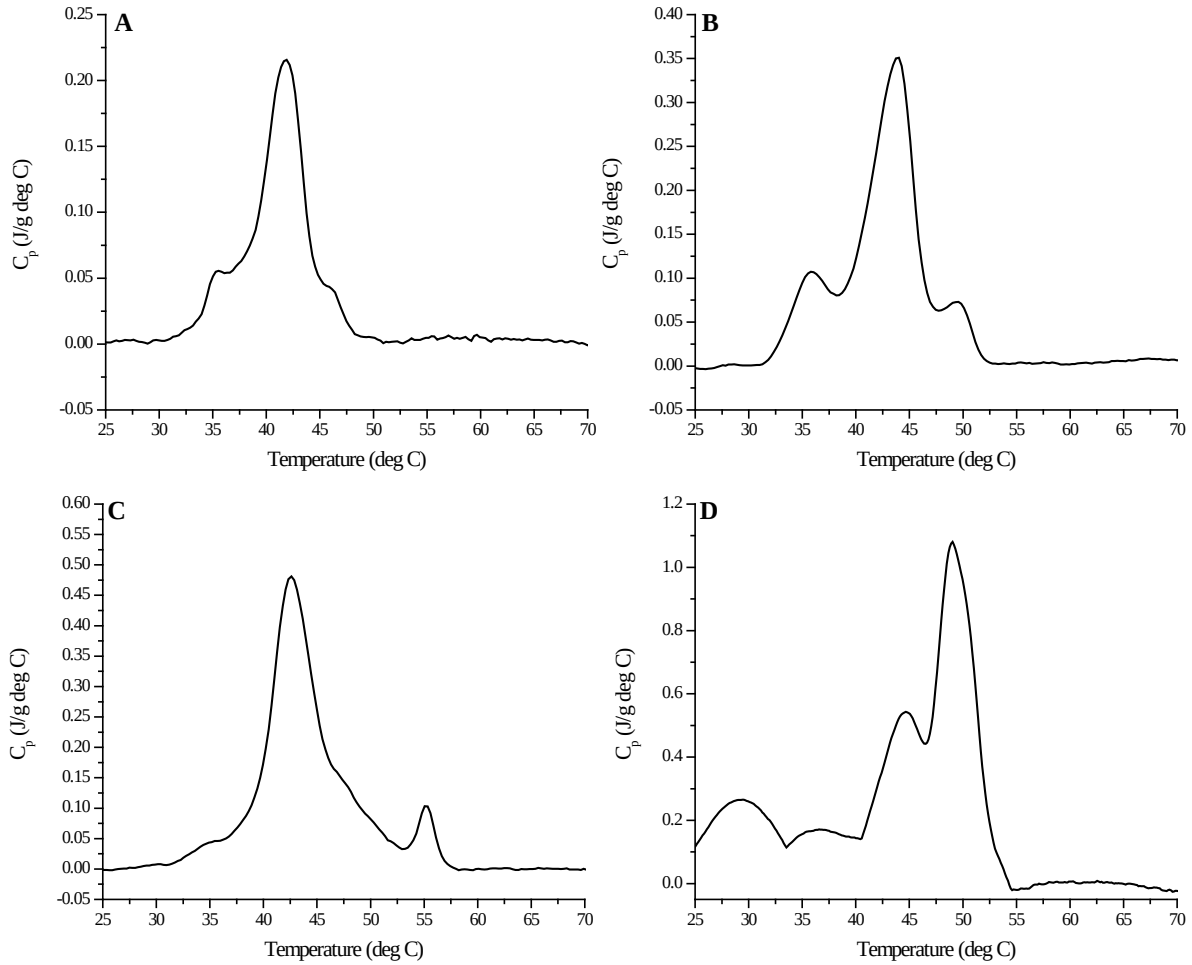

Figure 3.19. DSC endotherms for MeO-$EG_{44}CL_4$-OH (A), MeO-EG_{43}-CL_{11}-OH (B), MeO-EG_{43}-CL_{20}-OH (C) and MeO-EG_{53}-CL_{51}-OH (D).

with temperature increasing above the melting point of the cores of the micelles.

DSC was first performed on Generation III EG2000 micelles without anything loaded into the cores. The concentration was above the CMC for each of the sets of micelles. Figure 3.19 shows the DSC traces for all four of the polymer micelles. All traces were analyzed using MicroCal Origin VPDSC software. In general, the baseline was found for each of the micelle sets and then the area under the Heat Capacity vs. Temperature plot was found to 0, which gave the heat of fusion for the melting endotherms (ΔH). The height of the endothermic peak was taken to be the melting point for each of the traces.

Table 3.3 shows the results for each of the polymers for melting point (T_m), heat of fusion of micelles (ΔH_f), and the percent crystallinity (X_{CL}) for each set of Generation III micelles. The heat of fusion for bulk crystalline PCL (ΔH_{CL}) is 139.5 J/g.[4] This coupled with the information in table 3.3 for the observed heat of fusion of the micelles can be used with equation 3.1 to determine the percent crystallinity of the micelles.

Table 3.3. Generation III micelles solution phase DSC results including weight fraction of CL (ω_{CL}), melting points (T_m), heats of fusion (ΔH_f) and percent crystallinity (X_{CL}) for micelles.

Polymer	**ω_{CL}**	**T_m (°C)**	**ΔH_f *(J/g)***	**X_{CL} (%)**
MeO-EG_{44}-CL_4-OH	0.19	42	8.8	34
MeO-EG_{43}-CL_{11}-OH	0.40	44	13	23
MeO-EG_{43}-CL_{20}-OH	0.54	43	12	16
MeO-EG_{53}-CL_{51}-OH	0.71	49	9	9.6

$$X_{CL} = \frac{\Delta H_f}{\omega_{CL}\Delta H_{CL}} \times 100\% \qquad \textbf{Equation 3.1}$$

First, the area under the curve given in cal/mol was converted to J/g, this was taken to be ΔH_f, in equation 3.1. By dividing the ΔH_f by the heat of fusion of pure crystalline PCL (ΔH_{CL}) multiplied by the weight fraction of PCL in the sample (ω_{CL}) one can pull out the percent crystallinity of PCL in the sample of micelles from DSC. For the MeO-EG_{43}-CL_{20}-OH and MeO-EG_{53}-CL_{51}-OH copolymers multiple peaks were present; only the major peak is represented in the table. In general as the weight fraction of CL increased, the percent

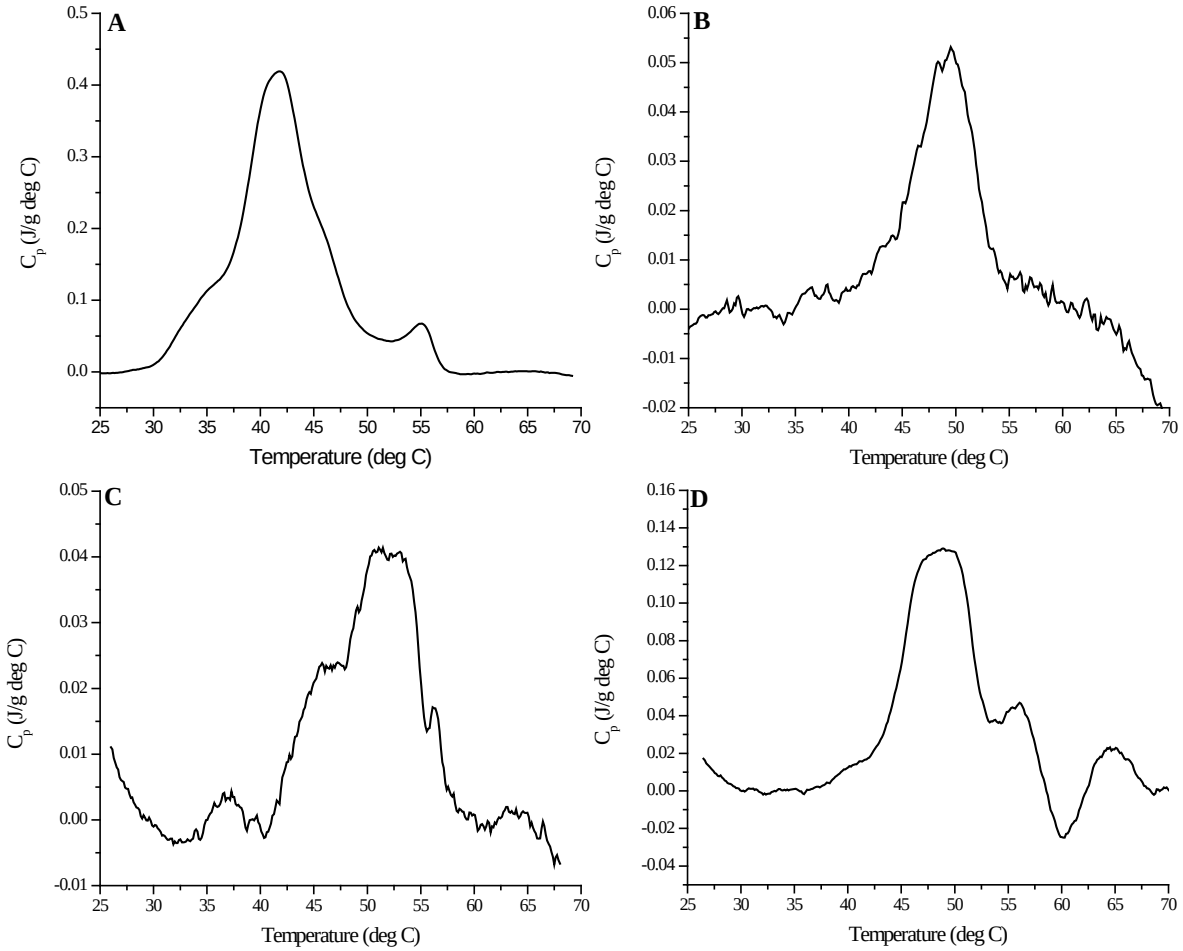

Figure 3.20. DSC melting endotherms for generation IV MeO-EG_{43}-CL_{20}-OH (A), MeO-EG_{111}-CL_{17}-OH (B), MeO-EG_{113}-CL_{107}-OH (C) and MeO-EG_{109}-CL_{48}-LA_{43}-OH (D) micelles.

crystallinity of the CL cores decreased. The melting point also increased, this is because it is known that melting point increases with CL length.[3]

Table 3.4. Generation IV micelles solution phase DSC results including weight fraction of CL (ω_{CL}), melting points (T_m), heats of fusion (ΔH_f) and percent crystallinity (X_{CL}) for micelles.

Polymer	**ω_{CL}**	**T_m (°C)**	**ΔH_f *(J/g)***	**X_{CL} (%)**
MeO-EG_{43}-CL_{20}-OH	0.54	42	13	17
MeO-EG_{111}-CL_{17}-OH	0.28	50	0.87	2.2
MeO-EG_{133}-CL_{107}-OH	0.71	51	0.27	0.3
MeO-EG_{109}-CL_{48}-LA_{43}-OH	0.41	49	1.2	2.1

The first DSC experiments were prepared by Generation III methods for EG2000 polymers. Later when Generation IV was determined to be the optimal preparation method, four polymers were prepared by Generation IV methods including MeO-EG_{43}-CL_{20}-OH (Figure 3.20 A). From that experiment it was shown that the two methods yielded similar crystallinity (Figure 3.19 C and 3.20 A). For Generation III MeO-EG_{43}-CL_{20}-OH micelles the percent crystallinity was shown to be 16 %, and for Generation IV it was 17 %. Because of this we could prepare micelles by Generation IV for EG5000 micelles including MeO-EG_{111}-CL_{17}-OH, MeO-EG_{113}-CL_{109}-OH and MeO-EG_{109}-CL_{48}-LA_{43}-OH copolymers. These copolymers were difficult to prepare using any other method because of their limited solubility in water and THF before self-assembly.

Unlike the EG2000 micelles (Figure 3.19 A—D and Figure 3.20 A), the micelles made from EG5000 copolymer (Figure 3.20 B—D) displayed much lower signal when melted. Also it was not possible to discern multiple peaks in the EG5000 micelles. One feature present in the MeO-EG_{109}-CL_{48}-LA_{43}-OH micelles not present in any other micelles was an apparent T_g which fell where pure LA would display a T_g (Figure 3.20 D). Additionally the heats of fusion and percent crystallinity of the micelles is much lower for the EG5000 micelles. Table 3.4 summarizes these results. MeO-EG_{113}-CL_{107}-OH showed the lowest percent crystallinity and heat of fusion at 0.3 % and 0.27 J/g respectively. This follows the trend from the EG2000 Generation III micelles in Table 3.3. Expected percent crystallinity should decrease with

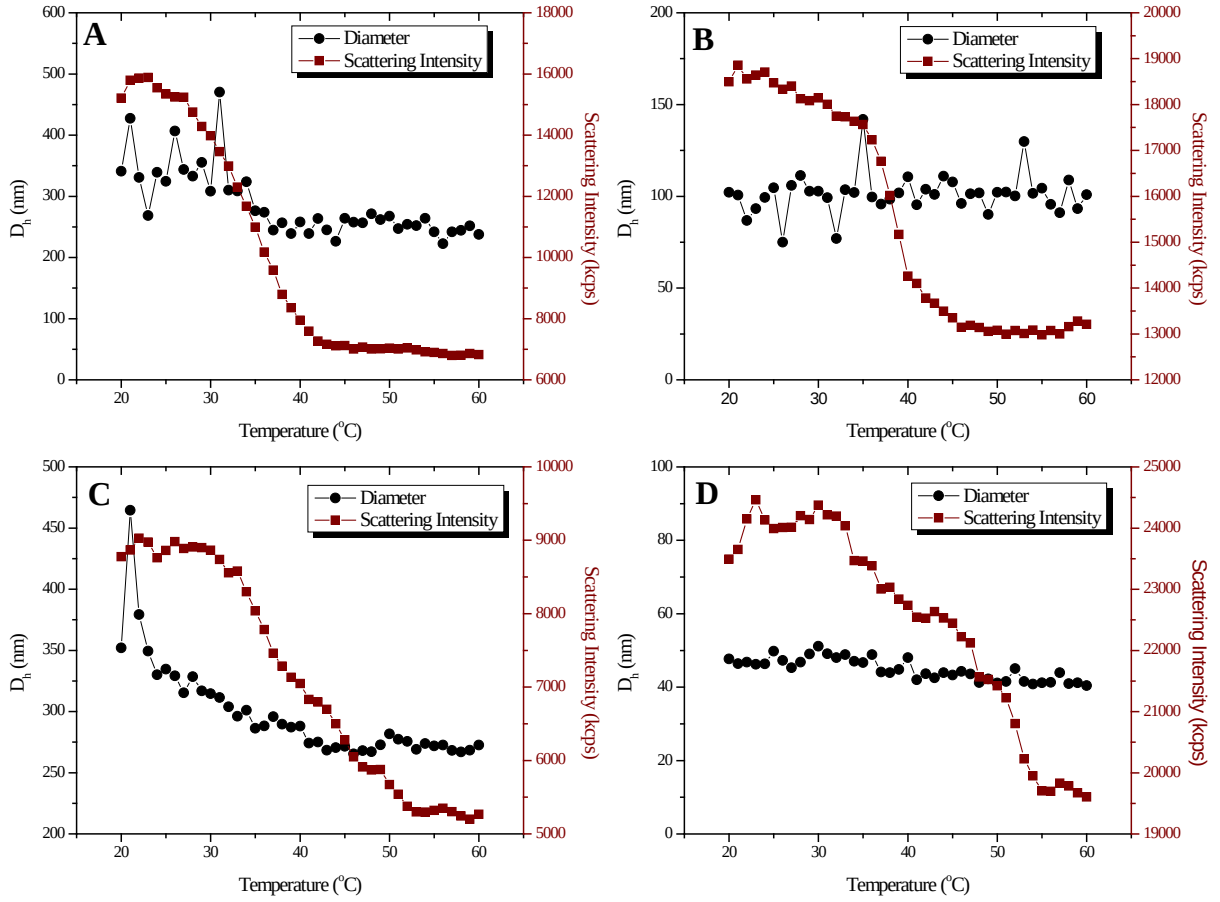

Figure 3.21. Temperature dependent DLS showing MeO-EG_{44}-CL_5-OH (A), MeO-EG_{43}-CL_{11}-OH (B), MeO-EG_{43}-CL_{20}-OH (C), and MeO-EG_{53}-CL_{51}-OH (D) scattering intensity decreasing across the melting ranges seen from DSC but size remaining constant.

increasing CL length. This was independent of the weight fraction of CL, demonstrated by the fact that MeO-EG_{53}-CL_{51}-OH micelles with a ω_{CL} equivalent to that of MeO-EG_{113}-CL_{107}-OH micelles had 30 times the crystallinity of MeO-EG_{113}-CL_{107}-OH micelles. Additionally, EG5000 versus EG2000 had a drastic effect on percent crystallinity, with a CL length of ~20 the top two polymers in table 3.3 should have similar crystallinities, but the heat of fusions are two order of magnitude lower for the EG5000 micelles making the crystallinity an order of magnitude lower than that of the EG2000.

From DSC it was determined that in order to make the crystallinity disrupted for the micelles the temperature of magnetic hyperthermia must locally reach above 45 to 55 °C depending on the copolymer. This is ideal because the ideal range for hyperthermia treatment in patients is ~45 °C.[5] Next, DLS was performed for the EG2000 copolymers to determine if the polymer micelles were breaking apart upon disrupting crystallinity. The original idea was that the micelles would burst apart upon heating and release their drug payload. The micelles were loaded into the DLS and heated from 10 °C to 60 °C at a degree per minute, and the sizes of the particles in solution were tracked by the DLS. It turned out that the size stayed relatively the same through heating although the scattering intensity did decrease. Crystallites would scatter more light than amorphous solid therefore the scatting intensity decrease made sense, Figure 3.21.

3.3 Conclusions

Polymer nanostructures made from the prepared diblock and triblock copolymers were found to be spherical with hydrodynamic diameters under 100 nm. These nanoparticles can therefore be defined as micelles. In order to incorporate hydrophobic drugs and nanoparticles in these micelles several methods, termed generations, were used to create the micelles. The final

method arrived at for the best core incorporation was Generation IV. Generation IV micelles were formed by using the selective solvent THF and probe sonication during self-assembly. Temperature dependent studies for the blank micelles showed that CMC was temperature dependent and increased with temperature. Additionally the cores of the micelles were semicrystalline with well-defined melting points. Micelles also remain intact upon heating above their melting points.

References

1. Shuai, X.; Ai, H.; Nasongkla, N.; Kim, S.; Gao, J., Micellar carriers based on block copolymers of poly(epsilon-caprolactone) and poly(ethylene glycol) for doxorubicin delivery. *Journal of Controlled Release : Official Journal of the Controlled Release Society* **2004,** *98* (3), 415-26.

2. Nasongkla, N.; Shuai, X.; Ai, H.; Weinberg, B. D.; Pink, J.; Boothman, D. A.; Gao, J., cRGD-Functionalized Polymer Micelles for Targeted Doxorubicin Delivery. *Angewandte Chemie International Edition* **2004,** *43* (46), 6323-6327.

3. Glover, A. L.; Nikles, S. M.; Nikles, J. A.; Brazel, C. S.; Nikles, D. E., Polymer Micelles with Crystalline Cores for Thermally Triggered Release. *Langmuir* **2012,** *28* (29), 10653-10660.

4. Masegosa, R. M.; Nava, D.; Prolongo, M. G.; Salom, C., Linear unsaturated polyester plus poly (epsilon-caprolactone) blends: Calorimetric behaviour and morphology. *Thermochim Acta* **2006,** *440* (1), 93-101.

5. Kuznetsov, A. A.; Leontiev, V. G.; Brukvin, V. A.; Vorozhtsov, G. N.; Kogan, B. Y.; Shlyakhtin, O. A.; Yunin, A. M.; Tsybin, O. I.; Kuznetsov, O. A., Local radiofrequency-induced hyperthermia using CuNi nanoparticles with therapeutically suitable Curie temperature. *J Magn Magn Mater* **2007,** *311* (1), 197-203.

CHAPTER 4

MICELLAR DRUG DELIVERY AND CELL TARGETING

Once it had been established that the prepared copolymers formed micelles that were crystalline and spherical, the next task was to put the pieces together with drugs to first mimic release at elevated temperatures. These experiments were performed in a shaker bath at several different temperatures isothermally. The isothermal drug release was performed first as single experiments with a surrogate drug, dibucaine, and then was run in triplicate with the dibucaine and finally doxorubicin. Dibucaine is used a local anesthetic or for horse and cattle euthanasia,

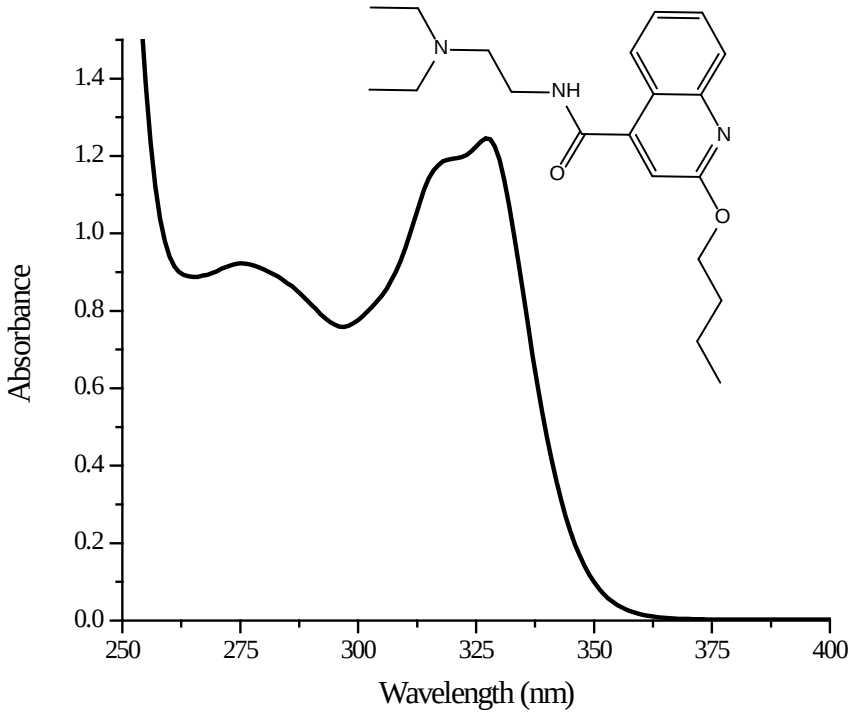

Figure 4.1. Absorption spectra and structure of dibucaine.

but worked well as a model drug because it is inexpensive and has limited water solubility. The electronic absorption spectra had a λ_{max} at 327 nm and a smaller peak at 317 nm, as shown in Figure 4.1. The anti-cancer drug doxorubicin, Figure 4.2, is used to treat many types of cancer and also has limited water solubility. Doxorubicin in highly colored and has a λ_{max} in its absorption spectra at 485 nm (Figure 4.2). Along with isothermal release, cell studies using the $\alpha_v\beta_3$ integrin targeting ligand, c-RGD*fk*. These were proof of concept experiments, to determine if a peptide that targets cells could be attached to the micelles and could that peptide indeed show enhanced micellar uptake. First, experiments were performed to ensure that the micelles were actually bound to the peptide using ^{1}H NMR. Then, HEK293 cell studies were performed to determine uptake of peptide labeled and non-labeled micelles. Finally, Jurkat cells were used to determine if the non-specific binding of micelles to cells could be reduced.

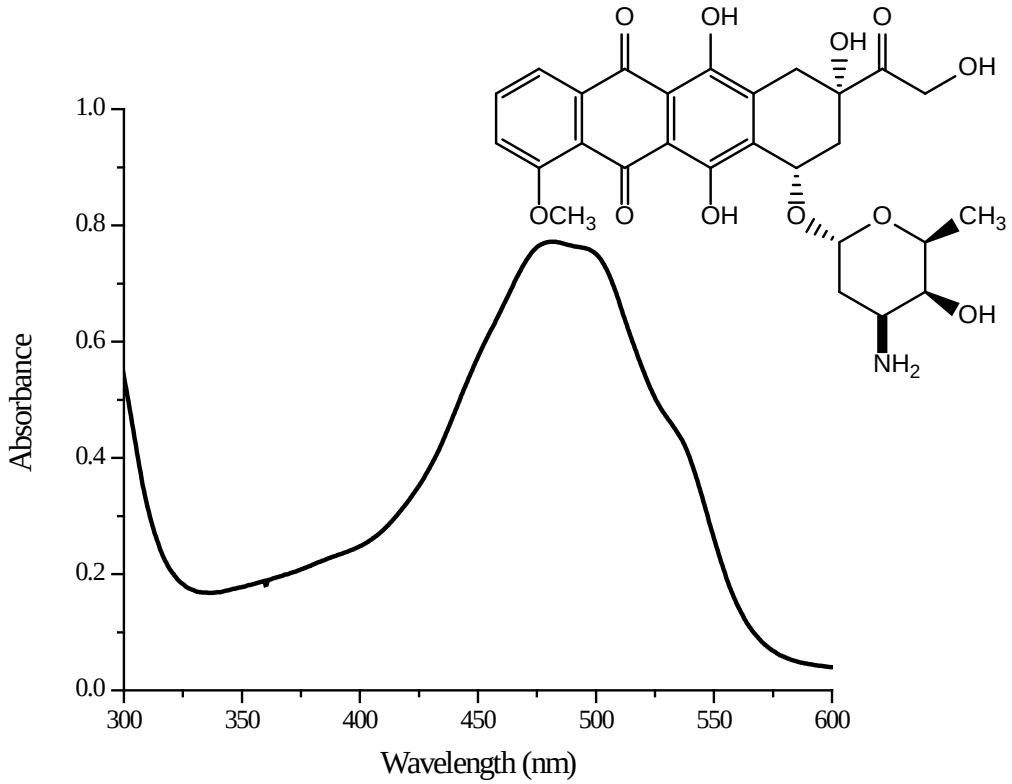

Figure 4.2. Absorption spectra and structure of doxorubicin.

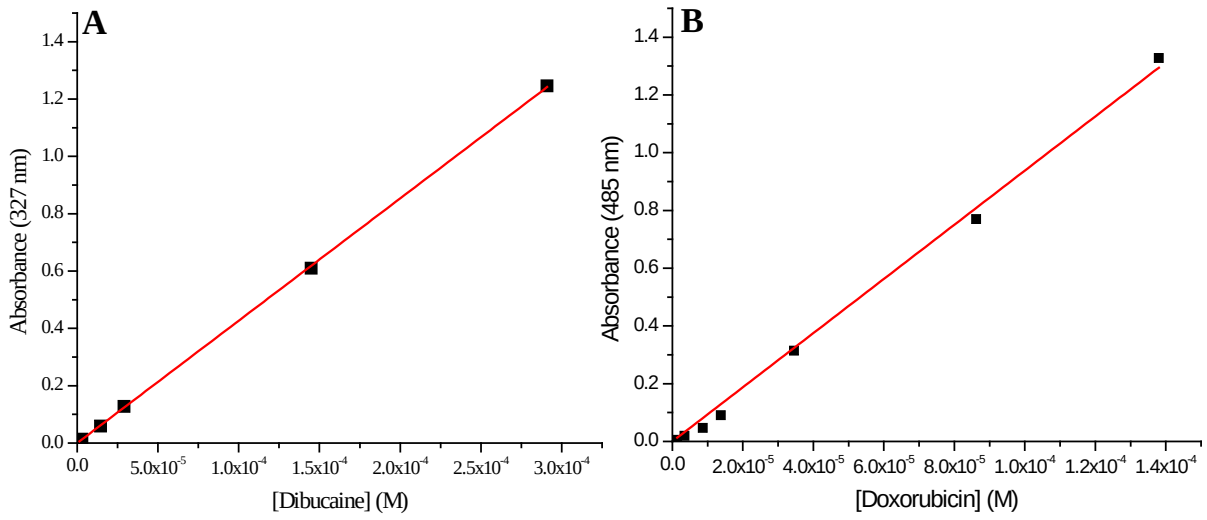

Figure 4.3. UV-Vis calibration curves for dibucaine (A) and doxorubicin (B).

4.1 Drug Loading Experiments

Drug loading experiments were performed in conjunction with drug release experiments. Calibration curves were created using UV-Vis spectroscopy for the both dibucaine at 327 nm (Figure 4.3 A) and doxorubicin at 485 nm (Figure 4.3 B). Plots of absorbance as a function of concentration were linear with a zero intercept. The slope gave values of the molar absorptivity for dibucaine (ε = 4268 $M^{-1}cm^{-1}$) and doxorubicin (ε = 9380 $M^{-1}cm^{-1}$). The R^2 values for the dibucaine and doxorubicin calibration curves were 0.9999 and 0.9989, respectively. These calibration curves were used to determine the drug loading for a given micelle set at a known volume and polymer content. Drug loading was then described in two ways, by total weight of the polymer or by total weight of the core of the micelles. Encapsulation efficiency is the amount of drug that made its way into the micelles after dialysis relative to the amount of drug initially loaded into the micelles.

4.1.1 Dibucaine Loading and Efficiency

Table 4.1 describes different drug loading for each copolymer using dibucaine and generation IV loading techniques. These data show that all of the parameters used to describe loading the copolymer MeO-EG_{111}-CL_{17}-OH and MeO-EG_{113}-CL_{107}-OH had the highest loading percentages with MeO-EG_{111}-CL_{17}-OH having more drug loaded per weight of the core than any other copolymer.

Table 4.1. Drug loading results for experiments using dibucaine as the surrogate drug using Generation IV loading techniques.

Polymer	Encapsulation Efficiency (%)	Loading (% by total weight)	Loading (% by core weight)
MeO-EG_{43}-CL_{11}-OH	15	6.9	21
MeO-EG_{43}-CL_{20}-OH	18	8.0	16
MeO-EG_{111}-CL_{17}-OH	25	11	48
MeO-EG_{113}-CL_{40}-OH	4.2	2.1	4.6
MeO-EG_{113}-CL_{107}-OH	28	12	20
MeO-EG_{109}-CL_{48}-LA_{43}-OH	15	6.8	11

As discussed in the previous chapter, one final method of loading was explored, self-assembly in water above the melting point of the micelles' cores (~90 °C). This method was used to explore if the kinetics of self-assembly had anything to do with the rate of crystallization. Table 4.2 describes the loading percentages and encapsulation efficiencies for polymer micelles self-assembled in hot water as the medium. Of all of the micelles tested this way Generation V micelles made from MeO-EG_{113}-CL_{117}-OH micelles had the best encapsulation efficiency and

drug loading of all of the polymer from either generation at 40 % of the drug loaded into the micelles being incorporated translating to 16 % loading by total weight and 28 % loading by only the core weight. For all core loading percentages, loading by core weight was over 15 % for every copolymer except the triblock copolymer. The micelles used for the dibucaine drug loading experiments were used to run isothermal drug release described in section 4.2.1 and 4.2.2.

Table 4.2. Drug loading results for experiments using dibucaine as the surrogate drug using Generation V loading techniques.

Polymer	Encapsulation Efficiency (%)	Loading (% by total weight)	Loading (% by core weight)
MeO-EG_{43}-CL_{11}-OH	12	5.5	17
MeO-EG_{43}-CL_{20}-OH	21	9.7	20
MeO-EG_{111}-CL_{17}-OH	16	7.5	31
MeO-EG_{113}-CL_{40}-OH	26	11	28
MeO-EG_{113}-CL_{107}-OH	40	16	28
MeO-EG_{109}-CL_{48}-LA_{43}-OH	12	5.5	8.9

4.1.2 Doxorubicin Loading and Efficiency

Table 4.3 describes the encapsulation efficiencies and loading percentages of generation IV polymer micelles loaded with doxorubicin. Contrary to the dibucaine results, the highest loading percentages for these copolymers are from the MeO-EG_{109}-CL_{48}-LA_{43}-OH micelles. This had higher drug loading than any other set of micelles, dibucaine or doxorubicin. Doxorubicin micelles made from MeO-EG_{113}-CL_{107}-OH micelles also showed high loading percentages and

encapsulation efficiency. However the doxorubicin micelles with a smaller PCL percentage, MeO-EG_{43}-CL_{11}-OH, showed very low loading and encapsulation efficiency.

Table 4.3. Drug loading results for experiments using doxorubicin as the surrogate drug using Generation IV loading techniques.

Polymer	Encapsulation Efficiency (%)	Loading (% by total weight)	Loading (% by core weight)
MeO-EG_{43}-CL_{11}-OH	6.2	2.0	5.9
MeO-EG_{113}-CL_{107}-OH	33	9.4	15
MeO-EG_{109}-CL_{48}-LA_{43}-OH	41	16.5	30

4.2 Drug Release from Polymer Micelles

Drug release was performed for polymer micelles using a shaker bath set to either ambient (27 °C), body (37 °C), hyperthermia (47 °C), or well above the core melting (57 °C) temperatures. Experiments were first run in singlet to determine the temperature profiles and then run in triplicate for the most promising polymer micelles.

4.2.1 Drug Release of Dibucaine from Polymer Micelles

Each of the copolymer micelles from drug loading experiments mentioned in tables 4.1.1 and 4.1.2 were used for single run drug release experiment for isothermal release. For these experiments, in general either close to ambient temperature (27 °C) or body temperature (37 °C) was used as controls to determine how the micelles behaved when drug should not be released from the cores. Elevated temperatures were used to mimic the environment inside the micelles during magnetic heating at either 47 °C or 57 °C. Dialysis membranes (50 kDa MWCO) were

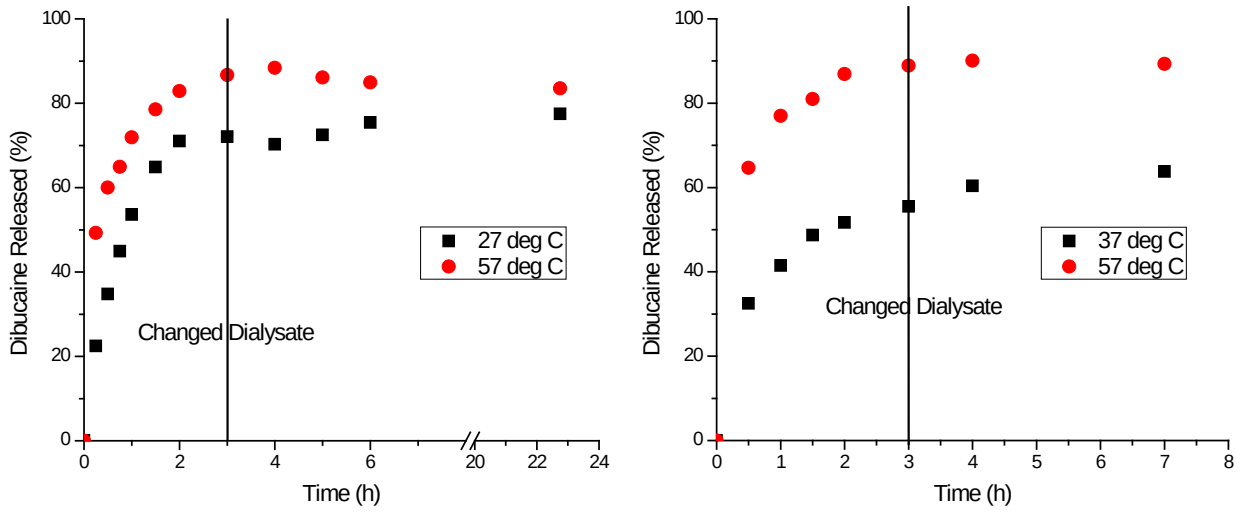

Figure 4.4. Isothermal drug release profiles from generation IV (left) and generation V (right) MeO-EG_{43}-CL_{11}-OH micelles loaded with dibucaine.

loaded with 2.00 mL of the micelle solution and put in jars with a 300 mL reservoir of ultrapure water. Dialysate was changed after 3 h to ensure the sink for the released drug was sufficient. At regular time intervals the micelle retentate were sample and replaced in the dialysis bags.

In Figure 4.4 a plot of the drug release profiles from the second smallest MeO-EG_{43}-CL_{11}-OH copolymer for Generation IV (left) and V (right) micelles. From Tables 4.1 and 4.2 there was not a lot of difference between the drug loading parameter between the two sets of micelles. The release profiles also looked similar at 57 °C with over 80 % of the payload being released in the first 2 hours. The difference between the two scenarios came with the fact that generation V releases less of its payload at 37 °C than Generation IV does at 27 °C with generation V micelles releasing only 45 % of its payload at 37 °C in the first 2 hours and IV micelles released 75 % of its payload in the first 2 hours of release. This indicated that somehow generation V micelles may have been less leaky than Generation IV micelles. To get a better handle on this phenomenon more experiments were run with higher PCL lengths.

Isothermal release was performed at 37 °C and 57 °C on MeO-EG_{43}-CL_{20}-OH Generation IV (Figure 4.5, left) and V (Figure 4.5 right) micelles next. For Generation IV micelles from MeO-EG_{43}-CL_{20}-OH micelles the drug release profiles at the two temperatures were very close to one another, so for Generation V micelles the leakiness of the cores was tested specifically. Once Generation V micelles were made from MeO-EG_{43}-CL_{20}-OH, the micelles were stored at 4 °C for one week before isothermal drug release was performed at 37 °C and 57 °C (Figure 4.5 right). From the drug release traces, the micelles released less of their payload overall, reaching a smaller maximal release percentage, M_∞, than the Generation IV micelles. Further, for the first hour of release, there was no difference in the amount of dibucaine released from the micelles indicative of free drug in solution. When there was a difference seen in the amounts of drug released it was less than 10% different indicating that the temperature difference of the medium may have been the only contribution to the diffusion coefficient differences between the release profiles rather than enhanced release from the polymer micelles.

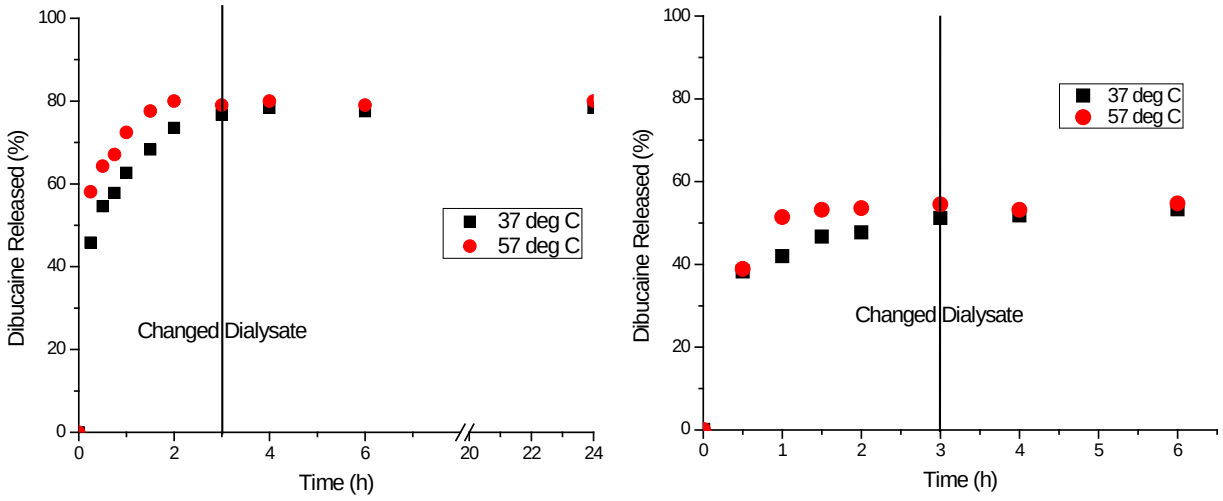

Figure 4.5. Drug release profiles from MeO-EG_{43}-CL_{20}-OH generation IV (left) and V (right) micelles loaded with dibucaine.

The PEG2000 micelles were leaky; therefore, the PEG5000 micelles were tested for isothermal release behavior next. For Generation IV micelles made from MeO-EG_{111}-CL_{17}-OH and MeO-EG_{113}-CL_{40}-OH (Figure 4.6 A and C) it was apparent that the micelles made from the higher molecular weight copolymer had a higher degree of separation between the low temperature and high temperature release profiles. When moving on to Generation V for the same micelles (Figure 4.6 B and D) up to about four hours the micelles behave relatively the

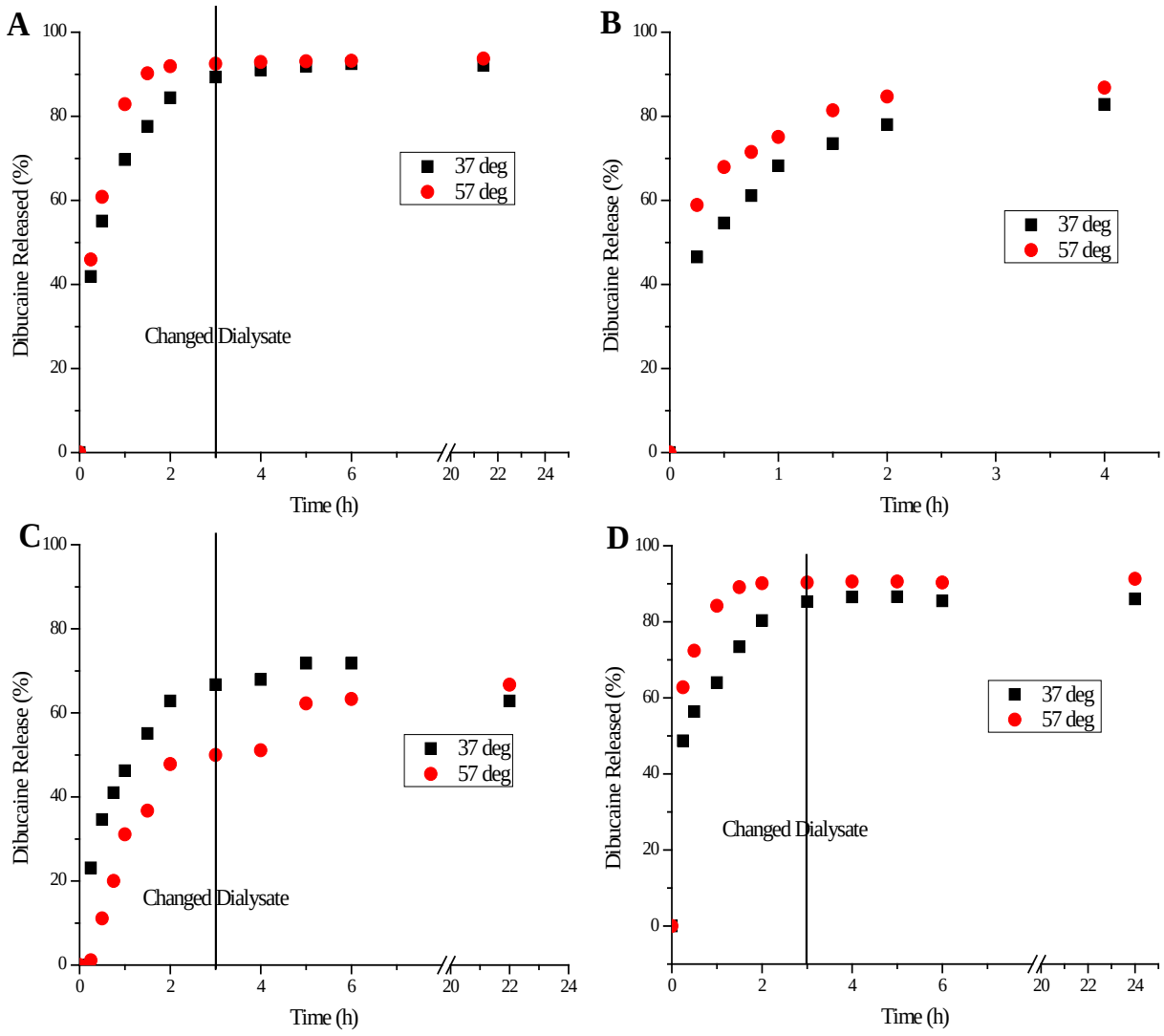

Figure 4.6. Isothermal dibucaine release from MeO-EG_{111}-CL_{17} generation IV (A) and V (B) micelles and MeO-EG_{113}-CL_{40}-OH Generation IV (C) and V (D) micelles.

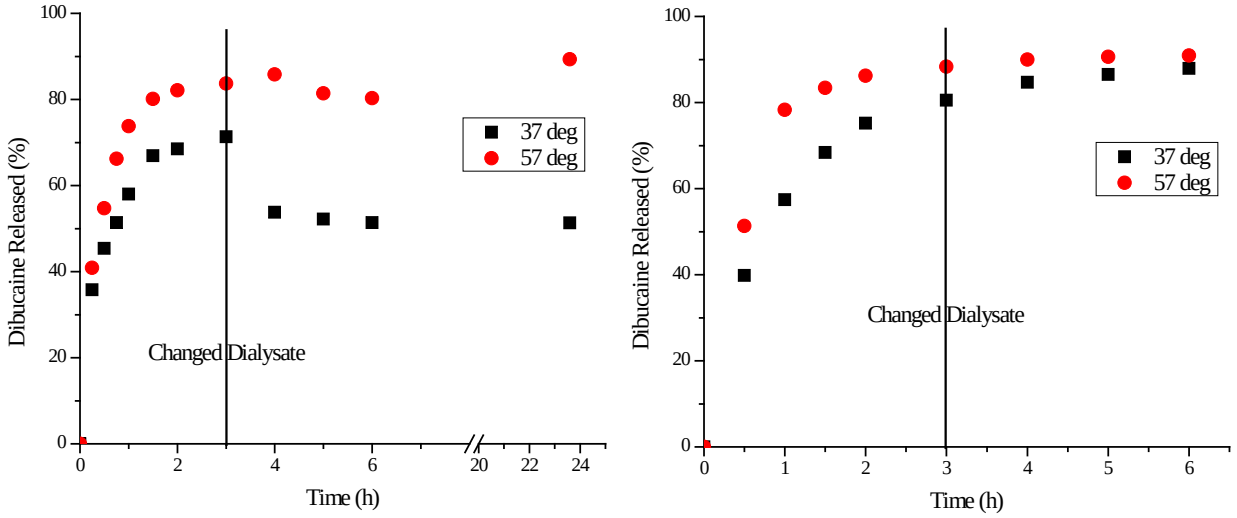

Figure 4.7. Isothermal drug release profiles from dibucaine loaded MeO-EG_{113}-CL_{107}-OH Generation IV (left) and V (right) micelles.

same with a small separation between the two release curves. On most all of the release profiles, after about three to four hours of release the profiles converge. This means that in patients the first several hours of treatment are critical to enhanced release and the possible synergistic effects of the chemotherapeutic and hyperthermia.

Figure 4.7 shows the dibucaine isothermal release profiles for Generation IV (left) and V (right) micelles made from MeO-EG_{113}-CL_{107}-OH micelles. Generation IV micelles shows a larger difference in release percentages at all times than generation V micelles did. After hour 4 for generation IV micelles one can see that some of the dibucaine in the dialysate must have returned to the interior of the dialysis membrane because release percentages decrease. For both sets of micelles the 57 °C isothermal release sample reaches about 80 % released by 3 hours into the experiment. Again a similar trend was seen that M_∞ was reached after 4 hours into the release and not much more was released into the dialysate from the micelles in the retentate. The result of decreased leakiness was promising and the next copolymer used was MeO-EG_{109}-CL_{48}-

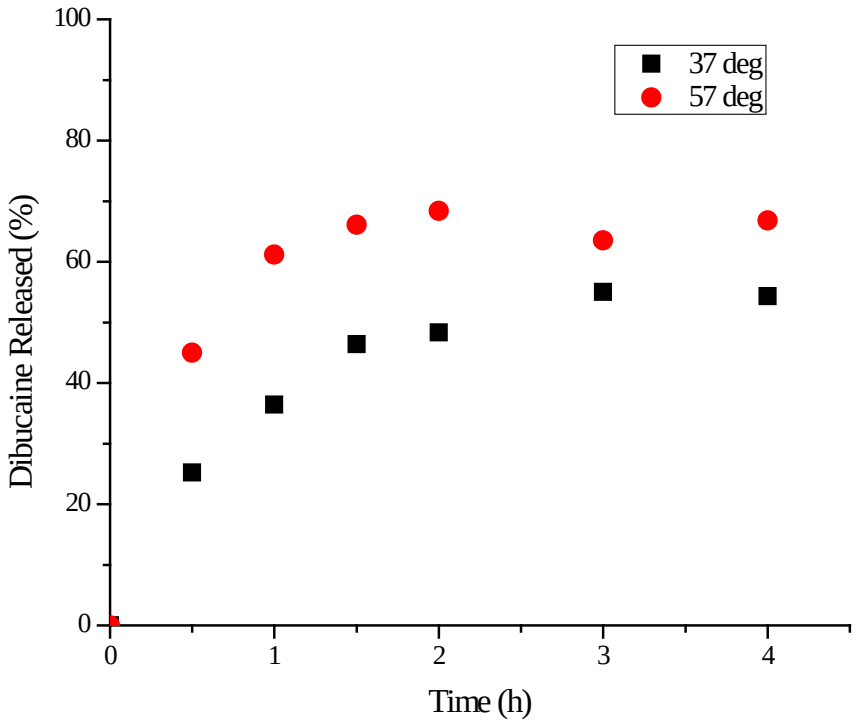

Figure 4.8. Isothermal drug release profile for dibucaine released from Generation V MeO-EG_{109}-CL_{48}-LA_{43}-OH micelles.

LA_{43}-OH. It was expected that the glassy PLA core of the micelle might help improve the leakiness at lower temperatures.

MeO-EG_{109}-CL_{48}-LA_{43}-OH dibucaine release was performed for generation V micelles (Figure 4.8). MeO-EG_{109}-CL_{48}-LA_{43}-OH did not show as rapid of a release, as did MeO-EG_{113}-CL_{107}-OH micelles, but it did show promise in solving the problem of leakiness from the micelles. This is because there was about 20 % difference in dibucaine released at 2 hours. For triplicate studies with dibucaine it was decided to use three copolymers: MeO-EG_{43}-CL_{20}-OH, MeO-EG_{113}-CL_{107}-OH, and MeO-EG_{109}-CL_{48}-LA_{43}-OH. There were several reasons for this decision including the fact that cell studies could be correlated to the copolymer micelles made from MeO-EG_{43}-CL_{20}-OH copolymer, the high M_∞ for MeO-EG_{113}-CL_{107}-OH and the large

difference in the percentage released from the micelles at body and elevated temperatures for MeO-EG_{109}-CL_{48}-LA_{43}-OH micelles.

4.2.2 Drug release of dibucaine from polymer micelles run in triplicate

Isothermal release was performed in triplicate for the aforementioned copolymers at four temperatures: 27 °C, 37 °C, 57 °C, and 67 °C. The two lower temperatures were chosen to determine the leakiness of the micelles at ambient and body temperatures. The two higher temperatures are higher than the range for hyperthermia but were chosen because the local temperature of the nanoparticles in the core should reach higher than the bulk temperature of

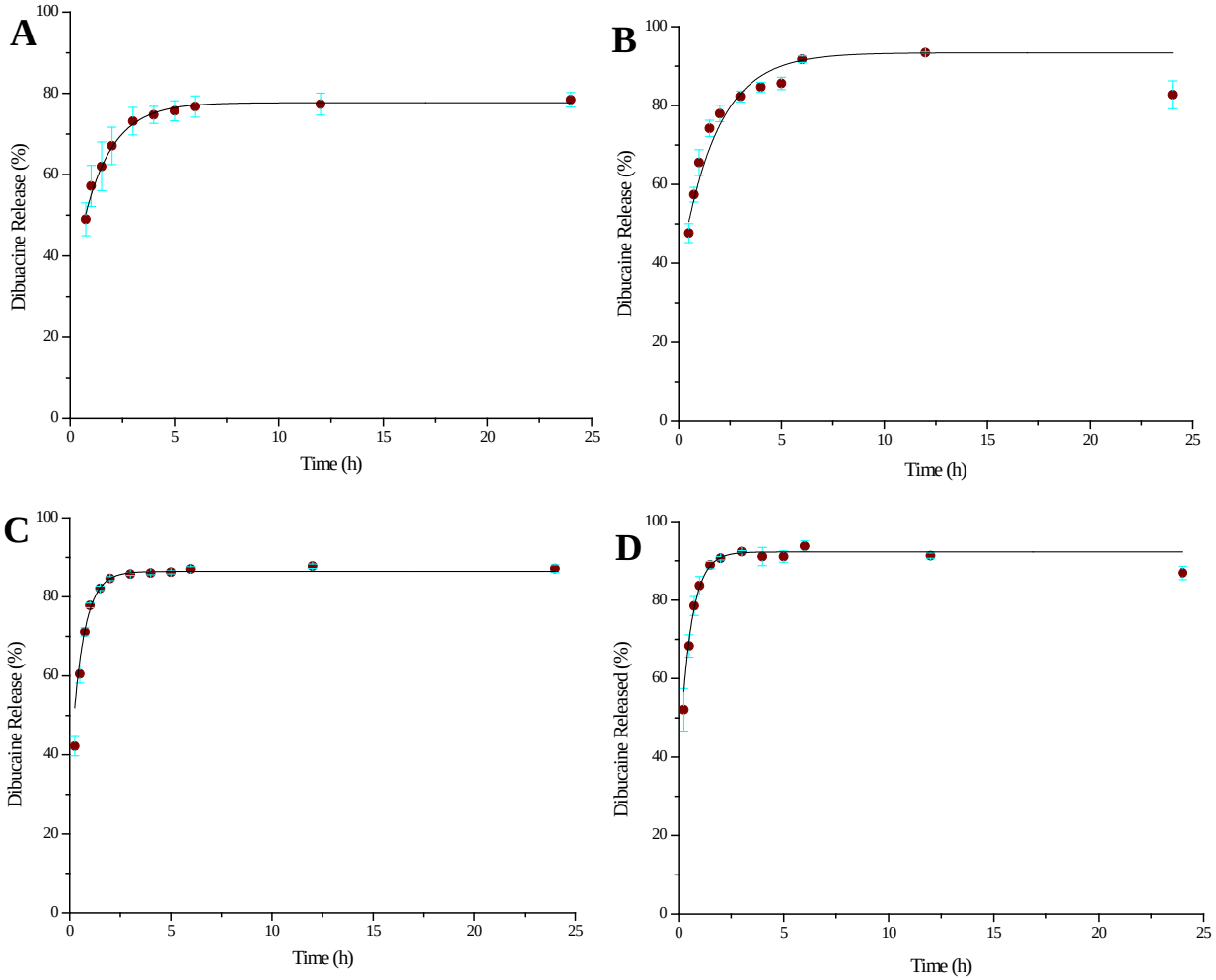

Figure 4.9. Isothermal release from MeO-EG_{43}-CL_{20}-OH dibucaine micelles at 27 °C (A), 37 °C (B), 57 °C (C) and 67 °C (D) fit to Crank's model for late diffusion from a polymer sphere.

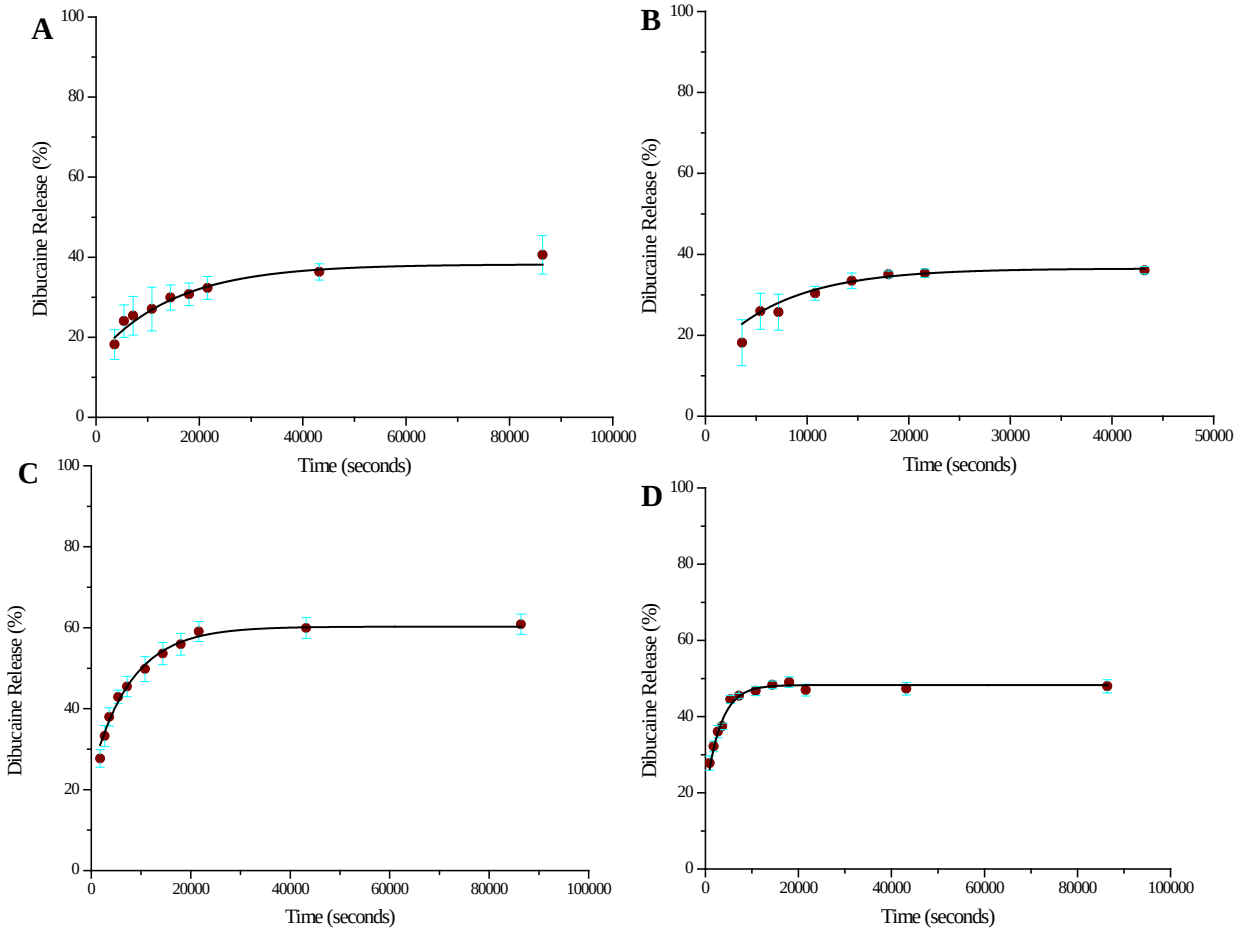

Figure 4.10. Isothermal release from MeO-EG$_{113}$-CL$_{107}$-OH dibucaine micelles at 27 °C (A), 37 °C (B), 57 °C (C), 67 °C (D) fit to Crank's model for late diffusion from a polymer sphere.

solution. The method was similar to the single run method where dialysis was performed at the isothermal temperature and samples were taken at various time points from the retentate. The percent release calculated (M_t) was a function of time and temperature.

The release profiles for dibucaine from polymer micelles done in triplicate were fit to Crank's Model of release of a small molecule from a spherical polymer for late diffusion (>40% released).[1] Equation 4.1 describes this model:

$$M_t = M_\infty \left(1 - \frac{6}{\pi^2} e^{\frac{-\pi D t}{r^2}}\right) \qquad \textbf{Equation 4.1}$$

In this equation D is the diffusion coefficient, r is the radius of the sphere (in this case a micelle), M_t is the release percentage at time (t) and M_∞ is the maximal release from the sphere at $t = \infty$. Figure 4.9 shows the release data from MeO-EG_{43}-CL_{20}-OH at 27 °C (A), 37 ° (B), 57 °C (C), and 67 °C (D) fit to Crank's model. The fits all had R^2 values above 0.9. At the first data point, or 15 min into the release, the release has already reached at least 40 % for each of the

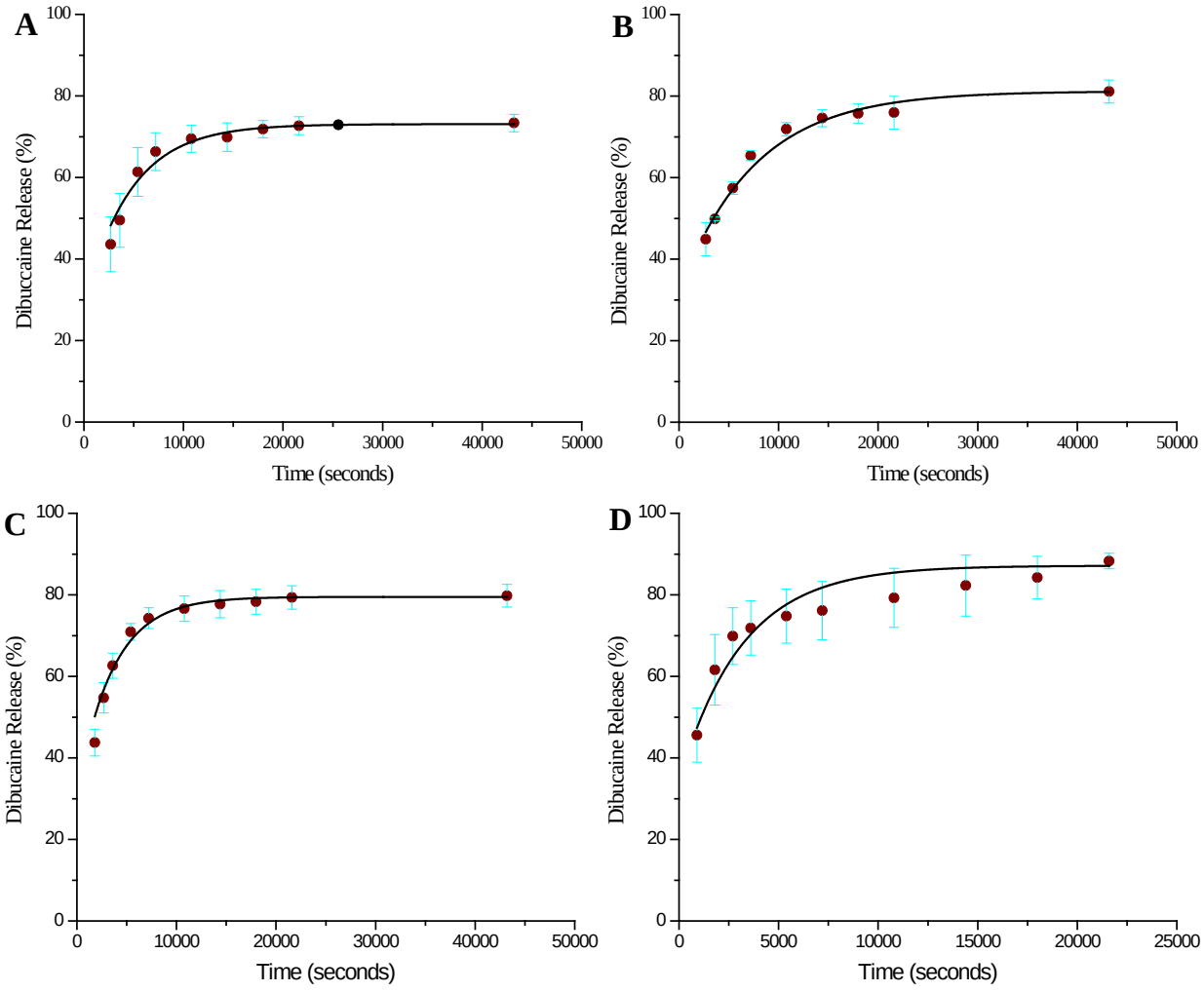

Figure 4.11. Isothermal release from MeO-EG_{109}-CL_{48}-LA_{43}-OH dibucaine micelles at 27 °C (A), 37 °C (B), 57 °C (C), 67 °C (D) fit to Crank's model for late diffusion from a polymer sphere.

Table 4.4. Values for infinite release (M_∞) and, the ratio of diffusion coefficient to radius squared and estimated diffusion coefficient for isothermal release from dibucaine loaded copolymer micelles.

Polymer	**T (°C)**	**M_∞ (%)**	**D/r^2 (s^{-1})**	**D (cm^2/s)***
MeO-EG_{43}-CL_{20}-OH	27	77.7 ± 0.4	2.1 ±0.1 x 10^{-5}	2 x 10^{-16}
	37	93.4 ±0.4	1.6 ±0.1 x 10^{-5}	2 x 10^{-16}
	57	86.4 ±0.3	4.7 ±0.2 x 10^{-5}	5 x 10^{-16}
	67	92.2 ±0.3	5.2 ±0.4 x 10^{-5}	5 x 10^{-16}
MeO-EG_{113}-CL_{107}-OH	27	38 ± 1	6.7 ±0.9 x 10^{-6}	2 x 10^{-17}
	37	37 ±1	1.4 ±0.1 x 10^{-5}	5 x 10^{-17}
	57	60 ± 1	1.3 ±0.1 x 10^{-5}	5 x 10^{-17}
	67	48 ± 1	3.2 ±0.2 x 10^{-5}	1 x 10^{-16}
MeO-EG_{109}-CL_{48}-LA_{43}-OH	27	73 ±1	2.0 ±0.2 x 10^{-5}	2 x 10^{-16}
	37	81 ± 1	1.4 ±0.2 x 10^{-5}	1 x 10^{-16}
	57	79 ± 1	2.8 ±0.3 x 10^{-5}	3 x 10^{-16}
	67	87 ± 1	3.2 ±0.4 x 10^{-5}	3 x 10^{-16}

*The radius of the hydrophobic core for the polymer micelles was estimated from the hydrodynamic diameter and radius of gyration for the PEG block; MeO-EG_{43}-CL_{20}-OH 32 nm (3.2 x 10^{-6} cm), MeO-EG_{113}-CL_{107}-OH 19 nm (1.9 x 10^{-6} cm), MeO-EG_{109}-CL_{48}-LA_{43}-OH 31nm (3.1 x 10^{-6} cm)

temperature trials meaning all of the release could be fit to Crank's model for late release. It took 5 hours for the 27 °C release to reach 75 % of the total payload released, where as it only took 30 min for the 67 °C isothermal release to reach 75 % M_t.

The PEG5000 micelles fit to Crank's model are shown in Figure 4.10 (MeO-EG_{113}-CL_{107}-OH) and Figure 4.11 (MeO-EG_{109}-CL_{48}-LA_{43}-OH). For 27 °C and 37 °C the M_∞ for MeO-EG_{113}-CL_{107}-OH didn't exceed 40 % released. M∞ values for MeO-EG_{113}-CL_{48}-LA_{43} values were much higher than for the CL107 polymer with all of the values exceeding 70 %. The data for M_∞, data for D/r^2 was obtained from the fits to Crank's model for late release. The diffusion coefficeints were then determined by subtracting the radius of gyration of PEG from the hydrodynamic radius obtained from DLS in Chapter 3. The radius of gyration of PEG was estimated using Equation 4.2.2.[2]

$$R_g = 0.0215 \cdot M_w{}^{0.583} \qquad \textbf{Equation 4.2}$$

The radius of gyration was calculated as 1.8 for PEG2000 and 3.1 for PEG5000. These results are tabulated for each copolymer in table 4.2.1. Diffusion coefficients for dibucaine were determined to be on the order of 10^{-17} cm/sec2 for the two polymers with higher M_∞ values (MeO-EG_{43}-CL_{20}-OH and MeO-EG_{109}-CL_{48}-LA_{43}-OH). MeO-EG_{113}-CL_{107}-OH had D values of 10^{-18}, meaning slower release rate, except for the 67 °C which was 10^{-17}. Sutton et. al. previously measured isothermal release of doxorubicin from PEG-PCL or PEG-PLA micelles at

37 °C and pH 7.4.[3] The PEG blocks were M_n ~ 5000 (n ~ 113) and the hydrophobic blocks were also M_n ~ 5000. For both polymers the fits to Crank's model gave identical values of D/r^2 at 2.5 x 10^{-7} s^{-1} for both polymers. After estimating the PEG corona to be twice the radius of gyration (6 nm) and was subtracted from the hydrodynamic radius. Their final diffusion coefficient was found to be 4.7 x 10^{-20} cm^2/s. This is two to three orders of magnitude slower than the diffusion coefficient found for dibucaine. From here, we set out to measure the isothermal release of doxorubicin from polymer micelles in triplicate.

4.2.3 Drug release of Doxorubicin from Polymer Micelles run in triplicate

Doxorubicin release run in triplicate was performed for MeO-EG_{113}-CL_{107}-OH and MeO-EG_{109}-CL_{48}-CL_{43}-OH micelles. Doxorubicin was converted to its hydrophobic form using triethylamine in situ during self-assembly preparation. For isothermal release at two temperatures, the procedure was modified slightly. This was because for the next chapter, isothermal release from magnetic micelles, it would be necessary to sample from the dialysate and determine the amount of doxorubicin released rather than the amount retained because the

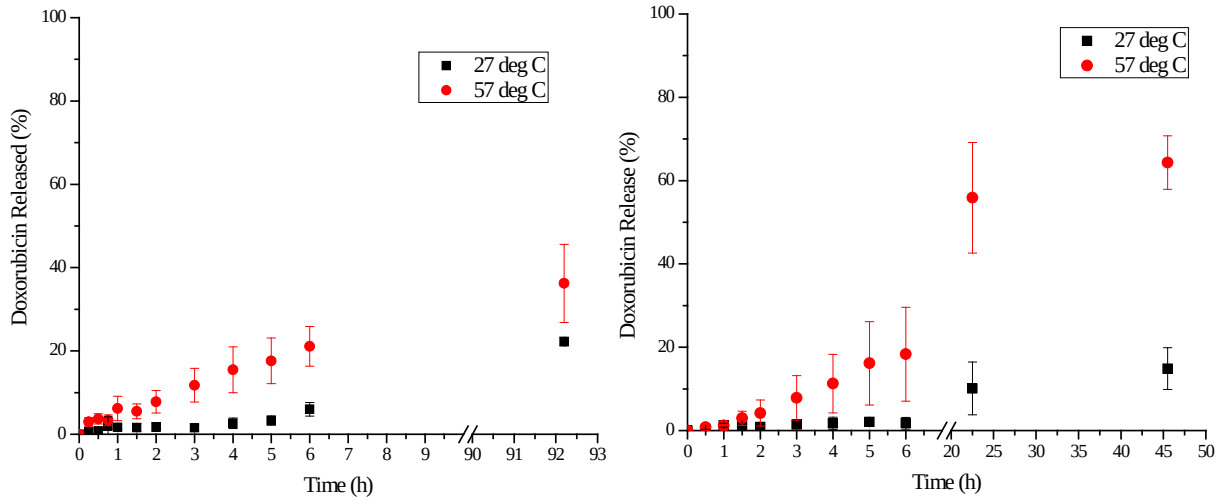

Figure 4.12. Doxorubicin release from MeO-EG_{113}-CL_{107}-OH (right) and MeO-EG_{109}-CL_{48}-LA_{43}-OH (left) micelles run in triplicate at 27 °C and 57 °C.

NPs incorporated into the cores would make the absorbance values increase for the retentate. The dialysate was sampled and fresh water was placed into the centrifuge tubes used as a reservoir for the release. Total doxorubicin released from the micelles was much lower than for the dibucaine micelles. For MeO-EG_{113}-CL_{107}-OH micelles total doxorubicin released in 94 hours was only about 30 % at both 27 °C and 57 °C (Figure 4.12, left). After 6 hours the total amount released was less than 10 % for 27 °C and about 20 % for 57 °C. Results were similar for MeO-EG_{109}-CL_{48}-LA_{43}-OH micelles where in 6 h only about 20 % was release from the 57 °C samples and less than 5 % was released from the room temperature samples (Figure 4.12, right). This was promising, even if not a lot of drug was released, the micelles had a larger difference in release from the 57 °C samples as compared to 27 °C.

4.3 Targeting Cells with c-RGD*fk* peptide

Triggered release has to be accompanied with targeting of the release device to the disease site. This was done by using the cyclic peptide cRGD*fk* with a thioacetyl group for convenient attachment to a moiety on the micelles, c[RGD*fk* (Ac-SCH_2CO)] (Figure 4.13).[4] This

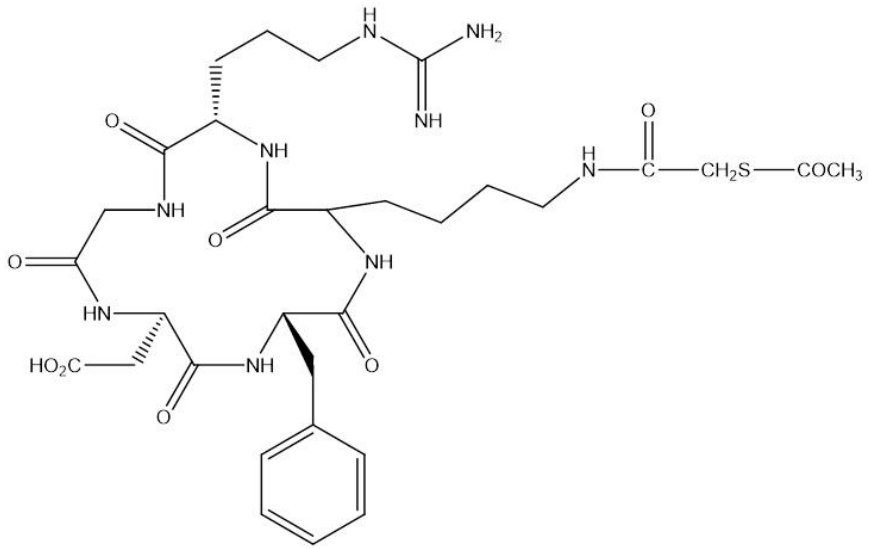

Figure 4.13. Cell targeting ligand c[RGD*fk* ($AcSCH_2CO$)].

cyclic peptide is used to target $\alpha_v\beta_3$ integrin receptors on cells. Because these control growth of cells they are overexpressed in cancer cells. The peptide used had a protected sulfide group on the end of it c[RGDfk ($AcSCH_2CO$)] which could be modified. First, PCL was grown off PEG monomaleimide (MAL-PEG-OH). This polymer was then added to the desired copolymer during self-assembly yielding micelles that were decorated with maleimide groups. Once

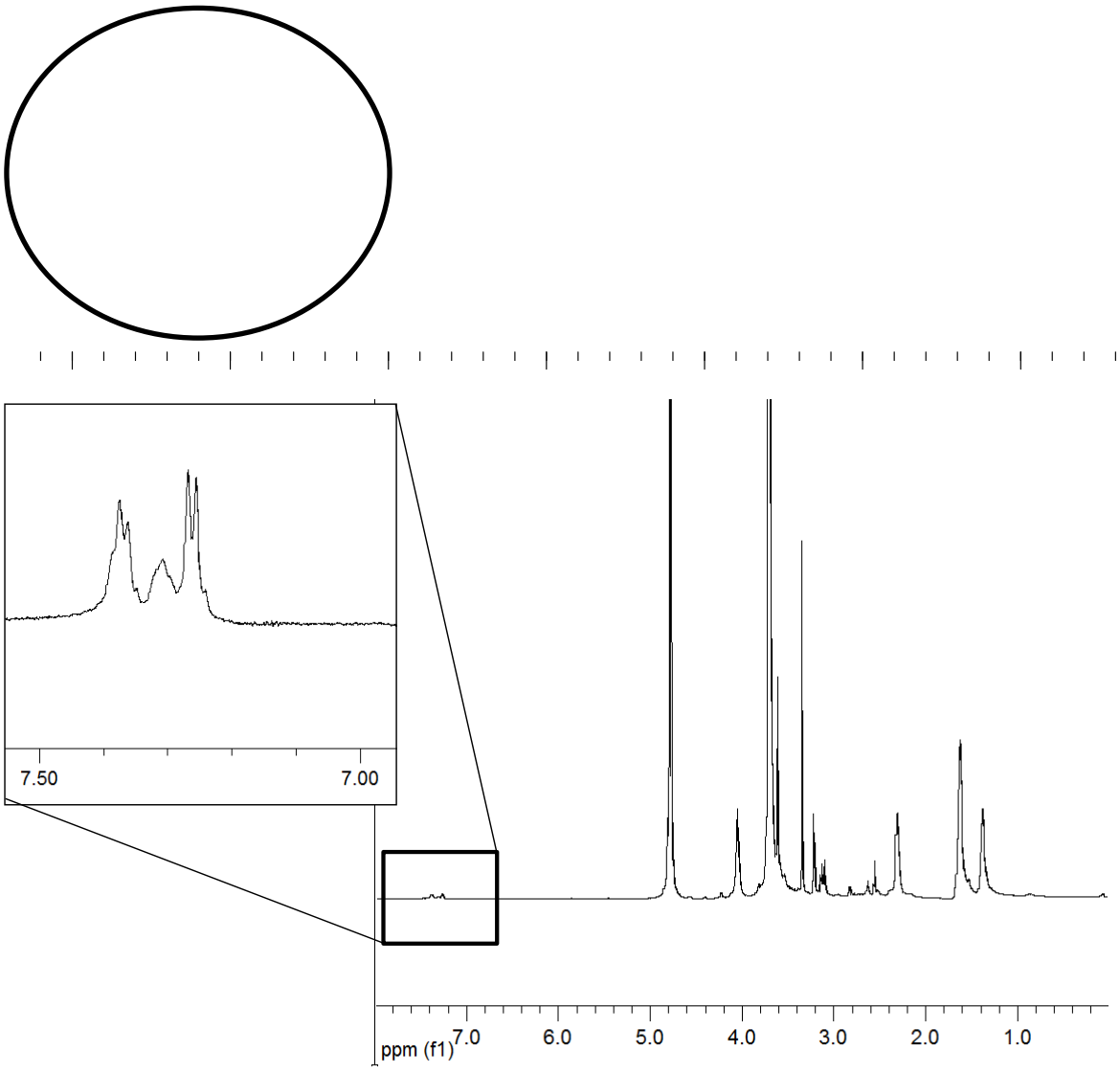

Figure 4.14. ^{1}H NMR of MAL-PEG-PCL-OH attached to c-RGD*fk* run in $CDCl_3$ showing the absence of the maleimide peak (top) and run in D_2O showing phenylalanine peaks in the aromatic region (bottom, inset)

assembled the micelles were incubated with deprotected c-RGDfk for 24 h. Then micelles, now decorated with cRGD*fk*, were dialyzed to remove any unreacted small peptide and remaining small molecules not incorporated into the micelles.

4.3.1 ^{1}H NMR of cRGD*fk* micelles

An experiment was performed with MAL-PEG-PCL-OH to determine if the Michael addition to attach cRGD*fk* to the micelles was occuring. For this cRGD*fk* was attached in high quantities to afford an NMR signal. The isolated c-RGDfk-PEG-PCL-OH polymer was then analyzed by ^{1}H NMR in both deuterated chloroform ($CDCl_3$) and deuterated water (D_2O). The chloroform ^{1}H NMR spectrum showed no peak for the maleimide, seen at 6.76 ppm in the original ^{1}H NMR of the MAL-PEG-PCL-OH (Figure 4.14, top). It did show all of the original PEG and PCL peaks. Because only a small fraction of the sample was peptide, the phenylalanine peaks were not visible in the $CDCl_3$ spectrum. The NMR run in D_2O shows the peptide's

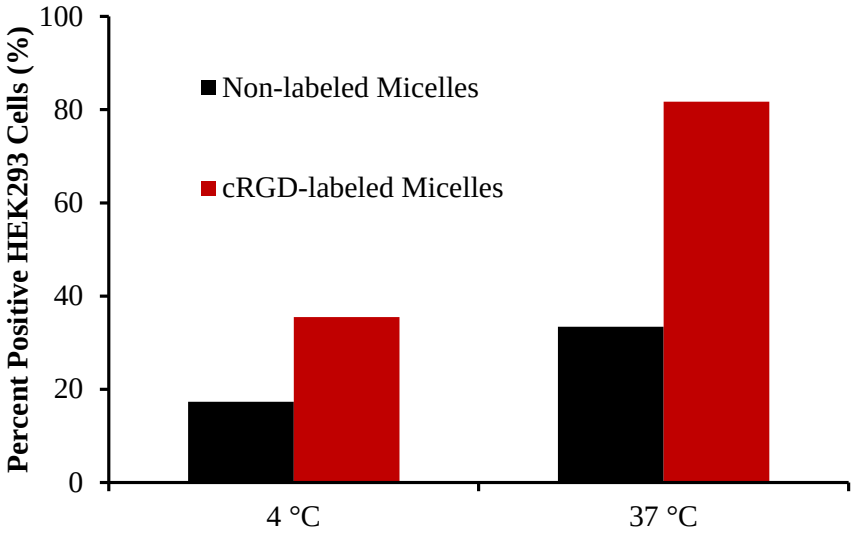

Figure 4.15. Results from incubating 40% labeled and non-labeled micelles with HEK293 cells. Percent positive cells are cells that have micelles attached.

phenylalanine peaks in the aromatic region (Figure 4.14, bottom insert).

4.3.2 c-RGD*fk* micelles with HEK293 and JURKAT Cells

Micelles were made with either 40 % MAL-PEG-PCL-OH or no MAL-PEG-PCL-OH and the copolymer MeO-EG43-CL20-OH. During self-assembly these micelles were loaded with a rhodamine derivative dye PKH26 generally used to stain cell membranes. Extensive dialysis (24 h) was performed to ensure any unincorporated dye had been removed from solution. These micelles were then fed to human embryonic kidney cells (HEK293) and incubated at either 4 °C or 37 °C for 1 h. These cells were then analyzed using flow cytometry and the percent positive cells were quantified at each temperature for each type of micelle. Figure 4.3.4 shows the results of that experiment. At 4 °C the percent positive cells was less than 20 % for non-labeled micelles and almost 40 % for c-RGDfk labeled micelles. When incubated at body temperature

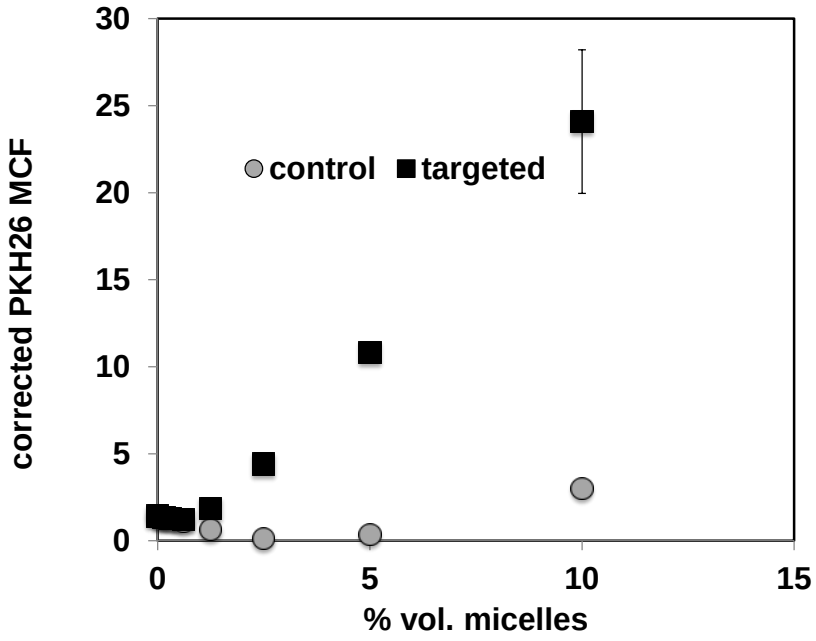

Figure 4.16. Results from incubating <5% labeled and non-labeled micelles with JURKAT cells showing less non-specific binding than seen with HEK293 cells.

the percent positive cells for the peptide labeled micelles increased to almost 80 % positive and the non-labeled micelles only showed about 30 % positive signal. This is a promising result in that the labeled micelles attached to cells at a higher percentage than did the non-labeled micelles.

A different cell line was tested to determine if non-specific binding could be reduced. T1, JURKAT cell line was incubated with micelles labeled with < 5 % c-RGDfk at varying percentages of micelle volume with the cells (from 0 % to 10 %). Figure 4.16 shows the results of incubating JURKAT cells with micelles labeled with the peptide or not labeled (control) at 45 °C for 30 min. This incubation temperature mimicked the temperatures desired to be reached by hyperthermia. At 10 % micelles volume in cells the mean channel fluorescence (MCF) is 5 time greater than for the non-labeled, control micelles.

References

1. Crank, J., The Mathematics of Diffusion. Oxford University Press: New York, 1975; pp 89-103.

2. Devanand, K.; Selser, J. C., Asymptotic behavior and long-range interactions in aqueous solutions of poly(ethylene oxide). *Macromolecules* **1991,** *24* (22), 5943-5947.

3. Sutton, D.; Wang, S.; Nasongkla, N.; Gao, J.; Dormidontova, E. E., Doxorubicin and beta-lapachone release and interaction with micellar core materials: experiment and modeling. *Exp Biol Med (Maywood)* **2007,** *232* (8), 1090-9.

4. (a) Nasongkla, N.; Bey, E.; Ren, J.; Ai, H.; Khemtong, C.; Guthi, J. S.; Chin, S.-F.; Sherry, A. D.; Boothman, D. A.; Gao, J., Multifunctional Polymeric Micelles as Cancer-Targeted, MRI-Ultrasensitive Drug Delivery Systems. *Nano Letters* **2006,** *6* (11), 2427-2430; (b) Nasongkla, N.; Shuai, X.; Ai, H.; Weinberg, B. D.; Pink, J.; Boothman, D. A.; Gao, J., cRGD-Functionalized Polymer Micelles for Targeted Doxorubicin Delivery. *Angewandte Chemie International Edition* **2004,** *43* (46), 6323-6327; (c) Toti, U. S.; Guru, B. R.; Grill, A. E.; Panyam, J., Interfacial Activity Assisted Surface Functionalization: A Novel Approach To Incorporate Maleimide Functional Groups and cRGD Peptide on Polymeric Nanoparticles for Targeted Drug Delivery. *Mol Pharmaceut* **2010,** *7* (4), 1108-1117.

CHAPTER 5

MAGNETIC MICELLES, CONCLUSIONS, AND FUTURE RECOMMENDATIONS

Once it was determined that cell targeting ligands could successfully be attached to the micelles and that drug indeed could be released at high temperatures the final piece of the puzzle had to be tried. This final piece of the puzzle was to incorporate magnetic nanoparticles (NPs) into the cores of the micelles. This was done using several different types of nanoparticles. First NPs were analyzed for their size and morphology. Then magnetic micelles were prepared, imaged and tested in the magnetic field for heating ability. The heating studies were initially done using an IR camera to measure bulk solution temperature. It was thought that perhaps the

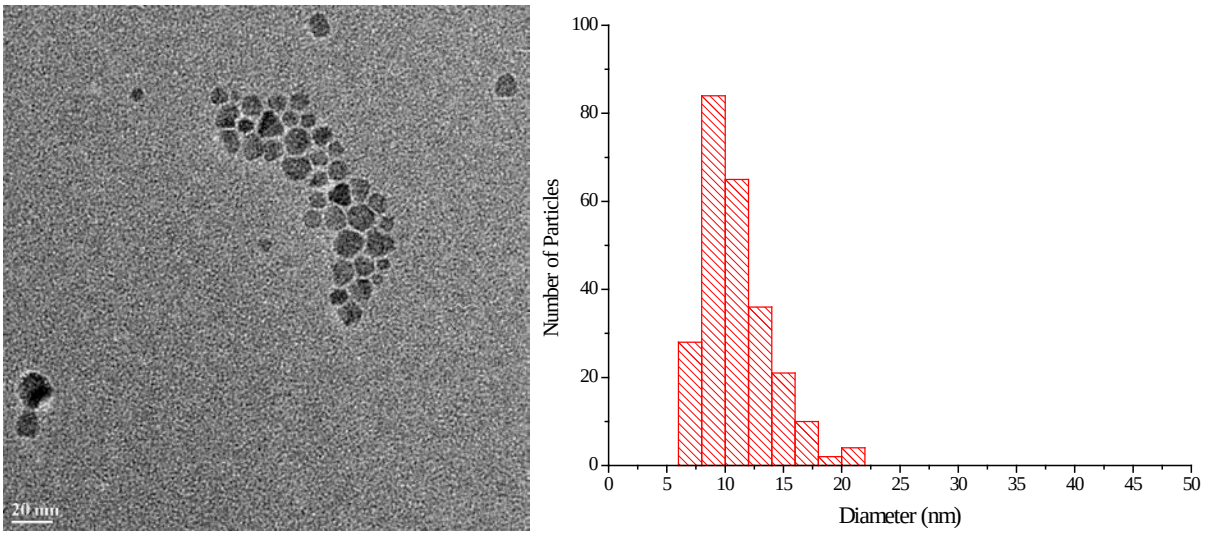

Figure 5.1. TEM of nanoparticles prepared from the Sun synthesis (scale bar 20 nm) and histogram representing 250 nanoparticles. From the histogram these nanoparticles were found to be 11 ± 3 nm.

surface of the NPs and the cores of the micelles were heating more than the bulk solution. This led to using quantum dots (QDs) as probes for nanotemperature changes. Finally, magnetically triggered release of dibucaine was attempted using large nanoparticles.

5.1 Magnetic Micelles

Initially several batches of NPs were prepared to test with magnetic heating. The first magnetic micelles were prepared with 11 nm NPs. Then a new batch of 10 nm NPs and a batch

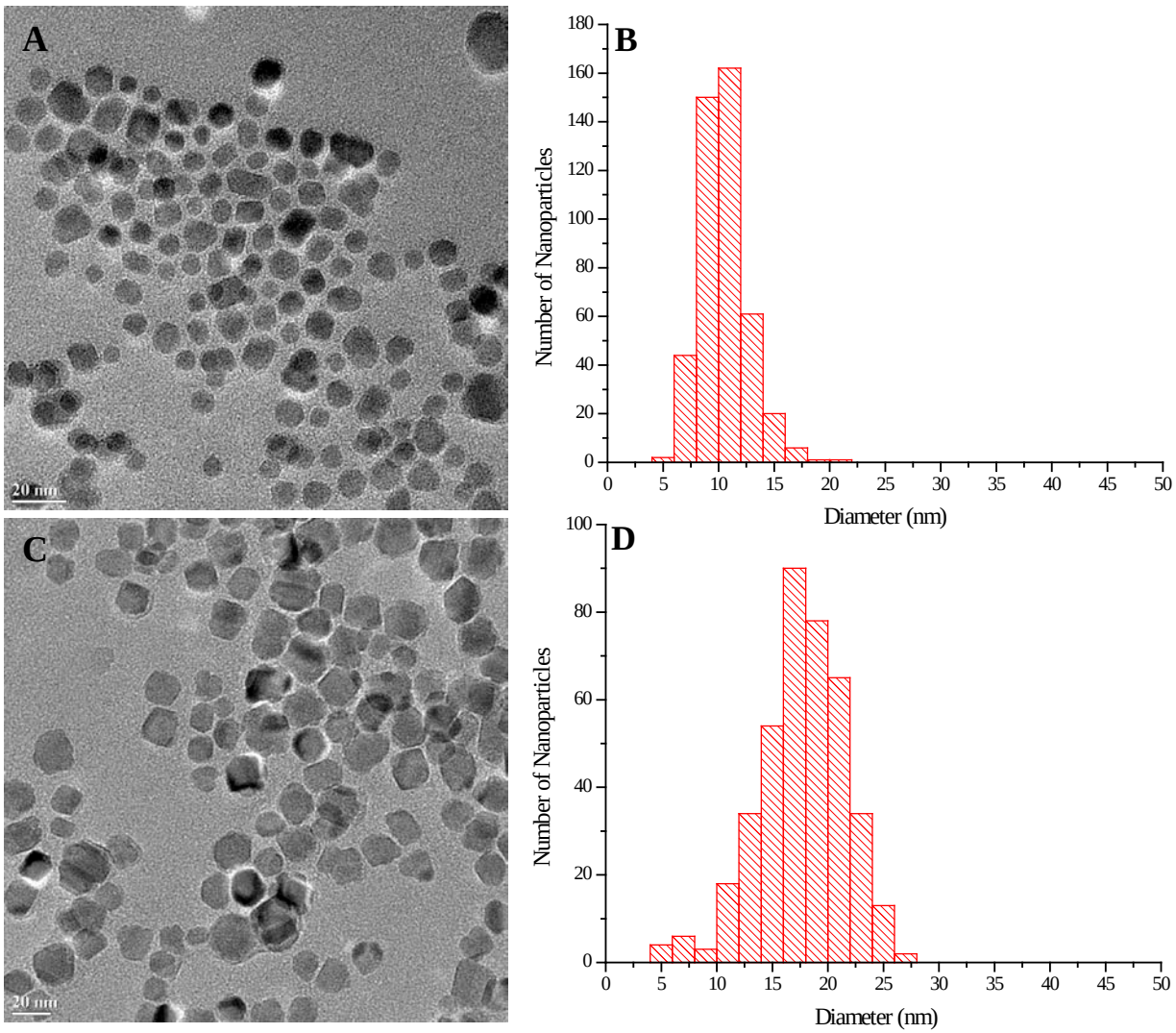

Figure 5.2. TEM images of nanoparticles seeded from smaller NPs. TEM scale bars are 20 nm. TEM showed 10 ± 2 nm particles (A, histogram of over 400 analyzed B) and 17 ± 2 nm (C, histogram of over 400 analyzed D).

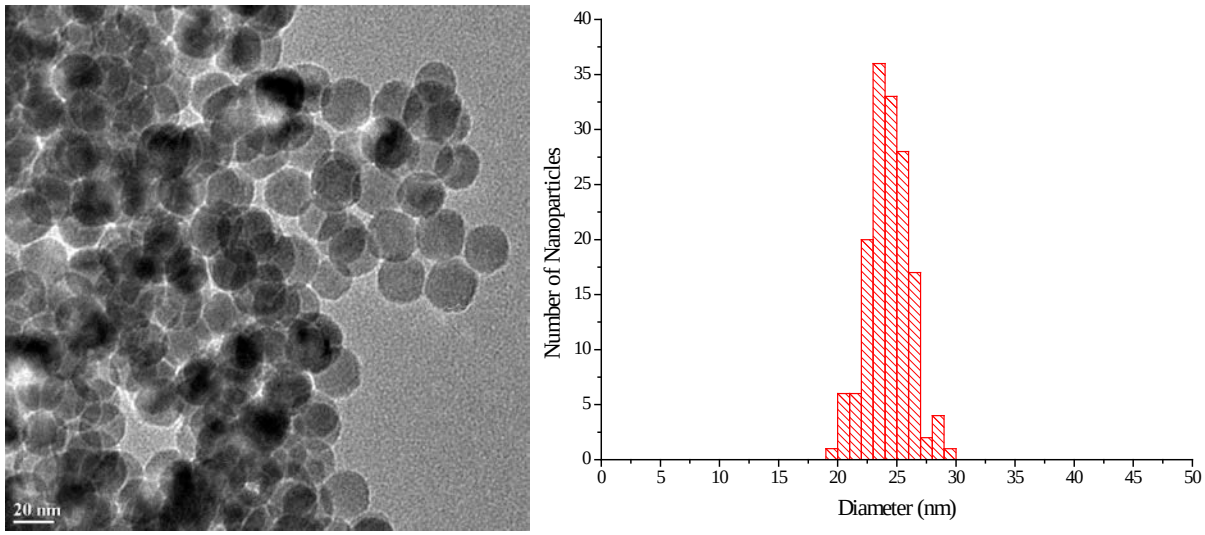

Figure 5.3. TEM image (right, scale bar 20 nm) of nanoparticles made to have a larger diameter and regular shape. 154 particles were analyzed to yield the histogram (left) showing 24 ± 2 nm diameter particles.

of 18 nm NPs were used to prepare magnetic micelles. The final batch of NPs used for heating was 24 nm. The first step in analyzing the heating from NPs was to determine the actual size of the NPs along with their shapes. Next micelles without drug were heated in the ac magnetic field and monitored for bulk solution temperature change. A method to probe internal temperatures of the micelles cores was also developed using quantum dots (QDs). This method allowed for the monitoring of fluorescence emission during exposure of samples to the radio frequency ac magnetic field. Finally, drug release from NP loaded micelles was attempted. Samples were exposed to the magnetic field for 5, 15, 30, or 60 min.

5.1.1 Nanoparticles for Magnetic Micelles

All nanoparticles were imaged by TEM to determine their actual sizes. The first synthesis of nanoparticles was supposed to yield 9 nm particles; however, the synthesis showed larger particles than that.[1] TEM showed that the nanoparticles were small and irregular, some being circular and some being octahedral in shape (Figure 5.1, left). The images from TEM

were again analyzed using NIH ImageJ software. After sampling 250 nanoparticles, the average diameter was found to be 11 ± 3 nm (Figure 5.1, right). Another batch of smaller particles was prepared this time using the Sun synthesis to prepare what were supposed to be 7 nm NPs. These NPs were then used to seed the preparation of two batches of NPs. Again the NPs were irregular in shape (Figure 5.2 A and C). After analysis, the particles were found to be 10 ± 2 nm and 17 ± 2 nm (histograms, Figure 5.2 B and D). The final set of nanoparticles used were prepared via the reduction of iron (III) oleate instead, in order to obtain the reported properties of a larger nanoparticle but also to have more uniform shape.[2] The nanoparticles synthesized were more spherical and very uniform in shape and size (Figure 5.3, left). ImageJ analysis of 154 particles showed an average size of 24 ± 2 nm, as shown in the histogram in Figure 5.3, right.

Table 5.1.1. Theoretical nanoparticle loading for magnetic micelles.

Nanoparticles (nm)	**Polymer Type**	**Theoretical [NP] (% by wt.)**	**Theoretical [NP] (g/L)**
11 ± 3	MeO-EG_{109}-CL_{48}-LA_{43}-OH	12	0.14
11 ±3	MeO-EG_{43}-CL_{20}-OH	28	0.50
10 ± 2	MeO-EG_{43}-CL_{20}-OH	67	10.4
10 ± 2	MeO-EG_{113}-CL_{107}-OH	68	10.9
17 ± 2	MeO-EG_{43}-CL_{20}-OH	66	10.1
17 ± 2	MeO-EG_{113}-CL_{107}-OH	66	10.1

5.1.2 Magnetic Heating of Magnetic Micelles

Once the nanoparticles were characterized, micelles containing the nanoparticles were analyzed in the presence of a magnetic field. For all of the described experiments, 4-turn copper coils were used at varying field strengths. Initially 11 ± 3 nm NPs were loaded into micelles at low concentrations, and tested in the magnetic field. Table 5.1 summarizes the theoretical loading of NPs into each set of micelles used for magnetic heating as well as the field strength used. The lowest field strength and NP loading was seen using 11 ± 3 nm nanoparticles and MeO-EG_{109}-CL_{48}-LA_{43}-OH micelles. For that experiment, the magnetic coils were set up with 400 V power and a frequency of 194 kHz. The sample holder, in the coils, was thermostatted with a water bath that kept the initial temperature at 37 °C. The idea was to see how high above body temperature the NP micelles would heat. After exposure to the magnetic field for 10 min,

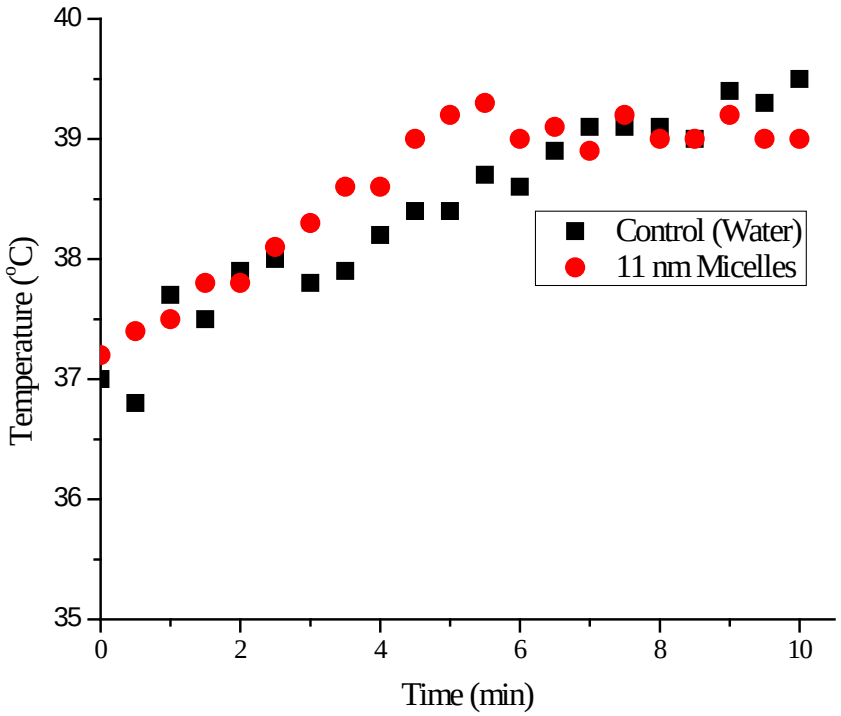

Figure 5.4. Heating curve resulting from heating MeO-EG_{109}-CL_{48}-LA_{43}-OH micelles loaded with 11 ± 3 nm NPs. The field applied was 400 V power with 194 kHz frequency.

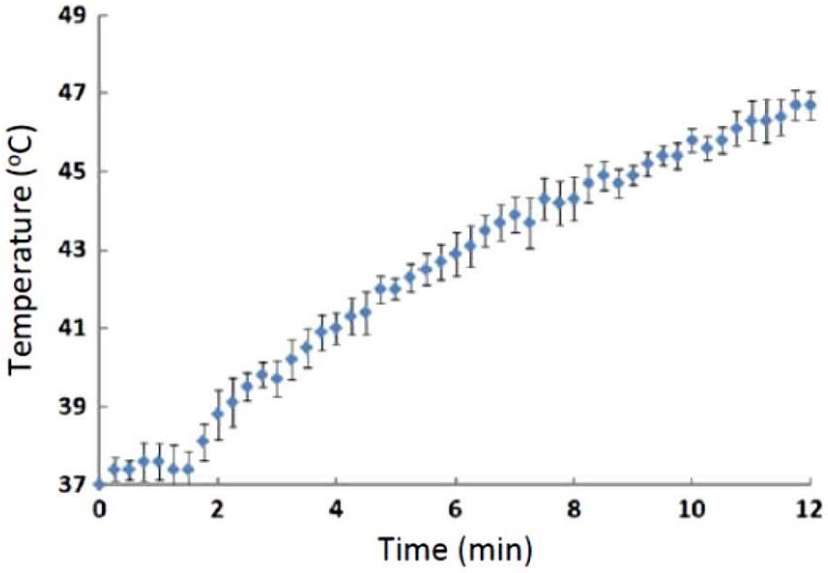

Figure 5.5. Magnetic heating curve for MeO-EG_{43}-CL_{20}-OH micelles made with 11 ± 3 nm NPs starting at 37 °C. The field strength was 75.4 kHz.

no appreciable heating was found. Figure 5.4 shows the heating curve of the micelles and ultrapure water in the same coil set up. There was no difference in heating between the two samples.

From this experiment, it was determined that the NP concentration had to be increased. For the next experiment the same set up with the coils was used however the NP concentration in the micelles was more than doubled to 28 % by weight or 0.50g/L. This time the micelles were prepared from MeO-EG_{43}-CL_{20}-OH. The experiment was run in triplicate and the initial temperature was still set at 37 °C with the same field strength as the previous experiment. This time the NP micelles heated 10 °C in 12 minutes, Figure 5.5. This was right on target for hyperthermia temperatures and melting the core of the MeO-EG_{43}-CL_{20}-OH micelles.

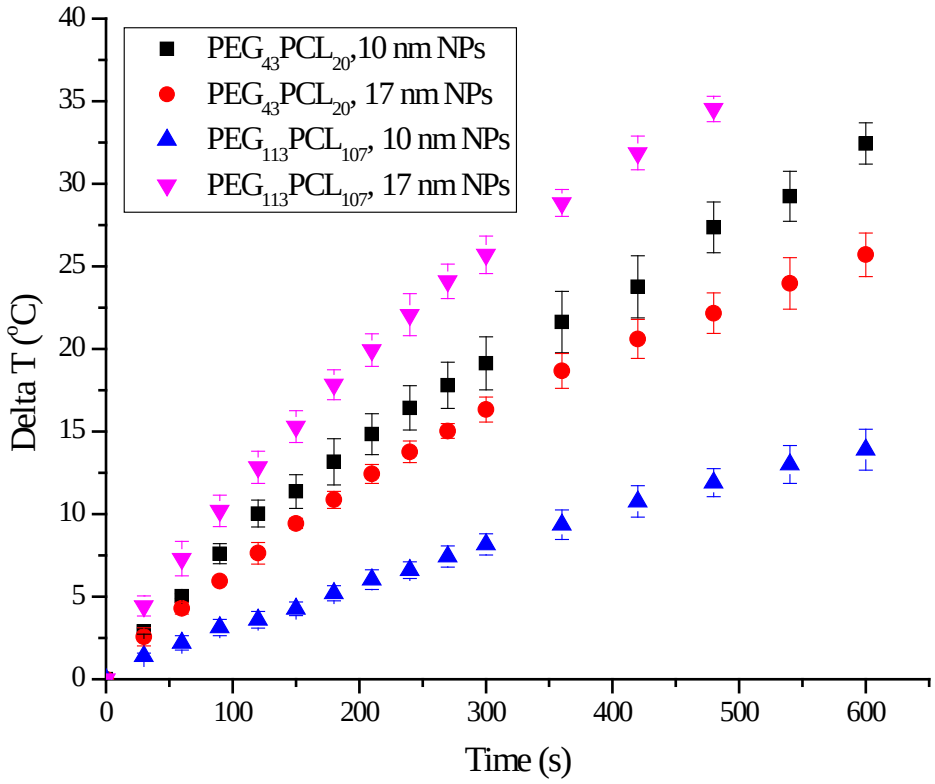

Figure 5.6. Heating of magnetic micelles made with two different copolymers and two different types of NPs. The field strength was 480 G.

Next, higher field strength and larger nanoparticles were tried to see if that would give good heating results. For this experiment MeO-EG_{43}-CL_{20}-OH and MeO-EG_{113}-CL_{107}-OH micelles were loaded with either 10 ± 2 nm NPs or 18 ± 2 nm NPs at very high concentrations. The magnetic field used was 480 G, and the coils were the same as above. A baseline of ultrapure water temperatures in the coils was subtracted from the temperature seen by the magnetic micelles. This gave a delta T (°C) of heating which was plotted as a function of time in Figure 5.6. The final change in temperature seen for the MeO-EG_{113}-CL_{107}-OH micelles housing the 18 ± 2 nm NPs was 34.5 °C after only 8 min. This was by far the highest temperature seen in any of the magnetic micelle experiments. In this series of micelles the second best heating was seen by the combination of MeO-EG_{43}-CL_{20}-OH micelles with 10 ± 2 nm nanoparticles in the

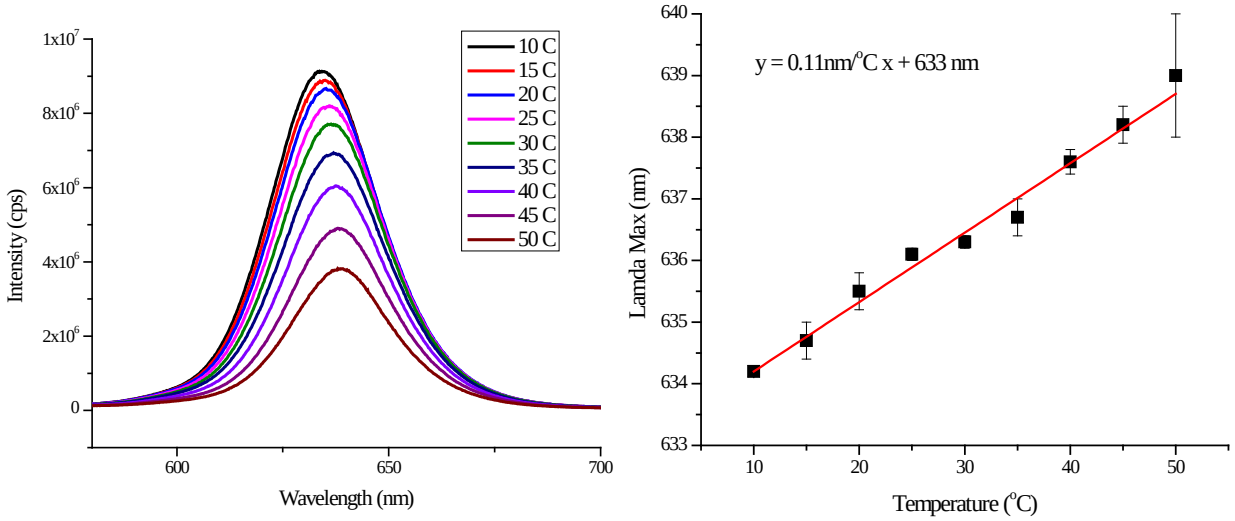

Figure 5.7. Emission spectra for NP/QD MeO-EG_{43}-CL_{20}-OH micelles showing a red shift in λ_{MAX} as temperature increased (right) and λ_{MAX} plotted against temperature (left) showing a 0.11 nm/°C red shift with increasing temperature.

core. These micelles heated 32.4 °C in 10 min. Interestingly, the micelles that heated the least of this set were the MeO-EG_{113}-CL_{107}-OH micelles loaded with the 10 ± 2 nm nanoparticles. This brings into question if certain chain lengths of PCL behave differently with different sized NPs in the cores or if there could be a correlation between chain length and NP incorporation during self-assembly.

5.1.3 Nanothermometers

In the previous experiments, bulk temperature readings were taken to determine the efficiency of magnetic heating. However, it was considered that the surface of the NPs would heat more than was seen for the bulk solution. It has been shown that QDs can be used to determine the local temperature of nano-environments such as cells.[3] The fluorescence emission maximum of the QDs experiences a red-shift of 0.1 nm/°C. First, 11 ± 3 nm NPs were loaded into the core of MeO-EG_{43}-CL_{20}-OH micelles with QDs. These micelles were then analyzed using a thermostatted fluorimeter. The temperature of the sample was increased at 2 °C from 10

°C to 50 °C. The resulting emission from 550 nm to 700 nm was analyzed for the emission maximum (λ_{max}). Figure 5.7 shows the resulting emission spectra (right) and the λ_{max} vs. temperature curve (left). This resulted in a calibration curve for determining the temperature from the λ_{max} with a slope comparable to the literature at 0.11 nm/°C.

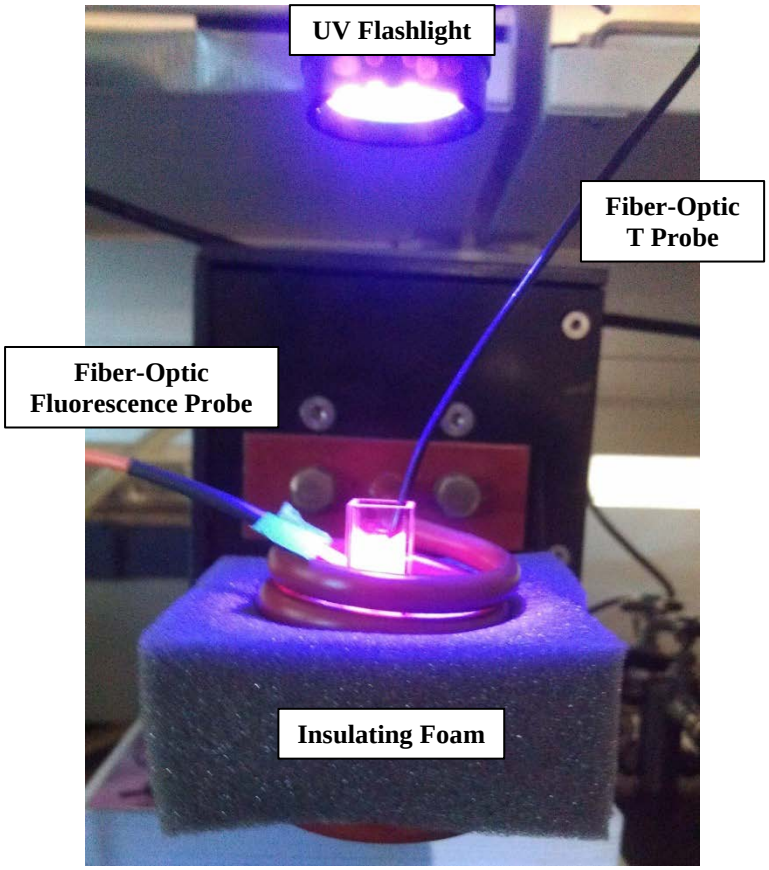

Figure 5.8. Magnetic coil set up for measuring fluorescence and temperature during magnetic induction heating.

The NP/QD micelles were again prepared for use in the ac magnetic field. The experimental set up for the experiments can be seen in Figure 5.8. The micelles, in a quartz cuvette suitable for fluorescence, were placed in the four-turn coils inside a piece of insulating foam. A portable spectrophotometer (Ocean Optics) was used that used a fiber optic cable as the detector. The fiber optic cable was equipped with a plastic end so that it would not heat up in the magnetic field. A UV capable flashlight with a emission at 400 nm was used to excite the QD fluorescence. Another fiber optic probe was used to determine the bulk solution temperature. When the NP/QD micelles were placed in the coils a spectrum was taken every half minute for 16 minutes in the field. The resulting emission peaks from the QDs were fit to a Gaussian curve using the computer program Origin and the peak maximum was taken to be the λ_{max} and was

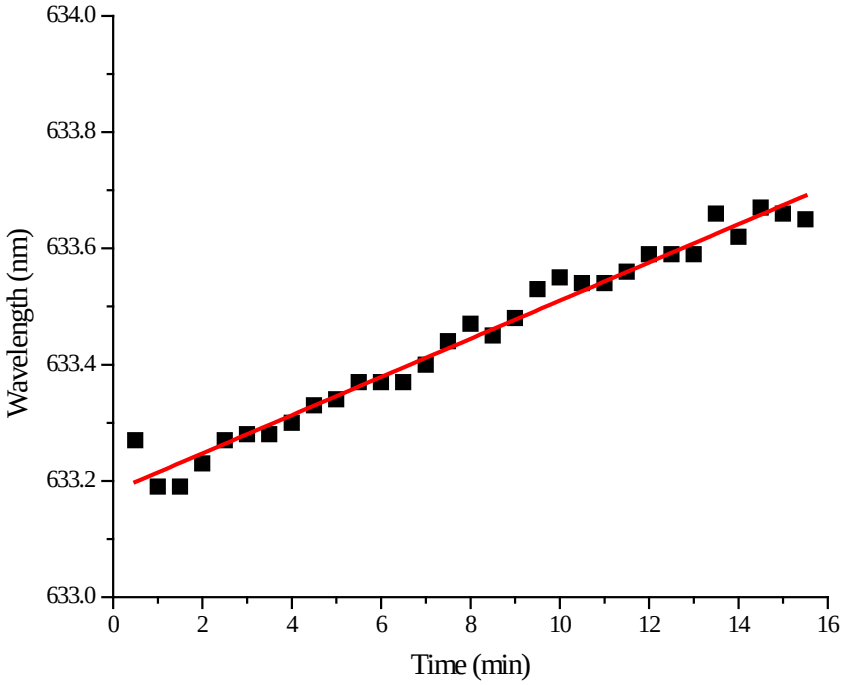

Figure 5.9. Magnetically triggered heating of NP/QD micelles showing a 0.034 nm/min slope which resulted in 5 °C heating in 16 min.

plotted against time as seen in Figure 5.9. The resulting curve had a slope of 0.034 nm/min. This translated to a 5 °C temperature change in 16 minutes. Compared to the moving average from the temperature probe, which also had a 5 °C response over the 16 minutes; it was concluded that the total temperature change seen from the QD fluorescence was a bulk temperature change.

This result could be explained by looking at the TEM images of the NP/QD micelles. The TEM image, Figure 5.10 left, shows NPs incorporated into the cores of the micelles with the QDs. However there were also instances of QDs not incorporated in the core of the micelles. Therefore it was concluded that the resulting spectrum from the QD heating was an average spectra of the core of the micelles and the bulk solution. To better understand the micelles 24 nm NPs were also incorporated into QD micelle solutions. The QDs made very nice, spherical

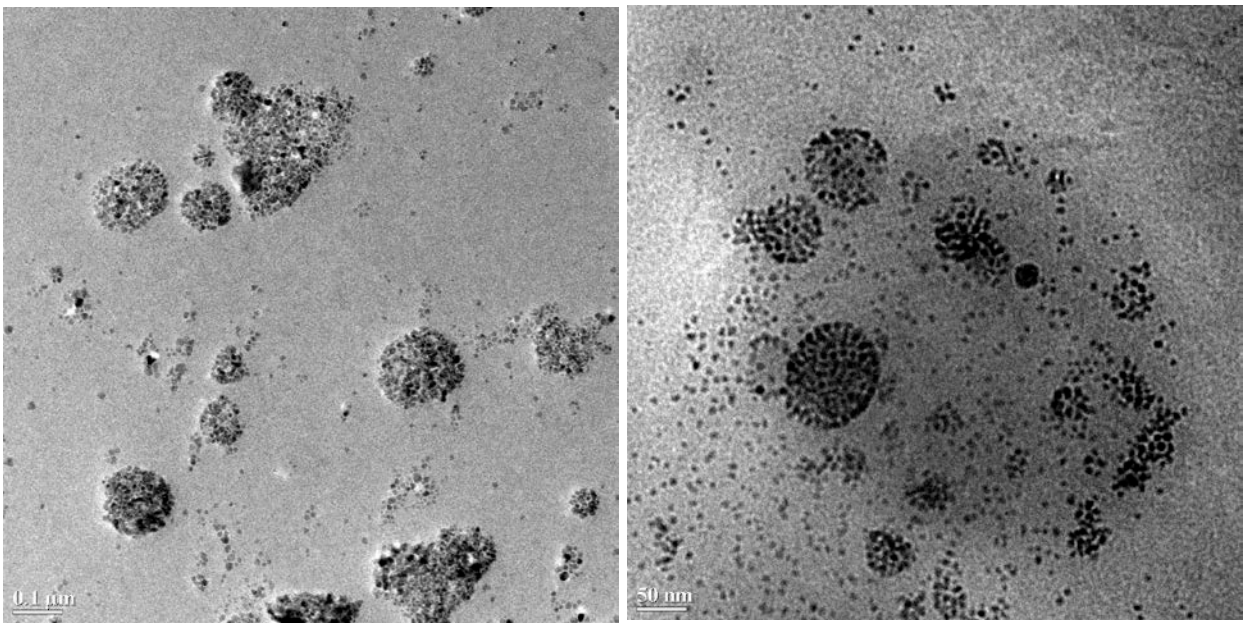

Figure 5.10. TEM images of 11 ± 3 nm NP/QD micelles (right, scale bar 0.1 μm) and 24 ± 2 nm NP/QD micelles showed QD exclude larger NPs (left, 50 nm scale bar).

micelles, however the huge difference in size between the 4 nm QDs and the 24 nm NPs meant that the QDs excluded the NPs completely from the cores of the micelles (Figure 5.10, right).

5.1.4 Magnetothermally Triggered Drug Release

Although the experiments to get a handle on the local temperature in the core of the micelles did not result in the desired nano temperature probes; it was still promising that QDs did show bulk heating for the sample. This meant, regardless of the nanotemperature, the magnetic NPs in solution had to be heating in the field. Therefore, experiments to determine if the ac magnetic field generated enough heat to release drug at an increased level from the micelles. NPs and dibucaine were loaded into MeO-EG_{43}-CL_{20}-OH and MeO-EG_{113}-CL_{107}-OH micelles. The NP and drug amounts used to makes these micelles was more than was used for isothermal release. This was because the final release experiment was done using Float-A-Lyzers and testing from the dialysate coming out of the Float-A-Lyzers, like was done for the doxorubicin

micelles in Chapter 4. The extinction coefficient for dibucaine is lower than for doxorubicin. This meant that more drug had to be loaded to get any signal when detecting the release amount.

Drug loading was determined by back calculation. The drug loading could not be directly determined because dibucaine signal could not be quantified above the NP absorption by using UV-Vis spectroscopy. There was a cleaning step in the preparation of the micelles. Each dialysate from cleaning was sampled and analyzed by UV-Vis and compared to the previously determined calibration curve. The total dibucaine removed from solution was subtracted from the total loaded into the micelles. This gave the loading percentages seen in Table 5.2. Both sets of micelles retained more dibucaine than had been previously retained by the copolymer micelles.

Table 5.2. Drug and NP loading results from MeO-EG_{43}-CL_{20}-OH and MeO-EG_{113}-CL_{107}-OH NP/dibucaine micelles.

Polymer	NP loading (g/L)	Dibucaine loading (% by total weight)	Dibucaine loading (% by core weight)	Encapsulation Efficiency (%)
MeO-EG_{43}-CL_{20}-OH	10.6	16	35	47
MeO-EG_{113}-CL_{107}-OH	2.1	34	74	74

This means the total drug loaded for isothermal release had been underestimated in experiments described in the previous chapter. Theoretically, the MeO-EG_{43}-CL_{20}-OH micelles retained 16 % dibucaine by weight and the MeO-EG_{113}-CL_{107}-OH micelles retained 34 % of the drug by weight. This was about two times the amount seen previously.

For magnetically triggered drug release, 1.2 mL of the micelle solutions were exposed to a 480 G magnetic field for 5 min or 15 min for the MeO-EG_{43}-CL_{20}-OH micelles and for 30 min or 60 min for MeO-EG_{113}-CL_{107}-OH micelles. The micelles exposed to the field were then loaded into Float-A-Lyzers and then kept in the shaker baths at 27 °C. Control samples were also put in the 27 °C shaker bath at the same time as the exposed samples. Dialysate samples were taken at 30 min for early time release determination, 120 min for middle time release, 500 min for the time when the micelles generally started to reach M_∞, and 24 hours for late time release and true M∞ values. Dibucaine release was quantified in mg for each of the samples. Figure 5.11 shows the final release curves from the micelles with CL20 on the left and CL107 on the right. The amount of dibucaine in each 1.2 mL sample was 1 mg for the MeO-EG_{43}-CL_{20}-OH micelles and 2 mg for the MeO-EG_{113}-CL_{107}-OH micelles. After 24 hours only about 0.3 mg or 33 % of the drug was released from MeO-EG_{43}-CL_{20}-OH micelles and 0.17 mg or 9 % was release from the MeO-EG_{113}-CL_{107}-OH micelles. These release numbers were for the control and for the exposed micelles samples. This meant that for the setup of the experiments no more

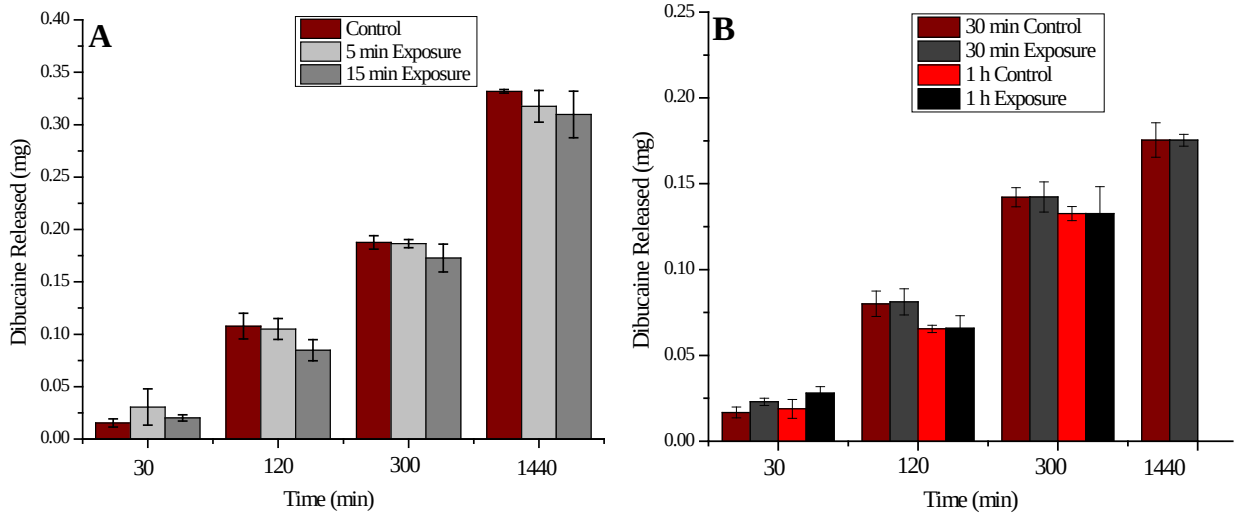

Figure 5.11. Magnetically triggered drug release curves for MeO-EG_{43}-CL_{20}-OH/dibucaine micelles (A) and MeO-EG_{113}-CL_{107}-OH/dibucaine micelles (left).

was released from the exposed samples than to the control samples. It was expected, from the results of the isothermal release, that the micelles made from the CL107 copolymer would release less than the CL20 copolymer micelles.

5.2 Conclusions from Magnetic Micelles

Magnetic heating experiments showed that, at least for bulk solution heating, micelles had to have at least 28 % NP loading by total weight, and more loading was better for heating. Also larger NPs heated more that smaller NPs in an ac magnetic field. There was a correlation between the type of copolymer and the size of nanoparticle during heating. In order to get a hold of the local temperatures of the NPs in micelle cores, QDs were used. Literature reports of the λ_{max} increasing with temperature were confirmed by traditional fluorescence. The micelles experiments failed to provide a heating change above the bulk solution. This was because the QD micelles were not successfully separated from free QDs in solution. Magnetothermally triggered release was performed using a combination of magnetic field exposure and dialysis. These experiments did not show more drug released from the cores of the micelle than for controls. This was perhaps due to the method of release used to determine release amounts. Drug may have been released at a higher rate for the exposed samples, but perhaps only during magnetic induction heating and not during subsequent isothermal room temperature release.

5.3 General Conclusions

The library of eight copolymers prepared via the tin catalyzed ring opening polymerization of ε-caprolactone onto polyethylene glycol monomethyl ether were used to create micelles. First, they were analyzed by ^{1}H NMR and GPC. From ^{1}H NMR it was possible to determine the degrees of polymerization and number average molecular weights for the copolymers. GPC did not agree very well with NMR results. This was because the polystyrene

standard used was inappropriate for the copolymers prepared. CMCs were determined via direct dissolution of the copolymers in an aqueous pyrene solution by fluorescence. They decreased with increasing PCL content. This was because of the fact that more PCL meant more hydrophobic interactions in water resulting in the polymer chains self-assembling sooner. DLS and TEM showed the nanostructures formed were spherical and generally below 200 nm in diameter. Some larger particles were seen for unfiltered solutions but these were removed in the final preparation of the loaded micelles which included a filtering step.

There were 5 generations of preparation methods for the micelles. Each method had advantages and disadvantages. It was determined for the best nanoparticle dispersions and self-assembly that generation 4 was the best method for preparing micelles. In this method a solvent selective for both blocks of the copolymer, THF, was used to dissolve or dispersed all components of the micelles. These solutions in THF were then added to room temperature ultrapure water drop wise with probe sonication. The probe sonication was able to disperse NPs more evenly than stirring methods. The THF was allowed to evaporate overnight and then the solution was dialyzed at 4 °C for 6 h to 24 h. The dialysis step was for removing unincorporated small molecules like drugs from the free solution. After dialysis, often there were NP or drug aggregates and crystals. This was the best way to improve the PDI of the micelles in solution as well as to remove any aggregates from components of the self-assembly matrix not incorporated into the cores of the micelles.

Blank micelles were characterized for their temperature dependent behavior. CMC was seen to increase with increasing temperature. This was determined to be because when at higher temperatures the equilibrium that exists between free chains and micelles in solutions favored dissolution. Micelles were also found to have semicrystalline cores. The percent crystallinity of

the cores of the micelles decreased with increasing hydrophobic character. This is also expected as it has been shown previously that the PCL homopolymer has smaller crystalline character as the length of the chains increased. Finally, it was shown that rather than simply falling apart when heated the micelles actually just scattered less light and the size remained mostly constant.

In Chapter 4 it was shown that the micelles were able to release higher drug at higher temperatures. In general, for early time release, the difference between the drug released at high temperature as compared to lower temperature was greater than the 10 % difference expected from the increase in diffusion at higher temperatures. From single replicate isothermal release it was decided that the favorite copolymers used were the MeO-EG_{43}-CL_{20}-OH, MeO-EG_{113}-CL_{107}-OH and MeO-EG_{109}-CL_{48}-LA_{43}-OH because of their ease of use, drug loading capacity and ability to retain drug at low temperatures (or minimal leakiness). These copolymers were used for triplicate doxorubicin release. Doxorubicin showed much less release than did dibucaine from single experiments. Only 20 % of the doxorubicin released from the cores of MeO-EG_{113}-CL_{107}-OH and MeO-EG_{109}-CL_{48}-LA_{43}-OH after about 6 h. Dibucaine studies were then revisited in triplicate for MeO-EG_{43}-CL_{20}-OH, MeO-EG_{113}-CL_{107}-OH and MeO-EG_{109}-CL_{48}-LA_{43}-OH. The resulting release curves were fit to Crank's model of diffusion from a polymer sphere which gave M_∞ and D/r^2 values. Taking into account the radius from DLS and the radius of gyration of PEG diffusion coefficients were determined for dibucaine release. It was found that the diffusion coefficients for dibucaine for the copolymers were 3 orders of magnitude faster than those previously reported for doxorubicin from similar copolymer micelles.

The targeting ligand c[RGDfk(Ac-SCH_2-CO)] was easily attached to the copolymer micelles made with a fraction of maleimide terminated PEG-PCL incorporated during self-

assembly. These micelles with 40 % peptide decorating the surface were able to attach to HEK293 cells at a higher percentage than non-peptide labeled micelles. However, some non-specific binding was seen from the non-labeled micelles. Jurkat cells were then used to prove that the non-specific biding would decrease with micelles containing < 5 % ligand at 10 % of the cells. This was a proof of concept experiment.

Finally, magnetic NPs were incorporated into the micelles. This incorporation was successful for a variety of sizes of NPs. These NPs showed heating of their solution in ac magnetic fields. Higher NP concentrations and higher field strengths increased the NP's ability to heat the aqueous solutions there were contained in. Attempts to probe the temperature at the surface of the NPs in the cores of the micelles were unsuccessful. However, the experiment was successful in developing a method that can be used in the future to probe fluorescence of a sample being exposed to an ac magnetic field. Finally, magnetically triggered drug release was attempted for two copolymers containing high quantities of dibucaine and NPs. These micelles did not show an increased release over controls after exposure to the ac magnetic field.

5.4 Future Recommendations

Copolymers that form less poly-dispersed molecular weights and less leaky micelles should be prepared. This could be done by perhaps simply changing the hydrophobic block to have CL at end of the triblock copolymer and LA in the center. This might increase the crystallinity of the CL block and provide a barrier that is glassy from LA to keep the drug in the center of the micelle. Other attempts should be made at synthesizing polymers with large PCL content and glassy blocks between the PEG and PCL blocks. The glassy polymer should be less porous than the crystalline copolymer and may be able to hold the drug in the micelles at low temperatures. Glass transitions of these copolymers should match up with the melting points of

the PCL block. For analysis of the copolymers, a more suitable standard should be found that mimics the diblocks hydrodynamic radius in organic solvent. This may increase the agreement between NMR and GPC. NMR should also be done with higher field NMRs. This is because from analysis, the peak used to set the integration for the rest of the copolymer is very small in high molecular weight polymers. This may skew the determination of the degrees of polymerization.

Temperature dependence should also be determined for drug and nanoparticle loaded micelles. This means DSC and temperature dependent DLS should be run for all of these micelles. For drug loaded micelles, comparing the crystallinity to blank micelles would give an idea of where the drug may reside in the core of the micelles as well as the mechanism for release. Isothermal release curves using doxorubicin should be used to determine doxorubcin's diffusion coefficients and M_∞ values for the copolymers being chosen for drug release. This would give a better idea of the dynamics of drug release for an actual drug that could be used in a clinical setting.

A method is needed to determine the amount of NP, drug, and targeting ligand incorporated with the micelles. Attempts have been made to analyze NP loading by atomic absorption spectroscopy (AA). This is accomplished by digesting the micelles containing nanoparticles in concentrated nitric acid or a combination of concentrated nitric acid and concentrated hydrochloric acid. This was successful with nanoparticles, but the amount of polymer contained in the micelles has made this difficult. This procedure should be revisited and refined to determine the amount of iron and consequently the amount of nanoparticles in the micelles. Thermogravametric analysis (TGA), where the mass of a sample is tracked upon thermal decomposition, could also be used to determine not only the nanoparticle mass in a

sample, but also the drug and the polymer masses of a sample of micelles. There is a possibility that even the targeting ligand will decompose at a specific temperature. Therefore each species that composes the micelles could be tracked by mass.

For biological studies, cell viability studies need to be performed with the NPs that will be used in the final application at a variety of different concentrations. This would determine the optimal concentration for use in animal studies. Cyclic arginine-glycine-aspartate peptides are shown to bind to integrins, which means the cRGD*fk* used in preliminary cell studies will only stick to the outside of the cells. A new peptide, antibody, or other targeting ligand should be chosen that will internalize the micelles into cancer cells. This new ligand should also be specific to one disease type. Integrins are overexpressed in most tumor cells because they are responsible for communication and cell growth. Therefore targeting these cells is not as specific as using a specific antibody for a receptor on the particular type of cancer being targeted.

Finally, determining the local temperature in the core of the micelles may be better done by using a fluorescent small molecule that has a temperature response that is quantifiable. Small molecules are more easily conjugated into the cores of the micelles or the surface of the nanoparticles. Unattached small molecules can be more readily removed with small MWCO dialysis membranes or magnetic separation and washing leading to less of a possibility of bulk temperature determination during heating experiments. The method developed for detecting fluorescence during ac magnetic field exposure should also be exploited for drug release studies. Pyrene, used in CMC determination studies, could also be used to determine where the drug is during heating. Other molecules should also be found that have a different fluorescence signal depending on the hydrophobicity or hydrophillicity of the surrounding environment. Additionally, electrochemical methods could be used to detect doxorubicin release by monitoring

the reduction of the 5,12-diquinone groups of doxorubicin.[4] This has been done for the approved liposomal doxorubicin delivery method DOXIL by recording square-wave voltammograms over the range of 0.3 V to 0.9 V. An advantage to this method is that it can be performed in a variety of solutions, such as phosphate buffered saline or human serum. This method would also elucidate release kinetics without the additional kinetics associated with crossing a dialysis membrane.

References

1. Sun, S. H.; Zeng, H.; Robinson, D. B.; Raoux, S.; Rice, P. M.; Wang, S. X.; Li, G. X., Monodisperse MFe_2O_4 (M = Fe, Co, Mn) nanoparticles. *J Am Chem Soc* **2004,** *126* (1), 273-279.

2. Park, J.; An, K.; Hwang, Y.; Park, J.-G.; Noh, H.-J.; Kim, J.-Y.; Park, J.-H.; Hwang, N.-M.; Hyeon, T., Ultra-large-scale syntheses of monodisperse nanocrystals. *Nat Mater* **2004,** *3* (12), 891-895.

3. Yang, J.-M.; Yang, H.; Lin, L., Quantum Dot Nano Thermometers Reveal Heterogeneous Local Thermogenesis in Living Cells. *Acs Nano* **2011,** *5* (6), 5067-5071.

4. Mora, L.; Chumbimuni-Torres, K. Y.; Clawson, C.; Hernandez, L.; Zhang, L.; Wang, J., Real-time electrochemical monitoring of drug release from therapeutic nanoparticles. *Journal of Controlled Release* **2009,** *140* (1), 69-73.